Orbital Theory of a Highly Eccentric Satellite Disturbed by a Massive Inner Satellite

Yoshimitsu MASAKI
Doctor of Science

Department of Astronomical Science
School of Mathematical and Physical Science
The Graduate University for Advanced Studies

2001 (School Year)

ABSTRACT

We have developed an analytical theory for a celestial body orbiting in a highly eccentric orbit under the perturbational influence of an inner body which revolves in a circular orbit around a central body. It is a form of restricted three-body problem. The theory is constructed using a canonical perturbation method of Lie type.

We avoided expanding the Hamiltonian in eccentricity and made it closed in form to the orbital eccentricity. Thus our analytical theory can be applied to any highly eccentric orbit. This is different from the process seen in ordinary perturbation methods that concern the celestial bodies of the Solar System which revolve in nearly circular orbits.

We confirmed that our theory is highly accurate by comparing numerically integrated results. However, the theory loses its high accuracy when the eccentricity of the outer body is very large. This is mainly due to the following: (1)The theory shows ill-convergence for short periodic perturbations. (2)Offset phenomena (the abrupt changes in the orbital elements that occur when the outer body passes through its pericenter) are shown in the numerical results. The magnitudes of the offsets are closely related to the spatial configurations of the two satellites.

The theory can be applied to some celestial bodies. The motion of the Neptunian satellite Nereid orbiting in a highly eccentric orbit ($e = 0.75$) perturbed by Triton is one example. Our theory provides a degree of accuracy, with results generally much better than 30Km in the (osculating) semimajor axis of Nereid. For some extrasolar planetary systems, a circularly revolving planet (sometimes called "Hot Jupiter") is known to be in the vicinity of the central star, and another new planet may exist in the outer field. The motion of these new planets can also be described by this theory.

Contents

Chapter 1

Introduction

1.1 Purpose of this study

In this thesis, we describe the motion of a celestial body (hereafter, we call it the 'outer') moving in a highly eccentric orbit around a pair consisting of the primary body and an inner revolving body (called the 'primary' and the 'inner', respectively). The mass of the inner body is small enough compared to the primary, and that of the outer can be neglected (i.e. mass-less particle). For brevity's sake, we can say that the inner body orbits around the primary star in a circular motion. It is one kind of restricted three-body problem.

1.2 Background

Astronomical ephemerides provide precise positions of celestial bodies in tabular form. These ephemerides are compiled from numerical integrations or using analytical theory.

In the numerical approach, the equations of motion are numerically integrated by computer. The results are usually obtained in the Cartesian coordinate system. Initial conditions and constants used for calculations determine all of the results uniquely.

Today, numerically integrated ephemerides are widely used in the world. DE (Development Ephemeris) series compiled by JPL are the most famous planetary ephemerides. For satellites, numerical ephemerides are also used.

In the analytical approach, the equations of motion are described in trigonometrical functions and their results are expressed as osculating elements which are functions of time. Therefore, we can calculate osculating elements at an arbitrary time without numerically integrating the equations of motion.

When we discuss the motion of a celestial body in the Solar System analytically, we usually handle a perturbation theory. From the dawn of celestial mechanics, many astronomers have devoted their efforts in the study of a perturbation theory to construct ephemerides of planets or satellites.

In the mid-20th century, canonical perturbation theories based on the Lie theory were proposed by some astronomers. Hori (1966) constructed a canonical perturbation theory through evaluating Poisson brackets of elements. A few years later, Deprit (1969) developed a different

type. These two formulations are mathematically equivalent. A canonical perturbation method is superior to other classical ones in the point that the theory is free from secular terms, like $\propto t^n$. Therefore, we don't face the steady (artifact) increase of orbital elements with time, which is seen in other perturbation methods. Thus, the theory's validity is long-term.

In a perturbation theory, we expand a perturbing function in a small parameter. Since most planets or satellites revolve in nearly circular orbits, i.e. orbital eccentricity $e \ll 1$, we usually expand a perturbing function in terms of powers of eccentricity.

However, a Neptunian satellite Nereid revolves on a highly eccentric orbit ($e = 0.75$), the power series of eccentricity converges quite slowly. Mignard(1975)'s study is the pioneered work on the motion of Nereid. Saad(2000) studied the motion of Nereid using a canonical perturbation method of Hori type. The inner orbiting satellite, Triton, is not taken into consideration in these studies because its perturbational effect is weaker than the Sun's and is not detected by astrometric observations from ground telescopes. However, if we would like to obtain a more precise ephemeris, the effect of Triton has to be included in the theory.

1.3 Newly adopted method

The problem in this study has the same orbital configuration as that of the Nereid system. Therefore, we can utilize previous work on Nereid under the perturbational influence of Triton, such as the research carried out by Oberti (1990), Segerman and Richardson (1997).

In their work, the motion of Nereid is described in the barycentric coordinate system of Neptune and Triton to express the problem in simple form. Oberti (1990) expanded the Hamiltonian in eccentric anomaly, thereafter Segerman and Richardson (1997) expanded the Hamiltonian in eccentricity. It is suspected that these theories are accurately calculated for a highly eccentric orbit. We cannot guess their accuracy from the authors' papers because they did not compare their analytical results with numerical ones.

In this study, we construct an analytical theory using a Lie-type canonical perturbation method, proposed by Hori (1966). Using this method, an analytical theory does not have secular trends in action variables (a, e, i) or (L, G, H) in Delauney's elements.

When evaluating an averaged value over the angular variable l, we integrate it by true anomaly f with $\frac{df}{dl}$. This approach does not require expanding in eccentricity. Hence it is suitable for a highly eccentric body.

We decompose the perturbing function in each degree of Legendre polynomials, such that we can estimate the truncational error of the Hamiltonian.

1.4 Application

We aim to construct this theory to describe the motion of Nereid. However, since our theory does not contain some numerical values which are peculiar to the Nereid system, it is applicable to other celestial bodies orbiting on highly eccentric orbits. See details in Ch. 8.

One example may be found in the extrasolar planetary system. In 1995, the first candidate for an extrasolar planet was reported by Mayor and Queloz (1995). After this discovery, several

tens of extrasolar planets have been found from radial-velocity observations as of 2001. Some of the planets are revolving near a primary star at small distances. These are called "Hot Jupiters". It is hoped that another planet will be discovered moving in the outer field of a Hot Jupiter system in near future. Our theory is also applicable to these planets.

Chapter 2

Methods of Analysis

2.1 Analytical formulation

2.1.1 A general expression of the problem in the barycentric coordinate system

Hereafter, we designate masses of the Primary, Inner and Outer as M, m_{In}, m, respectively. The subscript In is for a quantity of Inner, and no subscript (except M) is for Outer. The universal gravity constant is written by k^2.

In general, a force function of the three-body problem is expressed as follows:

$$U_0 = k^2 \left[\frac{M m_{In}}{r_{\text{Primary-Inner}}} + \frac{m_{In} m}{r_{\text{Inner-Outer}}} + \frac{mM}{r_{\text{Outer-Primary}}} \right]$$

where r is a mutual distance of two bodies of the set declared in the subscript.

When we consider the motion of the outer orbiting body, it is preferable to introduce the barycentric (Jacobi) coordinate system of the primary and the inner, because the time-variation in osculating elements is limited in the small magnitude (for example, Carusi et.al. (1985b, 1987)). Therefore, orbital elements of the Inner are referred to as the Primary-centric coordinate system, and those of the Outer as the Primary-Inner barycentric system as we see in Brouwer and Clemence (1961a), Oberti (1990) and Segerman and Richardson (1997).

From the definition written above, the radii of orbits are

$$\begin{aligned} r_{In} &\equiv r_{\text{Primary-Inner}} \\ r &\equiv r_{\text{(Barycenter of Primary and Inner)-Outer}}. \end{aligned}$$

So we can rewrite U_0 as

$$\begin{aligned} U_0 = k^2 \Bigg[& \frac{M m_{In}}{r_{In}} \\ & + \frac{m_{In} m}{r} \left\{ 1 + \frac{M}{M + m_{In}} \left(\frac{r_{In}}{r}\right) P_1(\cos S) \right. \\ & \left. + \left(\frac{M}{M + m_{In}}\right)^2 \left(\frac{r_{In}}{r}\right)^2 P_2(\cos S) \right. \end{aligned}$$

$$
\begin{aligned}
&\quad + \left(\frac{M}{M+m_{In}}\right)^3 \left(\frac{r_{In}}{r}\right)^3 P_3(\cos S) + \ldots \Big\} \\
&+ \frac{mM}{r} \Big\{ 1 - \frac{m_{In}}{M+m_{In}} \left(\frac{r_{In}}{r}\right) P_1(\cos S) \\
&\quad - \left(\frac{m_{In}}{M+m_{In}}\right)^2 \left(\frac{r_{In}}{r}\right)^2 P_2(\cos S) \\
&\quad - \left(\frac{m_{In}}{M+m_{In}}\right)^3 \left(\frac{r_{In}}{r}\right)^3 P_3(\cos S) - \ldots \Big\} \Big] \\
= \; & k^2 \Big[\frac{M m_{In}}{r_{In}} \\
&+ \frac{(M+m_{In})m}{r} \\
&+ \frac{M m_{In} m}{M+m_{In}} \frac{1}{r} \left(\frac{r_{In}}{r}\right)^2 P_2(\cos S) \\
&+ \frac{M m_{In} m (M-m_{In})}{(M+m_{In})^2} \frac{1}{r} \left(\frac{r_{In}}{r}\right)^3 P_3(\cos S) + \cdots \Big],
\end{aligned}
$$

where S is the elongation between Inner and Outer, and P_i is a Legendre polynomial of degree i.

For the motion of Outer, a force function has to be multiplied by a mass factor, $\frac{M+m_{In}+m}{(M+m_{In})m}$, i.e.

$$U = \frac{M+m_{In}+m}{(M+m_{In})m} U_0.$$

The unperturbed Hamiltonian of Outer (i.e. Kepler motion) is expressed as

$$H_0 = \frac{\mu}{2a}$$

where $\mu = k^2(M+m_{In}+m)$ and a is a semi-major axis of the orbit of Outer.

When a perturbation from Inner is added to the system, a (perturbed) Hamiltonian for Outer becomes,

$$F = \mu \left[\frac{1}{2a} + \frac{M m_{In}}{(M+m_{In})^2} \frac{r_{In}^2}{r^3} P_2(\cos S) + \frac{M m_{In}(M-m_{In})}{(M+m_{In})^3} \frac{r_{In}^3}{r^4} P_3(\cos S) + \cdots \right].$$

2.1.2 Simplification of the problem (Restricted problem)

After this, we simplify the problem:

- Inner moves on a circular orbit.
- Outer's perturbation does not affect the motion of the Primary or Inner (practically, it is equivalent to neglecting the mass of Outer, i.e. we study it as a restricted problem).

After neglecting Inner's eccentricity, the Hamiltonian is expressed simply:

$$F = \mu \left[\frac{1}{2a} + \frac{M m_{In}}{(M+m_{In})^2} \frac{a^3}{r^3} \frac{a_{In}^2}{a^3} P_2(\cos S) + \frac{M m_{In}(M-m_{In})}{(M+m_{In})^3} \frac{a^4}{r^4} \frac{a_{In}^3}{a^4} P_3(\cos S) + \ldots \right]$$

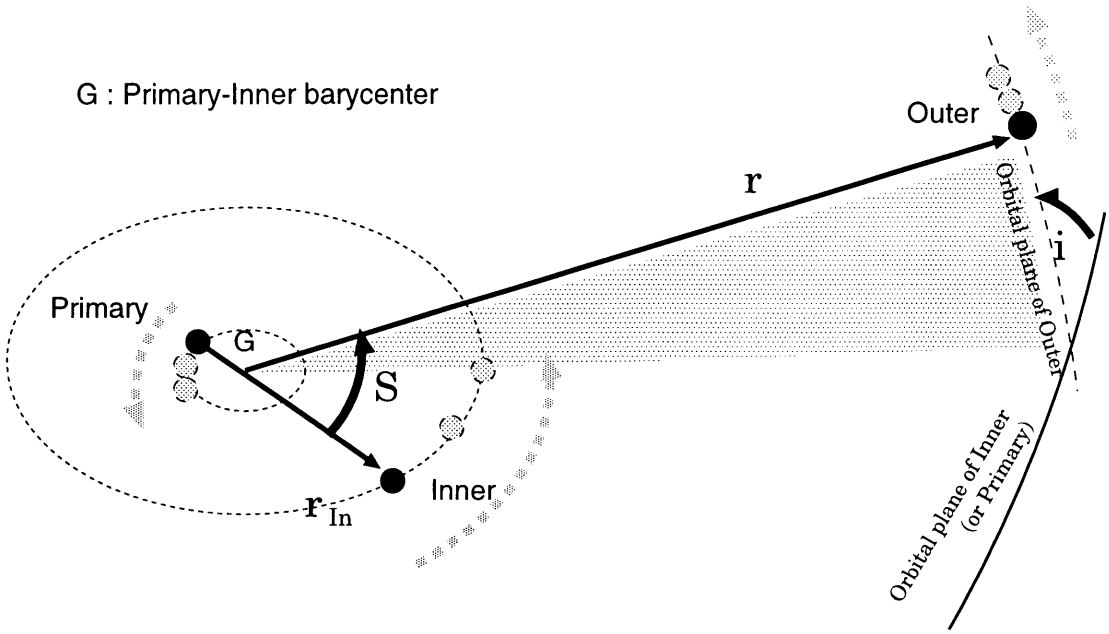

Figure 2.1: A schematically illustrated model of an inclined restricted problem

Legendre polynomials P_is are expanded as follows:

$$\begin{aligned} P_2(\cos S) &= \frac{1}{4}(3\cos(2S)+1) \\ P_3(\cos S) &= \frac{1}{8}(5\cos(3S)+3\cos S). \end{aligned}$$

An angular distance S is measured as an angle between Inner and Outer at the Primary-Inner barycenter. Using spherical trigonometry, S can be expressed by the angular orbital elements, f, ω, Ω and λ_{In} (See Figure 2.2) as follows:

$$\cos S = \cos(f+\omega)\cos(\lambda_{In}-\Omega) + \sin(f+\omega)\sin(\lambda_{In}-\Omega)\cos I$$

2.1.3 Representation in canonical form

When we consider a Kepler motion (non-perturbational problem), orbital elements of a, e, I eternally remain constant values. Now, we introduce Delaunay variables:

$$\begin{aligned} L &= \sqrt{\mu a} \\ G &= \sqrt{\mu a(1-e^2)} \\ H &= \sqrt{\mu a(1-e^2)}\cos I \\ l &= l \\ g &= \omega \\ h &= \Omega. \end{aligned}$$

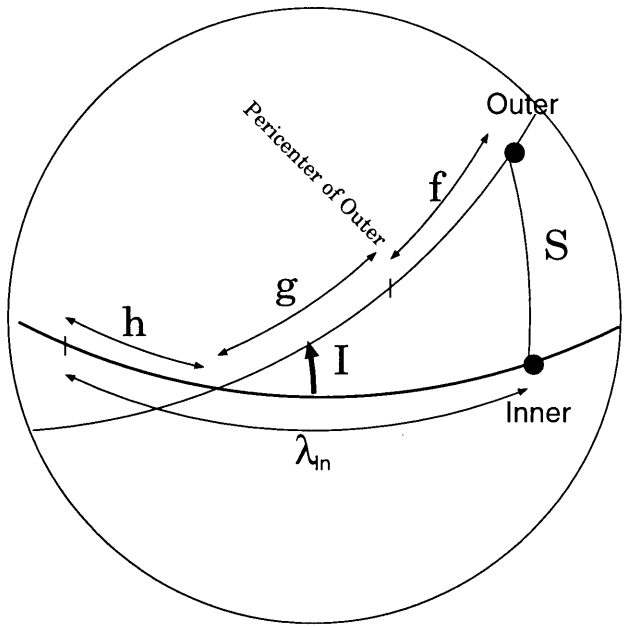

Figure 2.2: An angular distance S expressed by angular orbital elements.

Using these variables, equations of motion can be written in canonical form (as canonical equations), i.e.,

$$\begin{aligned}
\frac{dL}{dt} &= \frac{\partial F_0}{\partial l} \\
\frac{dG}{dt} &= \frac{\partial F_0}{\partial g} \\
\frac{dH}{dt} &= \frac{\partial F_0}{\partial h} \\
\frac{dl}{dt} &= -\frac{\partial F_0}{\partial L} \\
\frac{dg}{dt} &= -\frac{\partial F_0}{\partial G} \\
\frac{dh}{dt} &= -\frac{\partial F_0}{\partial H},
\end{aligned}$$

where F_0 is the Hamiltonian of the Kepler problem. In this case, F_0 does not depend on time explicitly, so F_0 is the energy integral. Needless to say, a set of angular variables l, g, h and the one of action variables L, G, H are canonical.

Thinking through a problem in canonical form has some advantages. One of the examples is: once we find a generating function suitable to the problem, equations of motion can be rewritten in another canonical form through a canonical transformation.

If we wish to separate periodic terms by their periodicity from a Hamiltonian, we have to define a generating function acting like that. Operating a canonical transformation on the Hamiltonian, we can eliminate periodic terms from it.

2.1.4 Elimination of time from Hamiltonian

As we have already seen in the previous section, the elongation S contains a variable λ_{In}, which depends on time:

$$\lambda_{In} \equiv k = n_{In}t + const..$$

Therefore, the Hamiltonian F depends on time t explicitly.

To make a Hamiltonian independent of time, we introduce a canonical conjugate action variable, K. The term $-n_{In}K$ has to be added to the Hamiltonian, then

$$\begin{aligned} F &= \frac{\mu}{2a} \\ &\quad -n_{In}K \\ &\quad +\mu\frac{Mm_{In}}{(M+m_{In})^2}\frac{a^3}{r^3}\frac{a_{In}^2}{a^3}\frac{1}{4}(3\cos(2S)+1) \\ &\quad +\mu\frac{Mm_{In}(M-m_{In})}{(M+m_{In})^3}\frac{a^4}{r^4}\frac{a_{In}^3}{a^4}\frac{1}{8}(5\cos(3S)+3\cos S) \\ &\quad +\ldots. \end{aligned}$$

There are three independent angular variables in this system:

$$f \quad , \quad g \quad \text{and} \quad h-k$$

i.e. there are three degrees of freedom.

After a suitable canonical transformation, we can deduce the Hamiltonian including only three sets of canonical variables, (y_1, x_1), (y_2, x_2) and (y_3, x_3). Suppose the canonical transformation

$$F(l,g,h,k,L,G,H,K) \longrightarrow F(y_1,y_2,y_3,x_1,x_2,x_3).$$

This transformation is obtained when the condition below is satisfied:

$$Ll + Gg + Hh + Kk = x_1y_1 + x_2y_2 + x_3y_3 + x_4y_4.$$

One example is:

$$\begin{aligned} y_1 &= l \\ y_2 &= g \\ y_3 &= h-k \\ y_4 &= k \\ x_1 &= L \\ x_2 &= G \\ x_3 &= H \\ x_4 &= K+H. \end{aligned}$$

Then the Hamiltonian becomes

$$\begin{aligned} F &= \mu\frac{1}{2a} \\ &\quad -n_{In}(x_4 - x_3) \\ &\quad +\mu\frac{Mm_{In}}{(M+m_{In})^2}\frac{a^3}{r^3}\frac{a_{In}^2}{a^3}\frac{1}{4}(3\cos(2S)+1) \\ &\quad +\mu\frac{Mm_{In}(M-m_{In})}{(M+m_{In})^3}\frac{a^4}{r^4}\frac{a_{In}^3}{a^4}\frac{1}{8}(5\cos(3S)+3\cos S) \\ &\quad +\ldots. \end{aligned}$$

The Hamiltonian does not depend on y_4 anymore, so we can eliminate x_4. Finally, the Hamiltonian is reduced to:

$$\begin{aligned} F &= \mu\frac{1}{2a} \\ &\quad +n_{In}x_3 \\ &\quad +\mu\frac{Mm_{In}}{(M+m_{In})^2}\frac{a^3}{r^3}\frac{a_{In}^2}{a^3}\frac{1}{4}(3\cos(2S)+1) \\ &\quad +\mu\frac{Mm_{In}(M-m_{In})}{(M+m_{In})^3}\frac{a^4}{r^4}\frac{a_{In}^3}{a^4}\frac{1}{8}(5\cos(3S)+3\cos S)+\ldots. \end{aligned}$$

This simplified Hamiltonian expression is used hereafter.

2.1.5 Simplification of the problem (Planar problem)

In the later chapter, to interpret results of complicated phenomena, another simplification is added to the problem,

- All bodies move on a common plane

(See Figure 2.3).

In this case, an angular distance S can be expressed as $f+\varpi-\lambda_{In}$, and the number of degrees of freedom in the system is reduced to two. Angular variables which are independent are:

$$f \quad \text{and} \quad g+h-k.$$

2.2 Hori's canonical perturbation theory

In this section, we briefly discuss Hori's canonical perturbation theory. See Hori(1966)'s work in detail. By applying this method, we can achieve decreasing degrees of freedom one by one in a Hamiltonian, to make a system integrable analytically.

2.2.1 Setting a new first integral

Suppose a canonical transformation such that

$$F(x,y) \longrightarrow F^*(x^*,y^*),$$

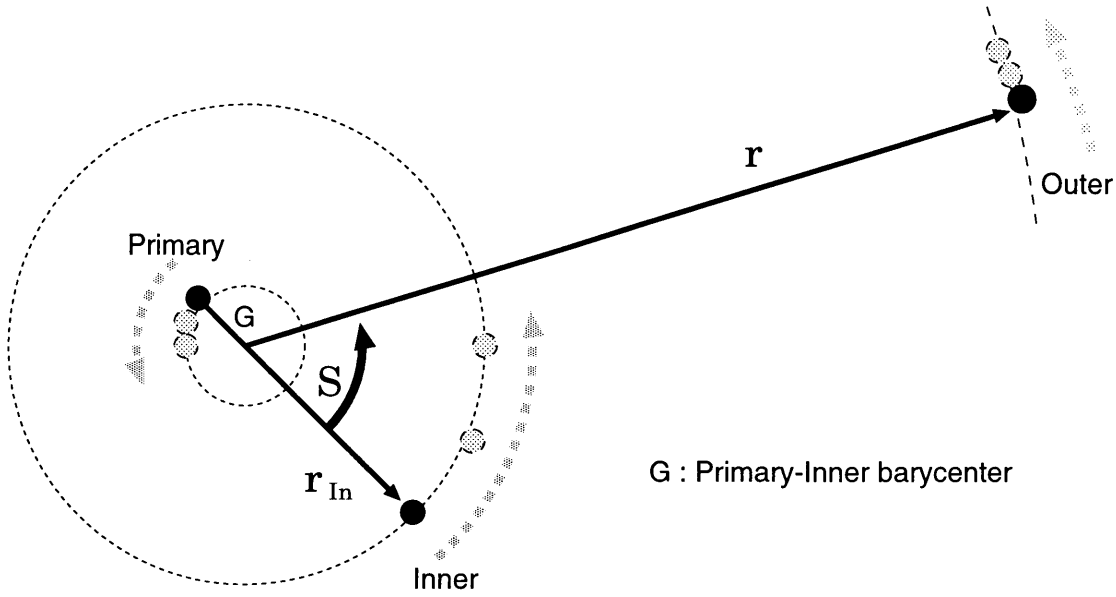

Figure 2.3: A schematically illustrated model of a planar restricted problem

where (x, y) and (x^*, y^*) are canonical variables, F and F^* are Hamiltonians, free from time t. These variables satisfy canonical equations, i.e.,

$$\begin{aligned} \frac{dx}{dt} &= \frac{\partial F}{\partial y} \\ \frac{dy}{dt} &= -\frac{\partial F}{\partial x} \end{aligned}$$

and

$$\begin{aligned} \frac{dx^*}{dt} &= \frac{\partial F^*}{\partial y^*} \\ \frac{dy^*}{dt} &= -\frac{\partial F^*}{\partial x^*}. \end{aligned}$$

Since a Hamiltonian F does not depend on time explicitly, F is the energy integral. Therefore F^* is also the energy integral which satisfies:

$$F^* \equiv const..$$

We suppose that a Hamiltonian contains perturbational terms, which are developed in powers of a small parameter ϵ,

$$F = F_0 + F_1 + F_2 + \ldots,$$

where F_0 is the Hamiltonian of the two-body problem and subscripts are orders of ϵ.

To solve equations of motion, we would like to obtain a first integral, F_0^*, to reduce by a degree of freedom after a canonical transformation:

$$F_0^* \equiv const.,$$

or, in other words, we would like to eliminate an angular variable through a transformation. For this reason, we set a canonical transformation such that

$$F_0 = F_0^*.$$

Therefore, F_0 is taken as an unperturbed Hamiltonian through this transformation.

Now, let us we consider the following equation (NOTE: in celestial mechanics, the Hamiltonian is usually reversed in its sign):

$$\frac{dF^*(x^*, y^*)}{dt^*}(\equiv 0) = \sum_i \left(\frac{\partial F^*}{\partial x_i^*} \frac{dx_i^*}{dt^*} + \frac{\partial F^*}{\partial y_i^*} \frac{dy_i^*}{dt^*} \right),$$

where t^* is defined as an artificial time parameter such that

$$\begin{aligned} \frac{dx^*}{dt^*} &= \frac{\partial F_0}{\partial y^*} \\ \frac{dy^*}{dt^*} &= -\frac{\partial F_0}{\partial x^*}. \end{aligned}$$

Then, the right hand side of the above equation can be rewritten as

$$\begin{aligned} \sum_i \left(\frac{\partial F^*}{\partial x_i^*} \frac{dx_i^*}{dt^*} + \frac{\partial F^*}{\partial y_i^*} \frac{dy_i^*}{dt^*} \right) &= \sum_i \left(\frac{\partial F^*}{\partial x_i^*} \frac{\partial F_0}{\partial y_i^*} - \frac{\partial F^*}{\partial y_i^*} \frac{\partial F_0}{\partial x_i^*} \right) \\ &= \{F^*, F_0\} \\ &= -\{F_0, F^*\}, \end{aligned}$$

where, $\{A, B\}$ is a Poisson bracket operation.

On the other hand, substituting canonical equations into $\frac{\partial F^*}{\partial y^*}$ and $\frac{\partial F^*}{\partial x^*}$ on the right hand side of the first equation,

$$\sum_i \left(\frac{\partial F^*}{\partial x_i^*} \frac{dx_i^*}{dt^*} + \frac{\partial F^*}{\partial y_i^*} \frac{dy_i^*}{dt^*} \right) (= \frac{dF_0}{dt}) = \{F_0, F^*\}$$

also holds.

Therefore, if we set a canonical transformation such that $F_0 = F_0^*$ (unperturbed) can be satisfied,

$$F_0^* = const.$$

is also satisfied.

2.2.2 Canonical transformations in Hori's method

Suppose Hamiltonians $F(x, y)$ and $F^*(x^*, y^*)$ are expanded in a small parameter ϵ, i.e.,

$$\begin{aligned} F &= F_0 + F_1 + F_2 + \ldots \\ F* &= F_0* + F_1* + F_2* + \ldots, \end{aligned}$$

where subscripts mean powers of ϵ.

An arbitrary function f of canonical variables (x, y) can be developed in a converged series of ϵ using the Lie theorem:

$$f(x,y) = \sum_{n=0}^{\infty} \frac{\epsilon^n}{n!} D_s^n f(x^*, y^*),$$

where D_s is an operator of n-times Poisson bracket with S , i.e.:

$$\begin{aligned} D_s^0 &= f \\ D_s^1 &= \{f, S\} \\ D_s^2 &= \{\{f, S\}, S\} \\ \ldots &= \ldots. \end{aligned}$$

Substituting a Hamiltonian F in f, we obtain F in a series of ϵ with variables (x^*, y^*). Comparing this expression with $F^*(x^*, y^*)$, we obtain the following equivalences for each power of ϵ:

$$\begin{aligned} F_0* &= F_0 \\ F_1* &= \{F_0, S_1\} + F_1 \\ F_2* &= \{F_0, S_2\} + \{F_1, S_1\} + \frac{1}{2}\{\{F_0, S_1\}, S_1\} + F_2 \\ F_3* &= \{F_0, S_3\} + \{F_1, S_2\} + \{F_2, S_1\} \\ &\quad + \frac{1}{2}\{\{F_0, S_2\}, S_1\} + \frac{1}{2}\{\{F_0, S_1\}, S_2\} + \frac{1}{2}\{\{F_1, S_1\}, S_1\} \\ &\quad + \frac{1}{6}\{\{\{F_0, S_1\}, S_1\}, S_1\} + F_3 \\ \ldots &= \ldots. \end{aligned}$$

Recalling a character of the Poisson bracket,

$$\begin{aligned} -\{F_0, S\} &= \sum_j \left(-\frac{\partial F_0}{\partial x_j^*}\frac{\partial S}{\partial y_j^*} + \frac{\partial F_0}{\partial y_j^*}\frac{\partial S}{\partial x_j^*} \right) \\ &= \sum_j \left(\frac{dy_j^*}{dt^*}\frac{\partial S}{\partial y_j^*} + \frac{dx_j^*}{dt^*}\frac{\partial S}{\partial x_j^*} \right) \\ &= \frac{dS}{dt^*} \end{aligned}$$

is satisfied. Therefore, we can obtain F_i^* and S_i as follows:

$$\begin{aligned} F_0* &= F_0 \\ F_1* &= [F_1]_{sec} \\ S_1 &= \int [F_1]_{per} dt^* \\ F_2* &= [\{F_1, S_1\} + \frac{1}{2}\{\{F_0, S_1\}, S_1\} + F_2]_{sec} \\ S_2 &= \int [\{F_1, S_1\} + \frac{1}{2}\{\{F_0, S_1\}, S_1\} + F_2]_{per} dt^* \\ F_3* &= [\{F_1, S_2\} + \{F_2, S_1\} \end{aligned}$$

$$
\begin{aligned}
&+\frac{1}{2}\{\{F_0,S_2\},S_1\}+\frac{1}{2}\{\{F_0,S_1\},S_2\}+\frac{1}{2}\{\{F_1,S_1\},S_1\}\\
&+\frac{1}{6}\{\{\{F_0,S_1\},S_1\},S_1\}+F_3\Big]_{sec}\\
S_3 &= \int[\{F_1,S_2\}+\{F_2,S_1\}\\
&+\frac{1}{2}\{\{F_0,S_2\},S_1\}+\frac{1}{2}\{\{F_0,S_1\},S_2\}+\frac{1}{2}\{\{F_1,S_1\},S_1\}\\
&+\frac{1}{6}\{\{\{F_0,S_1\},S_1\},S_1\}+F_3\Big]_{per}dt^*\\
\cdots &= \cdots.
\end{aligned}
$$

If an unperturbed Hamiltonian F_0 only depends on one action variable x_k^*, $\frac{dS}{dt^*}$ can be rewritten as

$$
\begin{aligned}
\frac{dS}{dt^*} &= -\{F_0,S\}\\
&= -\frac{\partial F_0}{\partial x_k^*}\frac{\partial S}{\partial y_k^*}.
\end{aligned}
$$

So, we can replace an artificial time t^* with an angular variable y_k^*,

$$
\int X\,dt^* = -\frac{1}{\frac{dF_0}{dx_k^*}}\int X\,dy_k^*.
$$

Note that separating the Hamiltonian F into a secular part F^* and a periodic one S means separating perturbations according to their periodicities. Therefore, defining F^* and S as above, we achieve the decomposition of short periodic perturbations of longer periodic ones.

2.2.3 Relation between variables before and after transformation

When you obtain osculating elements, variables before transformation, (x,y) require expression in variables (x^*,y^*). With Hori's theory, they are written:

$$
\begin{aligned}
x &= x* + \sum_{n=1}^{\infty}\frac{\epsilon^n}{n!}D_S^{n-1}\frac{\partial S}{\partial y^*}\\
&= x* + \epsilon\frac{\partial S}{\partial y^*}+\frac{1}{2}\epsilon^2\{\frac{\partial S}{\partial y^*},S\}+\ldots
\end{aligned}
$$

and

$$
\begin{aligned}
y &= y* - \sum_{n=1}^{\infty}\frac{\epsilon^n}{n!}D_S^{n-1}\frac{\partial S}{\partial x^*}\\
&= y* - \epsilon\frac{\partial S}{\partial x^*}-\frac{1}{2}\epsilon^2\{\frac{\partial S}{\partial x^*},S\}-\ldots.
\end{aligned}
$$

With an arbitrary function f,

$$
f = f^* + \{f,S\}+\frac{1}{2}\{\{f,S\},S\}+\ldots
$$

is also correct. It is noted that f can be replaced by canonical elements, i.e., x or y. If you substitute an angular variable y for f, it is not necessary to replace their signs with negative ones as in the former notation. In practical use, the latter expression is convenient for calculating osculating x and y.

2.2.4 Advantages of Hori's method compared to other canonical methods

In the field of celestial mechanics, some types of canonical transformation are widely used, such as:

- von Zeipel (1916) method
- Hori (1966) method.
- Deprit (1968) method

The von Zeipel method is a popular one, but it has some disadvantages. For example, variables before transformation are not expressed explicitly in terms of those after transformation. When you rebuild osculating elements, it is necessary to substitute variables iteratively until achieving the required accuracy. Moreover, von Zeipel's transformation does not hold its canonical character of a Hamiltonian. The Hori and Deprit methods do not have these disadvantages.

The latter two methods are based on the Lie theorem, mathematically equivalent. Both methods expand variables in a small parameter. You can see some differences in the expression of generating functions or in expressions of Hamiltonians expanded in their Poisson bracket for higher orders of ϵ. Using Deprit's method, the expression is slightly more complicated than using Hori's one.

2.3 Computational methods

2.3.1 Numerical approach

Today, our scientific studies are vastly supported by the aid of powerful and strong computational technology. Numerical simulations reveal to us new facts.

For example, in the field of celestial mechanics, experiments with numerical integrations have brought about a revolutionary change. Practically, the business of numerical ephemerides is prospering today. High accuracy numerical ephemerides (e.g. DE series by Standish/JPL) are widely distributed and utilized over the worldwide, taking the place of analytical ephemerides.

However, old-fashioned analytical ephemeris have advantages insofar as they:

- make it easy to understand each periodic contribution in the time-variation of orbital elements
- are quickly calculated
- do not depend on astronomic constants, such as mass of satellites/planets

In this work, we also handle numerically integrated results to check the accuracy of analytically derived results. Since this study focuses on the ephemeris of Outer (i.e. the motion of Outer for a short period), it is enough to consider for some centuries at most, not for the age of the Solar System.

Therefore, we adopt the extrapolation (Bulirsch-Stoer) integration code for numerical integrations, since it produces much more accurate results for short period problem.

We check these two results by calculating their residuals. Ideally, it is hoped that the residuals are zero for any given time, however, due to approximations by truncations of analytical expressions, or by round-off errors in numerical integrations, the residuals cannot be zero.

If residuals are not equal to zero, but small enough compared to a required accuracy, the divergences do not produce any problem. However, if they are beyond the expected accuracy, they create difficulties in terms of the accuracy of the results.

2.3.2 Machines and softwares

To accomplish this study, we utilize some powerful computational software.

- Mathematica (ver.4.0.2.0) copyrighted by Wolfram Research Inc.
- Fortran & C Package (ver.1.0) copyrighted by Fujitsu Kyushu System Engineering Ltd. (1999)

Mathematica is run on a Windows 2000 Operating System, and the Fortran compiler is operated on a Linux (Slackware 3.6) platform.

2.4 Checking accuracy (comparison with numerical integrations)

In an analytical approach, osculating elements are compounds of many periodic terms. When any time is given, the theory provides osculating elements. We calculate complicated arithmetic with the aid of a computational software, MATHEMATICA ver.4.

Astronomical constants, e.g. the masses of planets or satellites, are not determined from the theoretical study. It it necessary to combine the observational data with a theory to fix these constant values. Thereafter an analytical theory can be utilized as an ephemeris for the particular celestial bodies.

However, in this study, we do not aim to make an ephemeris peculiar to some celestial bodies, but we aim to construct a multipurpose analytical theory. Therefore, we do not give some numerical values for these constants.

The accuracy of ephemerides is assessed by comparing the results to observational data, i.e. calculating residuals of $O - C($ (observed) $-$ (calculated)). Observations are contaminated by noise, the constants are fit by methods of least squares.

In this work, we do not study for some specific celestial bodies, therefore we check the accuracy of our theory by comparing numerical integrations and calculating residuals of ((analyticals) $-$ (numericals)). We discuss the process in detail.

We assess the accuracy of our analytical expression through comparison with numerical results, or by calculating residuals in time sequence (See Figure 2.4). Numerical integration is performed by Bulirsch-Stoer ("extrapolation method") code in double-precision accuracy. This code provides high accuracy in results, suitable for our aim. We start integration with position and velocity values that are converted into Cartesian coordinates from a set of analytical

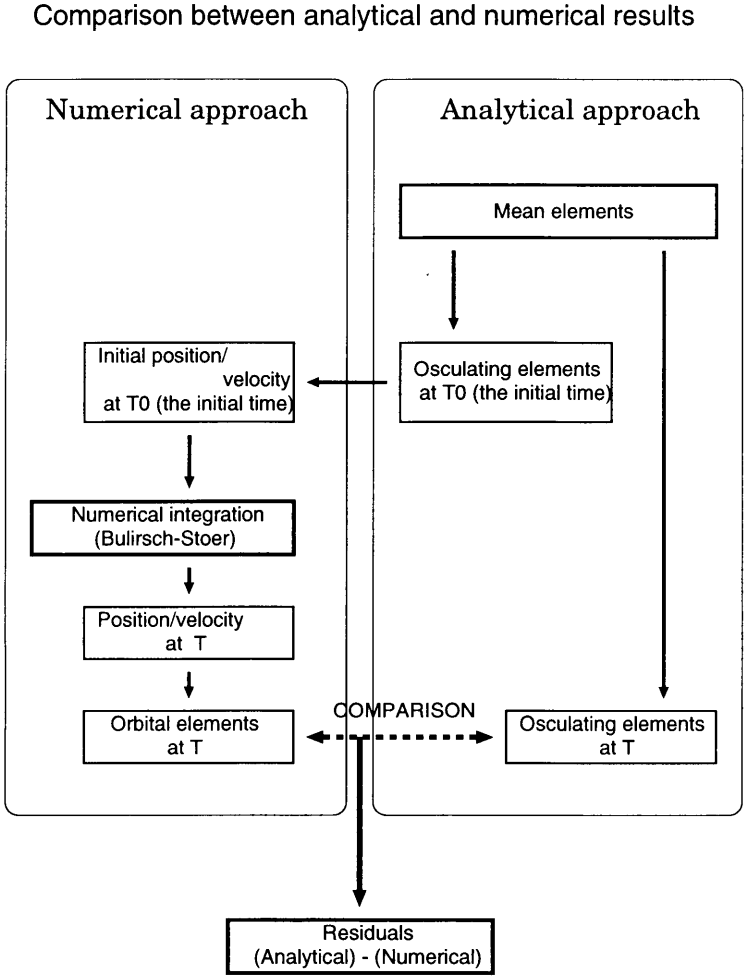

Figure 2.4: Flowchart for calculating residuals

Table 2.1: Mean elements for analytical calculation

Item	Inclined Problem	Planar Problem
Semimajor axis [Km]	5.5×10^6	5.5×10^6
Eccentricity	0.75	0.75
Inclination [deg]	132.40	-
Angular variable y_1 [deg]	0.0	0.0
Angular variable y_2 [deg]	0.0	0.0
Angular variable y_3 [deg]	0.0	-
Longitude of the Inner $\lambda_{In}[deg]$	0.0	0.0

osculating elements at the initial time. Then, at a time T, residuals (analytical results minus numerically integrated ones) are calculated as:

$$\text{(Residuals)} = \text{(Analytical results)} - \text{(Numerical results)}.$$

When we calculate residuals in angular variables, y_1, y_2 and y_3, secular trends (the slopes of regression line for raw data) are subtracted, not to hide fine structures in residuals for output figures.

We set the values in Table 2.1 for the mean elements in analytical calculations.

Chapter 3

Planar Restricted Problem

3.1 Preparations for solving the problem

In this section, we simplify the problem in a coplanar configuration, already mentioned in Chapter 2. The system has two degrees of freedom: angular variables corresponding to them are $y_1(=l)$ and $y_2(=g+h-\lambda_{Tri})$. Therefore, the outer body suffers periodic disturbances with the periodicities of the revolutions of y_1 and y_2.

Hereafter, we decompose perturbations into three parts according to their periodicities. They are:

- Short periodic perturbation caused by the revolution of the inner body (in Neptunian system case, the periodicity is $\sim$ 6 days)
- Long periodic perturbation caused by the revolution of the outer body (in Neptunian system case, the periodicity is $\sim$ 1 year)
- Secular perturbation .

Removal of each periodic contribution from the Hamiltonian means decreasing degrees of freedom of the Hamiltonian, and finally we can integrate equations of motion analytically. A briefly summarized flowchart is seen in Figure 3.1.

In this chapter, for the sake of brevity, we mainly follow equations only up to P_2 term of Legendre polynomial in the perturbed Hamiltonian. The following discussion can be applied when higher terms of P_i are included in the Hamiltonian.

3.1.1 Short periodic perturbation: Elimination of short periodic terms

First, we take a time-averaged Hamiltonian over the short periodic variable, y_2. Through this manipulation, we can obtain a new Hamiltonian, $F^*(y_1, x_1)$, which only contains one angular variable, y_1.

We consider a canonical transformation

$$F(y_1, y_2, x_1, x_2) \longrightarrow F^*(y_1, x_1)$$

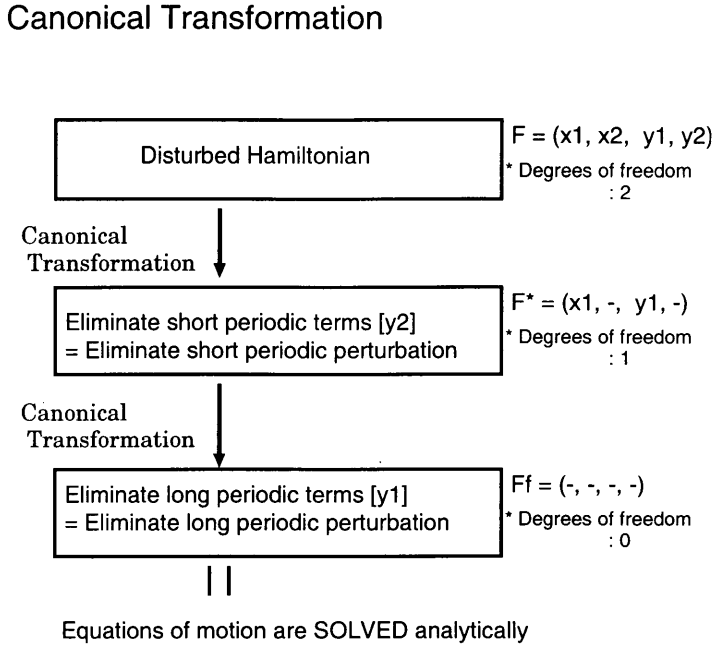

Figure 3.1: Flow chart of canonical transformations in the planar problem

such that

$$\begin{aligned} \frac{dx^*}{dt^*} &= \frac{\partial F_0}{\partial y^*} \\ \frac{dy^*}{dt^*} &= -\frac{\partial F_0}{\partial x^*}, \end{aligned}$$

where F_0 is taken as the unperturbed Hamiltonian.

From the second equation above, a fictitious time increment dt^* is replaced by an angular variable dy^*

$$dt^* = \frac{dy_2^*}{(-\frac{\partial F_0}{\partial x_2^*})} = \frac{dy_2^*}{(-n_{Tri})},$$

since F_0 only depends on x_2.

The original Hamiltonian (before transformation) is written as:

$$F = F_0 + F_1 + F_2$$

where,

$$\begin{aligned} F_0 &= n_{Tri} x_2 \\ F_1 &= \frac{\mu}{2a} \\ F_2 &= \mu \frac{M m_{Tri}}{(M + m_{Tri})^2} \frac{a^3}{r^3} \frac{a_{Tri}^2}{a^3} \frac{1}{4} (3\cos(2(f + y_2)) + 1). \end{aligned}$$

Subscripts are approximate orders of a small parameter $\frac{n}{n_{Tri}}$, the ratio of mean motions of the outer body to the inner one. In the Neptunian system, the value is $\sim \frac{1}{60}$.

However, a mass coefficient $\frac{m}{M+m_{Tri}}$ can act as a more efficient, small parameter. For example, in the case of Neptunian system, the value is $\sim 2 \times 10^{-4}$,

In fact, in the case of extrasolar planetary systems, it is possible to take various values. However, if we consider a typical one such that: a sun-like primary (for the F,G,K main sequence star, its mass is $\sim 1[M_\odot]$) with a brown dwarf companion (the upper limit of mass is $\sim 0.08[M_\odot]$) in neighbor and a planet revolving $> 1[AU]$ apart from the primary. For extra-solar systems, which satisfy these conditions, the mass coefficient $\frac{m}{M+m_{Tri}}$ can be regarded as an infinitesimal parameter.

Therefore, in the following discussion, we neglect $(\frac{m}{M+m_{Tri}})^2$ or higher order terms. Note that we continue to use subscripts for a small parameter $\frac{n}{n_{Tri}}$, but we sometimes truncate Poisson series by orders of $(\frac{m}{M+m_{Tri}})^1$.

We apply Hori's canonical perturbation method to F, a new Hamiltonian $F^* = \sum_i F_i^*$ and a generating function $S = \sum_i S_i$:

$$
\begin{aligned}
F_0^* &= F_0(\text{UNPERTURBED}) \\
F_1^* &= [F_1]_{sec} \\
&= \frac{\mu^2}{2x_1^2} \\
S_1 &= \int [F_1]_{per} dt^* \\
&= 0 \\
F_2^* &= [\{F_1, S_1\} + F_2]_{sec} \\
&= \frac{1}{4}\mu \frac{M m_{Tri}}{(M+m_{Tri})^2} \frac{a^3}{r^3} \frac{a_{Tri}^2}{a^3} \\
S_2 &= \int [\{F_1, S_1\} + F_2]_{per} dt^* \\
&= -\frac{3}{8} \frac{\mu}{n_{Tri}} \frac{M m_{Tri}}{(M+m_{Tri})^2} \frac{a^3}{r^3} \frac{a_{Tri}^2}{a^3} \sin 2(f+y_2) \\
F_3^* &= [\{F_1, S_2\}]_{sec} \\
&= 0 \\
S_3 &= \int [\{F_1, S_2\}]_{per} dt^* \\
F_4^* &= [\{F_1, S_3\}]_{sec} + O((\frac{m}{M+m_{Tri}})^2) \\
&= 0 \\
\cdots &= \cdots \\
F_i^* &= [\{F_1, S_{i-1}\}]_{sec} + O((\frac{m}{M+m_{Tri}})^2) \\
S_i &= \int [\{F_1, S_{i-1}\}]_{per} dt^* + O((\frac{m}{M+m_{Tri}})^2) \\
\cdots &= \cdots
\end{aligned}
$$

Here, $\{X, Y\}$ is an operation of Poisson bracket of X and Y. A conventional definition in the

field of celestial mechanics, the Hamiltonian sign is usually reversed. Therefore,

$$\{X, Y\} \equiv \sum_i \left[\frac{\partial X}{\partial x_i} \frac{\partial Y}{\partial y_i} - \frac{\partial X}{\partial y_i} \frac{\partial Y}{\partial x_i} \right].$$

An infinitesimal increment of time dt^* in indefinite integrals $\int \Box dt^*$ can be replaced by an angular variable, y_2, since F_0 depends only on x_2.

$$\begin{aligned} \int Q dt^* &= \int Q \frac{1}{(-\frac{\partial F_0}{\partial x_2^*})} dy_2^* \\ &= \int Q \frac{1}{-n_{Tri}} dy_2^* \end{aligned}$$

3.1.2 Long periodic perturbation: Elimination of long periodic terms

Next, we eliminate a long periodic angular variable y_1. After a canonical transformation, we can eliminate all of the angular variables y_i of the Hamiltonian expression, which means the problem is solved analytically, and equations of motion (canonical equations) are integrable.

A canonical transformation

$$F^*(y_1, x_1) \longrightarrow F^{**}$$

is defined by :

$$\begin{aligned} \frac{dx^{**}}{dt^{**}} &= \frac{\partial F_1^*}{\partial y^{**}} \\ \frac{dy^{**}}{dt^{**}} &= -\frac{\partial F_1^*}{\partial x^{**}}. \end{aligned}$$

A time increment dt^{**} is replaced by y_1^{**}:

$$dt^{**} = \frac{dy_1^{**}}{(-\frac{\partial F_1^*}{\partial x_1^{**}})} = \frac{1}{n} dy_1^{**},$$

since F_1 only depends on x_1.

The Hamiltonian (before transformation) is :

$$F^* = F_0^* + F_1^* + F_2^*$$

where,

$$\begin{aligned} F_0^* &= F_0 \\ F_1^* &= \frac{\mu^2}{2x_1^2} \\ F_2^* &= \frac{1}{4}\mu \frac{M m_{Tri}}{(M + m_{Tri})^2} \frac{a^3}{r^3} \frac{a_{Tri}^2}{a^3}. \end{aligned}$$

Hori's canonical perturbation method is applied to this Hamiltonian, neglecting $O((\frac{m}{M+m_{Tri}})^2)$, we obtain a new Hamiltonan $F^{**} = \sum_i F_i^{**}$ and a generating function $S^* = \sum_i S_i^*$:

$$\begin{aligned}
F_0^{**} &= F_0^* \\
F_1^{**} &= F_1^*(\text{UNPERTURBED}) \\
F_2^{**} &= [F_2^*]_{sec} \\
&= \frac{1}{4}\mu \frac{M m_{Tri}}{(M+m_{Tri})^2} \frac{1}{\eta^3} \frac{a_{Tri}^2}{a^3} \\
S_1^* &= \int [F_2^*]_{per}\, dt^{**} \\
&= \frac{1}{4}\mu \frac{M m_{Tri}}{(M+m_{Tri})^2} \frac{1}{n\eta^3} \frac{a_{Tri}^2}{a^3} (f + e\sin f - y_1) \\
F_3^{**} &= [\{F_2^*, S_1^*\}]_{sec} \\
&= O((\frac{m}{M+m_{Tri}})^2) \\
S_2^* &= \int [\{F_2^*, S_1^*\}]_{per}\, dt^{**} \\
&= O((\frac{m}{M+m_{Tri}})^2) \\
\cdots &= \cdots
\end{aligned}$$

Here, an indefinite integral with t^{**} is replaced by

$$\begin{aligned}
\int Q dt^{**} &= \int Q \frac{1}{(-\frac{\partial F_1^*}{\partial x_1^{**}})} dy_1^{**} \\
&= \int Q \frac{1}{n} dy_1^{**}.
\end{aligned}$$

3.1.3 Secular perturbation

We have obtained a Hamiltonian F^{**} which does not depend on any angular variables. To summarize again, it forms :

$$F^{**} = F_0^{**} + F_1^{**} + F_2^{**}$$

where,

$$\begin{aligned}
F_0^{**} &= F_0^* \\
F_1^{**} &= F_1^* \\
F_2^{**} &= \frac{1}{4}\mu \frac{M m_{Tri}}{(M+m_{Tri})^2} \frac{1}{\eta^3} \frac{a_{Tri}^2}{a^3}.
\end{aligned}$$

This Hamiltonian also satisfies canonical equations, i.e.:

$$\begin{aligned}
\frac{dx^{**}}{dt} &= \frac{\partial F^{**}}{\partial y^{**}} (\equiv 0) \\
\frac{dy^{**}}{dt} &= -\frac{\partial F^{**}}{\partial x^{**}}
\end{aligned}$$

From the first equation, we obtain

$$x^{**} = const.,$$

and from the second one,

$$y^{**} = (-\frac{\partial F^{**}}{\partial x^{**}})t + const..$$

If we calculate real values of $\frac{\partial F^{**}}{\partial x^{**}}$,

$$\begin{aligned}
\frac{\partial F^{**}}{\partial x_1^{**}} &= -\frac{\mu^2}{x_1^3} - \frac{3}{4}\mu\frac{Mm_{Tri}}{(M+m_{Tri})^2}\frac{a_{Tri}^2}{na^5\eta^3} \\
&= -n - \frac{3}{4}\frac{n}{a^2}\frac{Mm_{Tri}}{(M+m_{Tri})^2}\frac{a_{Tri}^2}{\eta^3} \\
\frac{\partial F^{**}}{\partial x_2^{**}} &= n_{Tri} - \frac{3}{4}\mu\frac{Mm_{Tri}}{(M+m_{Tri})^2}\frac{a_{Tri}^2}{na^5\eta^4} \\
&= n_{Tri} - \frac{3}{4}\frac{n}{a^2}\frac{Mm_{Tri}}{(M+m_{Tri})^2}\frac{a_{Tri}^2}{\eta^4}
\end{aligned}$$

and substitute values into them,

$$\begin{aligned}
y_1^{**} &= (-\frac{\partial F^{**}}{\partial x_1^{**}})t + const. \\
y_2^{**} &= (-\frac{\partial F^{**}}{\partial x_2^{**}})t + const..
\end{aligned}$$

In other words, action variables x^{**} are constants, and angular variables y^{**} increase (or decrease) linearly with time t. This means the action variables, or a semimajor axis a^{**} and an eccentricity e^{**}, does not have secular trends, while the angular variables, or a mean anomaly l^{**} and a longitude of perihelion ϖ^{**}, have secular trends linearly with time.

3.1.4 Mean elements

Orbital elements $a^{**}, e^{**}, l^{**}, \varpi^{**}$ deduced from x^{**} and y^{**} are mean orbital elements.

Their real values are not obtained from dynamical theories, which only indicates that these values are constants. We have to merge results of astrometrical positions to get real numerical values for Nereid.

In this study, we do not identify numerical values for them because they do not affect the construction of an analytical theory.

3.1.5 Deriving osculating elements

Osculating elements E for canonical variables can be summed up by the following contributions:

- Mean elements E^{**}
- Contribution from long periodic perturbation δE^{*}
- Contribution from short periodic perturbation δE .

I.e., we first calculate

$$E^* = E^{**} + \delta E^*,$$

and after that, we evaluate

$$E = E^* + \delta E.$$

When we obtain a quantity of E^*, we have to evaluate δE^* with values of E^{**}. Similarly, a value E is calculated with E^* on the right hand side of the above equation.

From the relationship between old and new variables of Hori's canonical perturbation method (see Ch. 2), δE^* and δE are expressed as:

$$\begin{aligned} \delta E^* &= \{E^*, S^*\} + \frac{1}{2}\{\{E^*, S^*\}, S^*\} + \dots \\ \delta E &= \{E, S\} + \frac{1}{2}\{\{E, S\}, S\} + \dots . \end{aligned}$$

If we neglect $O((\frac{m}{M+m_{Tri}})^2)$ terms, all we have to do is take the Poisson bracket once, then,

$$\begin{aligned} \delta E^* &= \{E^*, S^*\} \\ \delta E &= \{E, S\}, \end{aligned}$$

since S or S^* contains at least a factor of $(\frac{m}{M+m_{Tri}})^1$. They are equivalent to the following operations.

$$\begin{aligned} \delta x_i^* &= \{x_i^*, S^*\} = \frac{\partial S^*}{\partial y_i^*} \\ \delta y_i^* &= \{y_i^*, S^*\} = -\frac{\partial S^*}{\partial x_i^*} \\ \delta x_i &= \{x_i, S\} = \frac{\partial S}{\partial y_i} \\ \delta y_i &= \{y_i, S\} = -\frac{\partial S}{\partial x_i} \end{aligned}$$

Deriving osculating elements expressed in orbital elements, we can use variational equations between orbital elements and canonical ones:

$$\begin{aligned} \delta a &= \frac{2x_1}{\mu}\delta x_1 \\ \delta e &= -\frac{1}{e}\left[\frac{x_2}{(x_1)^2}\delta x_2 - \frac{(x_2)^2}{(x_1)^3}\delta x_1\right] \\ \delta l &= \delta y_1 \\ \delta \varpi &= \delta y_2. \end{aligned}$$

The last equation is derived from $\delta\varpi = \delta y_2 + \delta k$ and k has no effect on the Nereid's motion since $k \equiv n_{Tri}t + const.$ is supposed.

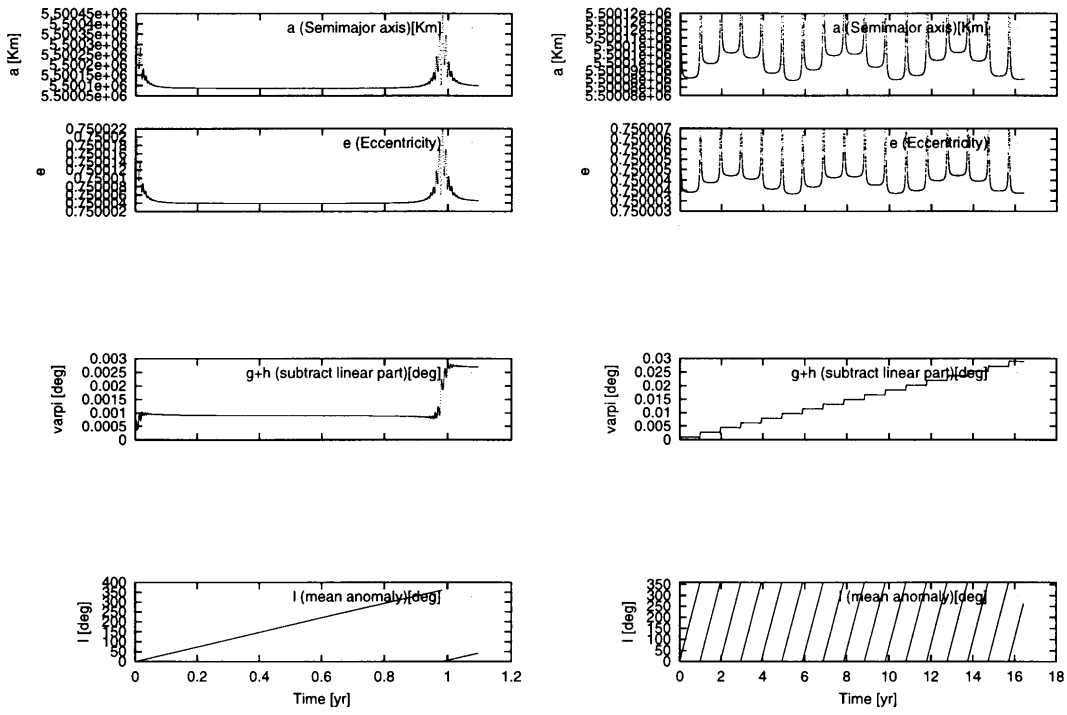

(a) (b)Trimmed for the vertical axis and zoomed up offsets

Figure 3.2: Numerical results (a)for one year (b)for 15 years (Note: for panel (b), the vertical axis is trimmed to reveal offsets in semimajor axis and eccentricity). The initial values for this calculation use the mean elements instead of the initial osculating elements generated by an analytical theory. Secular trends of residuals in angular variables are subtracted.

Table 3.1: Preliminary analytical models

Model Name	Hamiltonian expression (P_i of Legendre polynomials are considered)	Generating Function (S_i for short periodic terms are considered)	Direction of Triton's revolution
P2S2p	P_2	S_2	Prograde
P2S4p	P_2	S_2, S_3, S_4	Prograde
P3S2p	P_2, P_3	S_2	Prograde
P3S2r	P_2, P_3	S_2	Retrograde

3.2 Results and discussion

3.2.1 Numerical results

Figure 3.2 shows numerical results for one year and 15 years (Only these two calculations start with initial conditions of mean elements, rather than osculating elements). In semimajor axis and eccentricity, they exhibit many rapid-changing variations with a period of six days, superposed on eminent bowl-shaped variations with a period of one-year. Amplitudes of the former variations grow larger with Nereid's approaching its pericenter.

It is noted that the bottom level of the latter variations is offset slightly to one of the next revolutional periods. This phenomenon is caused by the phase of Neptune-Triton system against its barycenter when the Nereid passes through its pericenter. The pericentric distance of Nereid is $\sim 1.4 \times 10^6$ [Km] from the barycenter, which is only four times that of the Triton's distance from the barycenter. In a planar problem, a configuration of close approach occurs, which often creates difficulties in building accurate ephemerides.

3.2.2 Preliminary analytical results and residuals

We calculated residuals preliminarily, and they are shown in Figures 3.3 and 3.4. The analytical models we used are listed in Table 3.1.

To summarize, there exist large discrepancies between analytical results and numerical ones. If we take up to smaller quantities (e.g. up to higher small parameter of generating functions or up to higher Legendre polynomials) into consideration in the analytical calculation, discrepancies become small, but unpleasantly, large residuals still remaine.

Comparing the two models, with Triton orbits either in prograde or retrograde, we can see significant differences in residuals (see Figure 3.4). A retrograde model decreases its residuals drastically.

Hereafter, we use mainly prograde orbiting models. If we consider retrograde orbiting ones, residuals are smaller than those of the prograde models.

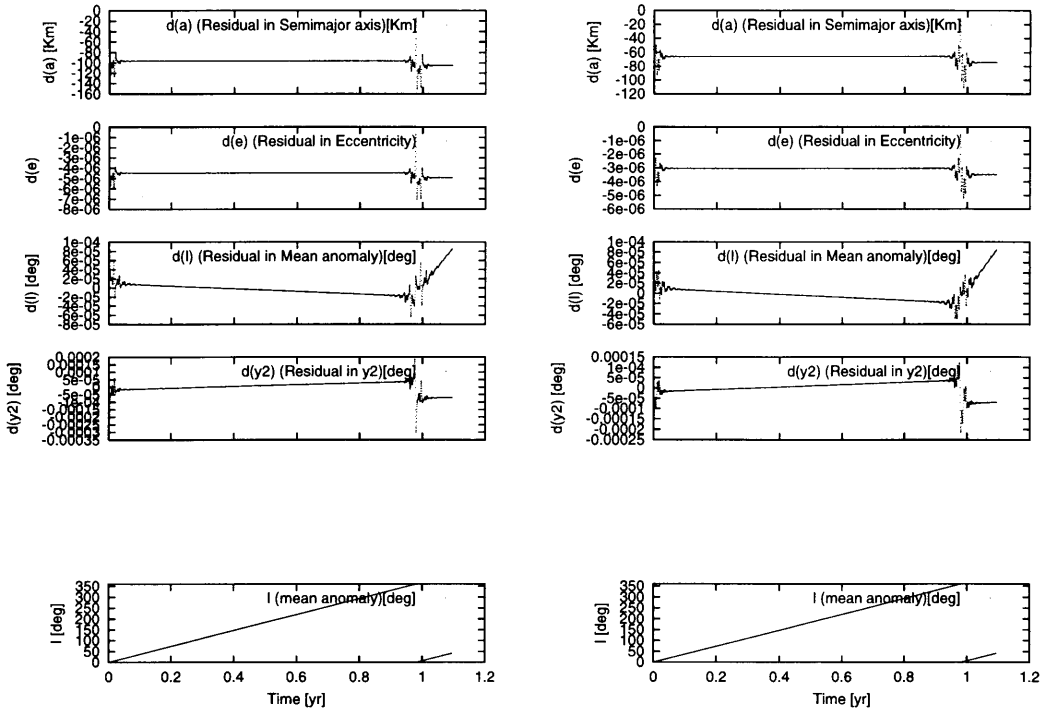

Figure 3.3: Preliminary results. Residuals are shown for each model. (a)model P2S2p, (b)model P2S4p

3.2.3 Influence on residuals of truncation of Legendre polynomials

If we consider the problem fully, we have to deal with a full expression of the Hamiltonian, i.e. infinite series of Legendre polynomials. However, we simplify the Hamiltonian for convenience, which may cause discrepancies between analytical and numerical results. To check the influence of truncation of Legendre polynomials,

(Full numerical results) − (Numerical results including up to P_i Legendre polynomials)

are calculated. The direction of Triton's revolution is prograde.

The full numerical calculation considers forces on Nereid from circular-orbiting Neptune and Triton, while a numerical calculation with truncated Legendre polynomials considers the model such that:

- a perturbing function is formulated into Cartesian coordinates. A P_2 potential is taken as an example:

$$\begin{aligned} F(P_2) &= \mu \frac{M m_{Tri}}{(M+m_{Tri})^2} \frac{r_{Tri}^2}{r^3} \frac{1}{2}(3\cos^2 S - 1) \\ &= \frac{1}{2}\mu \frac{M m_{Tri}}{(M+m_{Tri})^2} \left[\frac{3}{r^5}(\boldsymbol{r}\cdot\boldsymbol{r}_{Tri})^2 - \frac{r_{Tri}^2}{r^3} \right], \end{aligned}$$

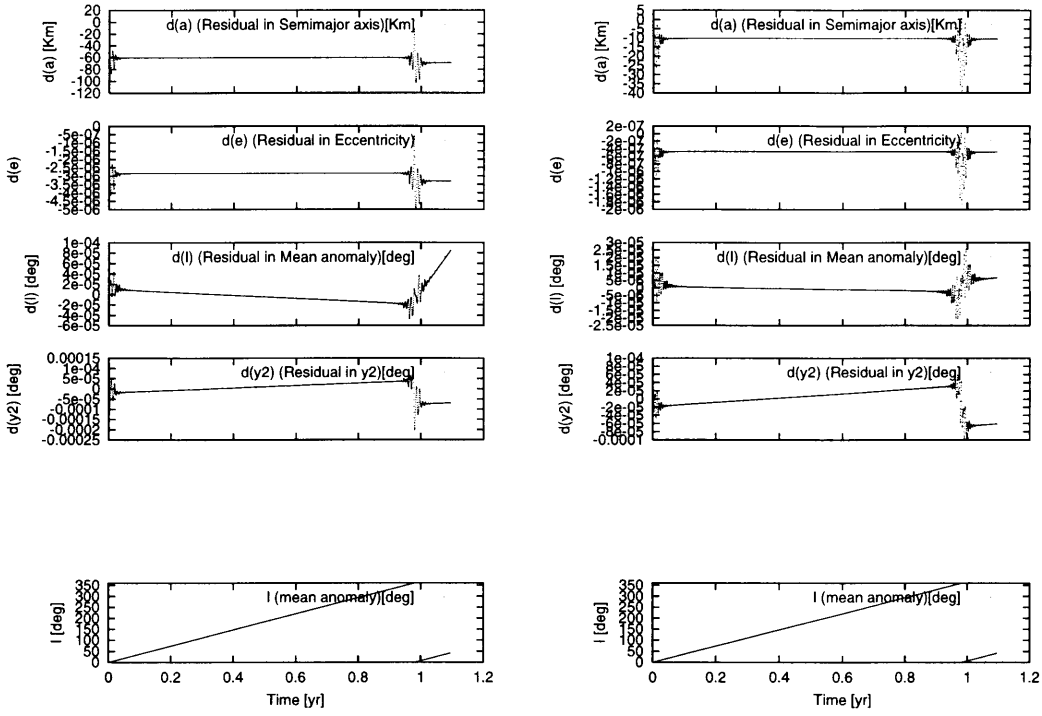

Figure 3.4: Preliminary results (continued). Residuals are shown for each model. (a)model P3S2p, (b)model P3S2r

where $(A \cdot B)$ is an operation of the inner product for A and B.

- acceleration is calculated through differentiating the potential.

These results are shown in Figure 3.5. If we expect to achieve accuracy of sub-Km in the semimajor axis (in the case of Triton revolving in prograde), we have to take terms up to P_5 in the Hamiltonian into account.

3.2.4 Influence on residuals of truncation of generating functions

Next, we assess the influence of truncational errors of short periodic generating functions S_i. The full expression of the short periodic generating function is

$$S = \sum_{i}^{\infty} S_i.$$

To check the contribution from truncational effects, we introduce a Hamiltonian, which includes only the P_n term of Legendre polynomial, for both numerical and analytical calculations. I.e.,

$$\left(\begin{array}{l} \text{Numerical results} \\ \text{including only } P_n \end{array} \right) - \left(\begin{array}{l} \text{Analytical results including only } P_n \text{ and} \\ \text{up to } S_i \text{ of generating functions for short periodic} \end{array} \right).$$

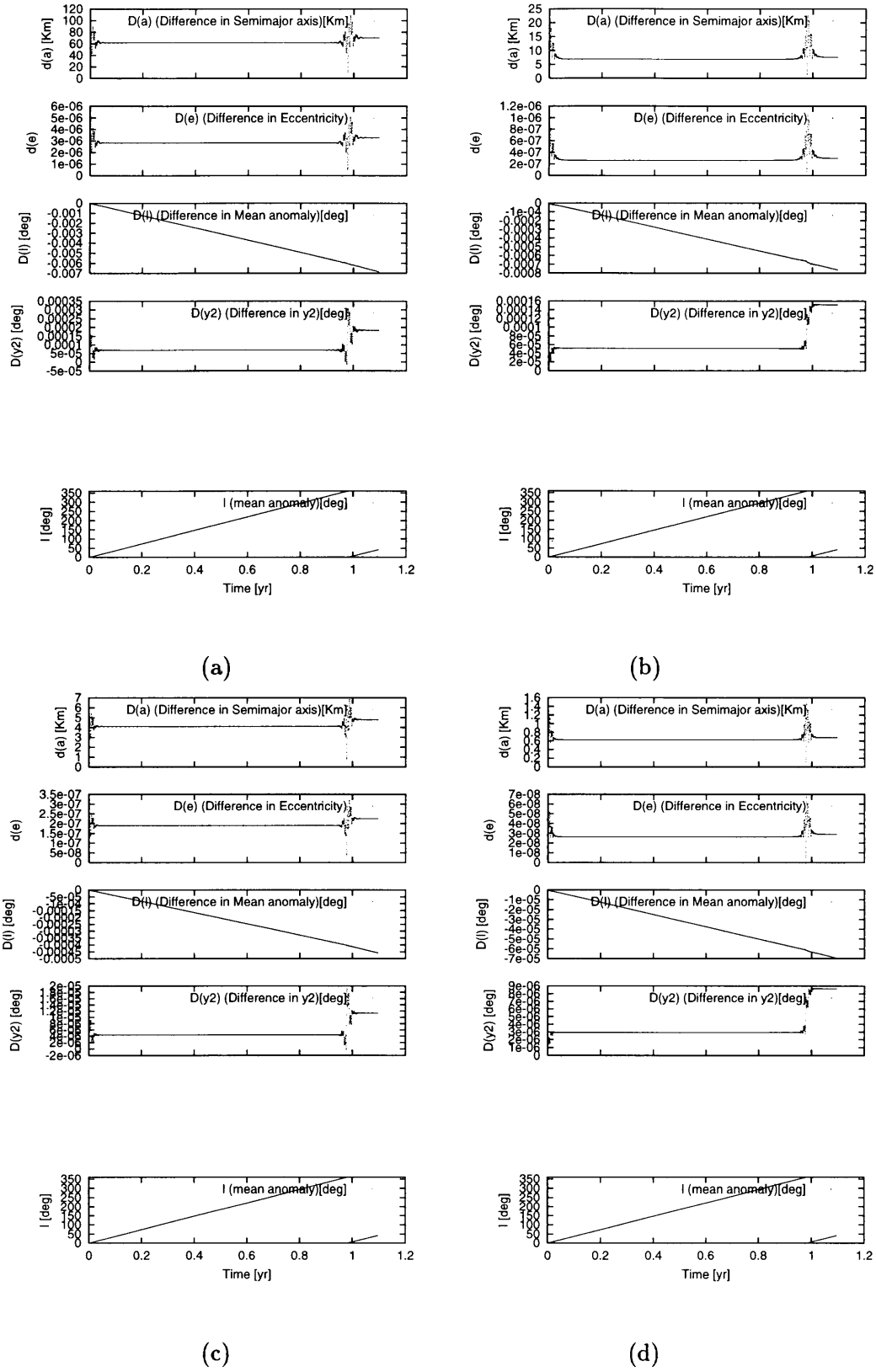

Figure 3.5: Residuals of full numerical results minus numerical results up to Legendre P_i terms in the Hamiltonian. (a)up to P_2 term, (b)up to P_3 terms, (c)up to P_4 terms, (d)up to P_5 terms

In this calculation, Triton revolution is prograde.

Results are in Figures 3.6 and 3.7. In the case of P_2-limited problem, residuals are converged below sub-Km in the semimajor axis when we take up to S_7 terms of a generating function into account. This means that it must include higher orders of a small parameter, $\frac{n}{n_{Tri}}$, in calculations. This slow-converging property is reflected from the character of closely approaching problems. Since S_i is calculated as (neglecting $(\frac{m}{M+m_{Tri}})^2$):

$$\begin{aligned} S_i &= \int \{F_1, S_{i-1}\} dt^* \\ &= -\frac{n}{n_{Tri}} \int \frac{\partial S_{i-1}}{\partial y_1} dy_2, \end{aligned}$$

however $\frac{\partial S_{i-1}}{\partial y_1}$ are converted into

$$\frac{\partial S_{i-1}}{\partial y_1} = \frac{\partial f}{\partial y_1} \frac{\partial S_{i-1}}{\partial f},$$

a term

$$\begin{aligned} \frac{\partial f}{\partial y_1} &= \frac{(1+e\cos f)^2}{\eta^3} \\ &\sim 10.583 \text{(at the pericenter)} \end{aligned}$$

dilutes the converging factor of $\frac{n}{n_{Tri}} \sim \frac{1}{60}$ and prevents series of S_i from rapidly converging.

Moreover, in the case of the P_3-limited problem, another phenomenon troubles us. This is shown in Figure 3.8. Eminent offsets on the bottom level in semimajor axis or eccentricity are shown for each revolution of Nereid. These offsets caused by the longitude of Triton when Nereid passes through its pericenter are discussed in the section on Numerical results. The offsets observed in the P_3-limited problem and the P_5-limited one are nearly comparable to the offset in numerical results, which means the offsets for each revolution of Nereid are mainly explained by contributions of P_3 and P_5 terms of Legendre polynomials in the Hamiltonian.

If Triton orbits in retrograde, residuals are decreased.

In any case, eminent discrepancies between analytical and numerical results when Nereid approaches its pericenter are observed, especially in low degrees of S_i. This phenomenon seems to be caused by (1)a slowly varying frequency with time near the pericenter, and (2)approximations in trigonometic functions of an offset function .

Near the point of close approach of Nereid with Neptune (or Triton), the synodic period between them is continuously varying, which means a time-variation profile of orbital elements cannot be described using a single frequency of trigonometric series. A compound expression of trigonometric functions with many frequencies is required.

In fact, shown in Figures, time-series profiles of residuals are more simple and smoother when we take higher S_is into account. These are shown in the Appendix; the number of trigonometric terms are increasing for higher S_is.

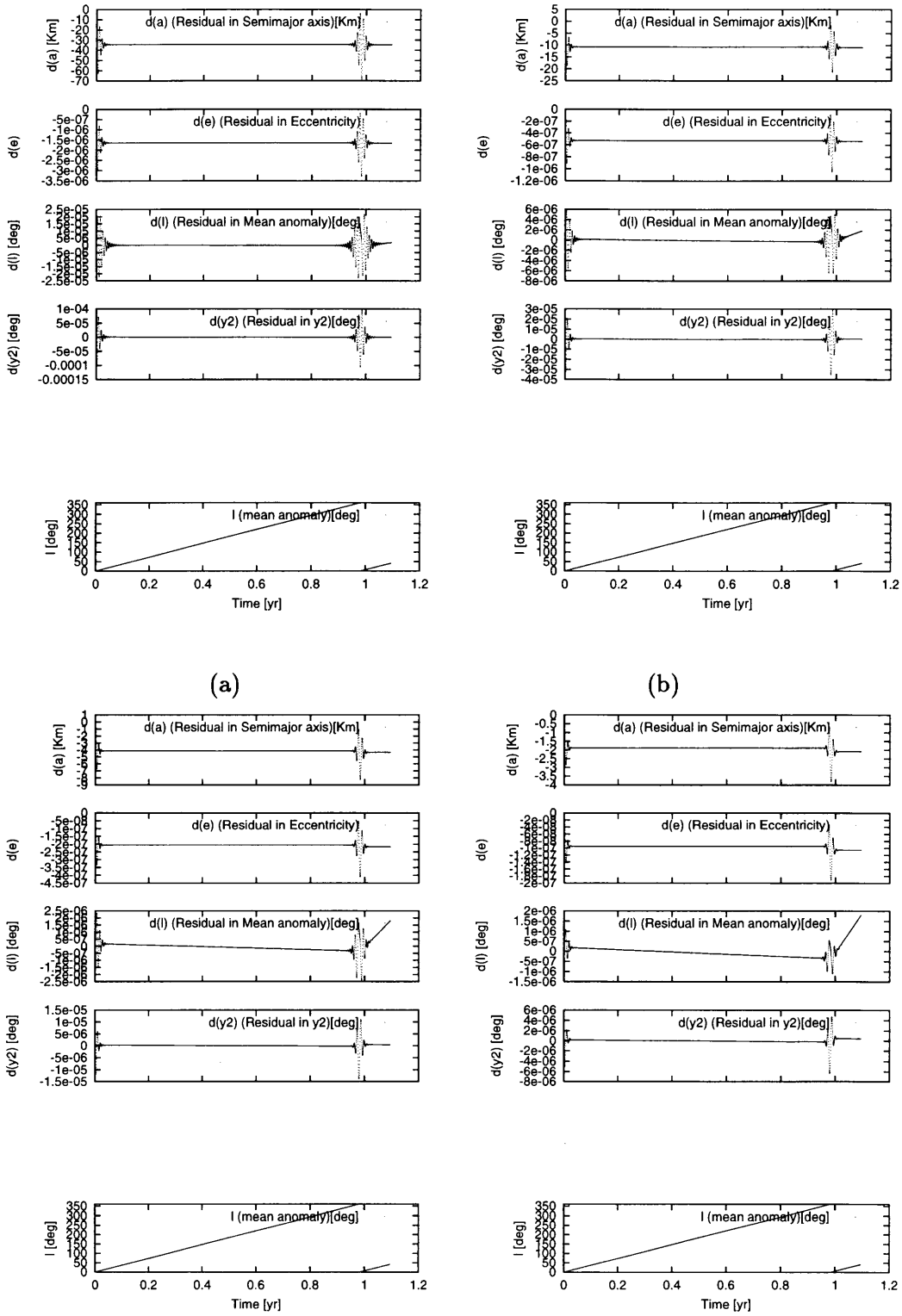

Figure 3.6: Residuals of numerical results minus truncated S_i results for a Hamiltonian limited only by Legendre P_2 contribution. Secular trends of residuals in angular variables are subtracted. (a)up to S_2 terms, (b)up to S_3 terms, (c)up to S_4 terms, (d)up to S_5 terms

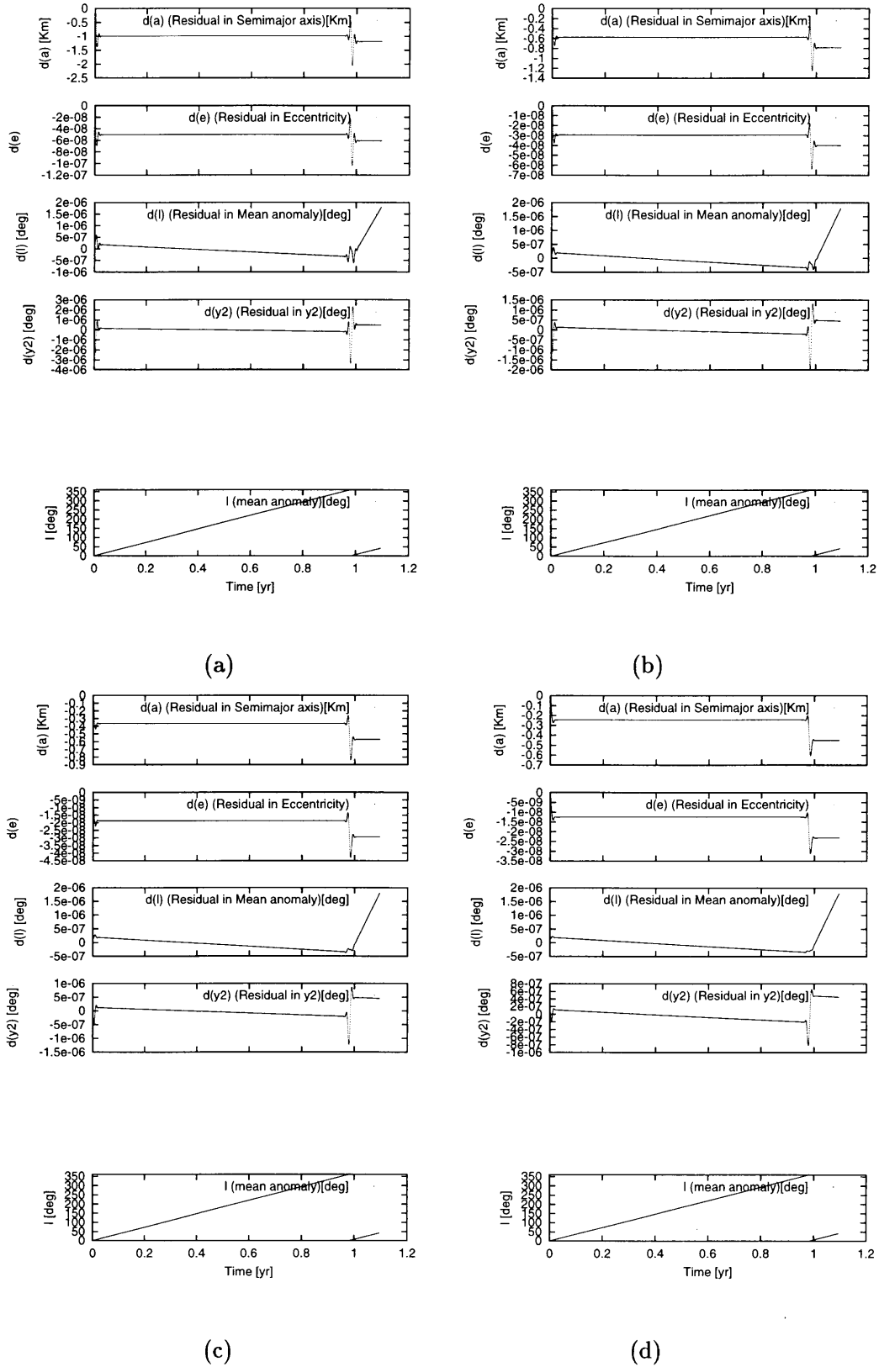

Figure 3.7: Residuals of numerical results minus truncated S_i results for a Hamiltonian limited only by Legendre P_2 contribution (continued). Secular trends of residuals in angular variables are subtracted. (a)up to S_6 terms, (b)up to S_7 terms, (c)up to S_8 terms, (d)up to S_9 terms

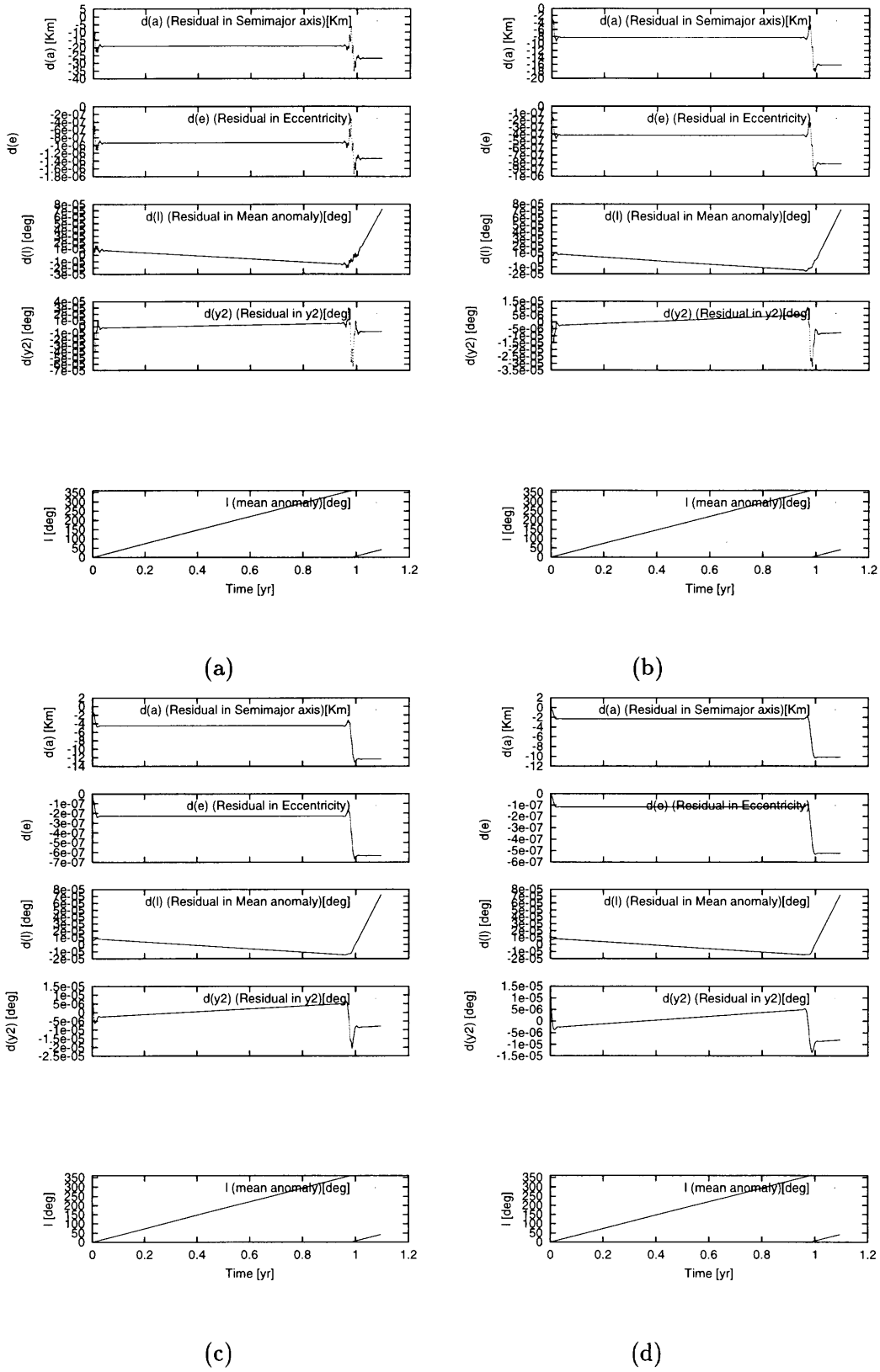

Figure 3.8: Residuals of numerical results minus truncated S_i results for a Hamiltonian limited only by Legendre P_3 contribution. Secular trends of residuals in angular variables are subtracted. (a)up to S_2 terms, (b)up to S_3 terms, (c)up to S_4 terms, (d)up to S_5 terms

Chapter 4

Inclined Restricted Problem

4.1 Preparations for solving the problem

In this section, we discuss the inclined problem, applicable to any mutual inclinations of the orbital planes of the inner and outer bodies. The system has three degrees of freedom; angular variables corresponding to these are $y_1(=l), y_2(=g)$ and $y_3(=h-\lambda_{Tri})$.

Hereafter, as we did in the planar problem (Chap.3), we break down perturbations into four parts according to their periodicities. They are:

- Short periodic perturbation caused by the revolution of the inner body (in the Neptunian system, the periodicity is $\sim$ 6 days)
- Intermediate periodic perturbation caused by the revolution of the outer body (in the Neptunian system, the periodicity is $\sim$ 1 year)
- Long periodic perturbation caused by the circulation of the pericenter of the outer body (in the Neptunian system, the periodicity is of order $\sim 10^5$ year)
- Secular perturbation .

A summarized flowchart of the process is in Figure 4.1.

In this chapter, we mainly describe the equations for the perturbed Hamiltonian only up to P_2 terms of Legendre polynomials for the short or intermediate periodic perturbations, and up to P_6 terms for the long periodic ones.

4.1.1 Short periodic perturbation: Elimination of short periodic terms

We average the Hamiltonian over the short periodic variable, y_3 and decrease the number of degrees of freedom by one. The Hamiltonian is transformed into:

$$F(y_1, y_2, y_3, x_1, x_2, x_3) \longrightarrow F^*(y_1, y_2, x_1, x_2)$$

such that

$$\begin{aligned} \frac{dx^*}{dt^*} &= \frac{\partial F_0}{\partial y^*} \\ \frac{dy^*}{dt^*} &= -\frac{\partial F_0}{\partial x^*}, \end{aligned}$$

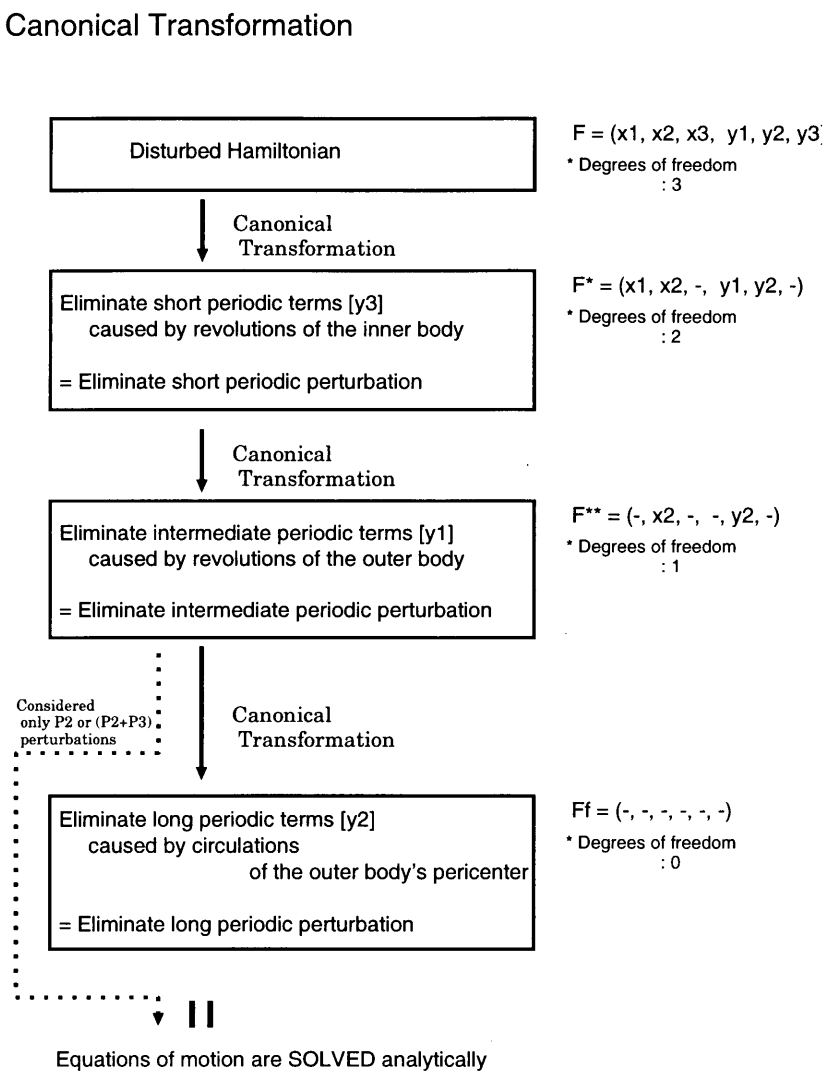

Figure 4.1: Flow chart of canonical transformations in the inclined problem

where F_0 is unperturbed. An artificial time increment dt^* is replaced by an angular variable dy^*

$$dt^* = \frac{dy_3^*}{(-\frac{\partial F_0}{\partial x_3^*})} = \frac{dy_3^*}{(-n_{Tri})},$$

since F_0 only depends on x_3.

The original Hamiltonian (before transformation) is written as:

$$F = F_0 + F_1 + F_2$$

where,

$$\begin{aligned}
F_0 &= n_{Tri}x_3 \\
F_1 &= \frac{\mu}{2a} \\
F_2 &= \mu\frac{Mm_{Tri}}{(M+m_{Tri})^2}\frac{a^3}{r^3}\frac{a_{Tri}^2}{a^3}\left[\frac{1}{8}(-1+3\theta^2)\right. \\
&\qquad +\frac{3}{8}(1-\theta^2)\cos(2f+2y_2) \\
&\qquad +\frac{3}{16}(1-\theta)^2\cos(2f+2y_2-2y_3) \\
&\qquad +\frac{3}{8}(1-\theta^2)\cos(2y_3) \\
&\qquad \left.+\frac{3}{16}(1+\theta)^2\cos(2f+2y_2+2y_3)\right],
\end{aligned}$$

and

$$\theta \equiv \cos I.$$

As we have seen in Chap. 3, subscripts are approximate orders of a small parameter $\frac{n}{n_{Tri}}$, and from here on, the expressions are neglected $(\frac{m}{M+m_{Tri}})^2$ or higher order terms.

A new Hamiltonian $F^* = \sum_i F_i^*$ and a generating function $S = \sum_i S_i$ are:

$$\begin{aligned}
F_0^* &= F_0(\text{UNPERTURBED}) \\
F_1^* &= [F_1]_{sec} \\
&= \frac{\mu^2}{2x_1^2} \\
S_1 &= \int [F_1]_{per}\, dt^* \\
&= 0 \\
F_2^* &= [\{F_1, S_1\} + F_2]_{sec} \\
&= \frac{1}{8}\mu\frac{Mm_{Tri}}{(M+m_{Tri})^2}\frac{a^3}{r^3}\frac{a_{Tri}^2}{a^3}\left[(-1+3\theta^2)+3(1-\theta^2)\cos(2f+2y_2)\right] \\
S_2 &= \int [\{F_1, S_1\} + F_2]_{per}\, dt^* \\
&= -\frac{\mu}{n_{Tri}}\frac{Mm_{Tri}}{(M+m_{Tri})^2}\frac{a^3}{r^3}\frac{a_{Tri}^2}{a^3}\left[-\frac{3}{32}(1-\theta)^2\sin(2f+2y_2-2y_3)\right. \\
&\qquad \left.+\frac{3}{16}(1-\theta^2)\sin(2y_3)\right.
\end{aligned}$$

$$+\frac{3}{32}(1+\theta)^2\sin(2f+2y_2+2y_3)\Big]$$

$$\begin{aligned}
F_3^* &= [\{F_1, S_2\}]_{sec} \\
&= 0 \\
S_3 &= \int [\{F_1, S_2\}]_{per} dt^* \\
F_4^* &= [\{F_1, S_3\}]_{sec} + O((\frac{m}{M+m_{Tri}})^2) \\
&= 0 \\
\cdots &= \cdots \\
F_i^* &= [\{F_1, S_{i-1}\}]_{sec} + O((\frac{m}{M+m_{Tri}})^2) \\
S_i &= \int [\{F_1, S_{i-1}\}]_{per} dt^* + O((\frac{m}{M+m_{Tri}})^2) \\
\cdots &= \cdots
\end{aligned}$$

Here, $\{X, Y\}$ is an operation of the Poisson bracket of X and Y.

$$\{X, Y\} \equiv \sum_i \left[\frac{\partial X}{\partial x_i}\frac{\partial Y}{\partial y_i} - \frac{\partial X}{\partial y_i}\frac{\partial Y}{\partial x_i}\right].$$

An infinitesimal increment of time dt^* in indefinite integrals $\int \Box dt^*$ can be replaced by an angular variable, y_3, since F_0 depends only on x_3.

$$\begin{aligned}
\int Q dt^* &= \int Q \frac{1}{(-\frac{\partial F_0}{\partial x_3^*})} dy_3^* \\
&= \int Q \frac{1}{-n_{Tri}} dy_3^*
\end{aligned}$$

4.1.2 Intermediate periodic perturbation: Elimination of intermediate periodic terms

Next, we eliminate an intermediate periodic perturbation by using a canonical transformation

$$F^*(y_1, y_2, x_1, x_2) \longrightarrow F^{**}(y_2, x_2).$$

Auxiliary equations are

$$\begin{aligned}
\frac{dx^{**}}{dt^{**}} &= \frac{\partial F_1^*}{\partial y^{**}} \\
\frac{dy^{**}}{dt^{**}} &= -\frac{\partial F_1^*}{\partial x^{**}},
\end{aligned}$$

therefore a time increment dt^{**} is

$$dt^{**} = \frac{dy_1^{**}}{(-\frac{\partial F_1^*}{\partial x_1^{**}})} = \frac{1}{n} dy_1^{**},$$

since unperturbed Hamiltonian F_1 only depends on x_1.

The Hamiltonian (before transformation) is :

$$F^* = F_0^* + F_1^* + F_2^*$$

where,

$$\begin{aligned} F_0^* &= F_0 \\ F_1^* &= \frac{\mu^2}{2x_1^2} \\ F_2^* &= \frac{1}{8}\mu \frac{M m_{Tri}}{(M+m_{Tri})^2} \frac{a^3}{r^3} \frac{a_{Tri}^2}{a^3} \left[(-1+3\theta^2) + 3(1-\theta^2)\cos(2f+2y_2)\right]. \end{aligned}$$

Neglecting $O((\frac{m}{M+m_{Tri}})^2)$, we obtain a new Hamiltonan $F^{**} = \sum_i F_i^{**}$ and a generating function $S^* = \sum_i S_i^*$:

$$\begin{aligned} F_0^{**} &= F_0^* \\ F_1^{**} &= F_1^* (\text{UNPERTURBED}) \\ F_2^{**} &= [F_2^*]_{sec} \\ &= \frac{1}{8}\mu \frac{M m_{Tri}}{(M+m_{Tri})^2} \frac{1}{\eta^3} \frac{a_{Tri}^2}{a^3} (-1+3\theta^2) \\ S_1^* &= \int [F_2^*]_{per}\, dt^{**} \\ &= \mu \frac{M m_{Tri}}{(M+m_{Tri})^2} \frac{1}{n\eta^3} \frac{a_{Tri}^2}{a^3} \left[\frac{1}{8}(-1+3\theta^2)(f + e\sin f - y_1)\right. \\ &\quad \left. + \frac{3}{8}(1-\theta^2)\left\{\frac{1}{2}e\sin(f+2y_2) + \frac{1}{2}\sin(2f+2y_2) + \frac{1}{6}e\sin(3f+2y_2)\right\}\right] \\ F_3^{**} &= [\{F_2^*, S_1^*\}]_{sec} \\ &= O((\frac{m}{M+m_{Tri}})^2) \\ S_2^* &= \int [\{F_2^*, S_1^*\}]_{per}\, dt^{**} \\ &= O((\frac{m}{M+m_{Tri}})^2) \\ \ldots &= \ldots \end{aligned}$$

In the above results, S_1^* does not satisfy the condition that the time-averaged value of S^* be zero, since $\sin(mf + 2y_2)$ is decomposed into $\sin(mf)\cos(2y_2)$ and $\cos(mf)\sin(2y_2)$, the y_1-averaged quantity of the latter has some non-zero value. So, we have to add additional terms for S_1^* to avoid contaminating secular trends in angular variables.

Moreover, an indefinite integral with t^{**} is replaced by

$$\begin{aligned} \int Q dt^{**} &= \int Q \frac{1}{(-\frac{\partial F_1^*}{\partial x_1^{**}})} dy_1^{**} \\ &= \int Q \frac{1}{n} dy_1^{**}. \end{aligned}$$

Finally we obtain the Hamiltonian F^{**} and a generating function S^{*} as follows:

$$
\begin{aligned}
F_0^{**} &= F_0^{*} \\
F_1^{**} &= F_1^{*}(\text{UNPERTURBED}) \\
F_2^{**} &= \frac{1}{8}\mu\frac{Mm_{Tri}}{(M+m_{Tri})^2}\frac{1}{\eta^3}\frac{a_{Tri}^2}{a^3}(-1+3\theta^2) \\
S_1^{*} &= \mu\frac{Mm_{Tri}}{(M+m_{Tri})^2}\frac{1}{n\eta^3}\frac{a_{Tri}^2}{a^3}\left[\frac{1}{8}(-1+3\theta^2)(f+e\sin f-y_1)\right. \\
&\quad +\frac{3}{8}(1-\theta^2)\left\{\frac{1}{2}e\sin(f+2y_2)+\frac{1}{2}\sin(2f+2y_2)+\frac{1}{6}e\sin(3f+2y_2)\right\} \\
&\quad \left.-\frac{1}{16}(1-\theta^2)\frac{1}{e^2}(2-3e^2-2\eta^3)\sin(2y_2)\right] \\
F_3^{**} &= O((\frac{m}{M+m_{Tri}})^2) \\
S_2^{*} &= O((\frac{m}{M+m_{Tri}})^2) \\
\ldots &= \ldots.
\end{aligned}
$$

4.1.3 Long periodic perturbation: Elimination of long periodic terms

Finally, we eliminate the long periodic variable y_2 from the Hamiltonian and obtain a new Hamiltonian F^{***} free from any angular variables y.

However, we have seen in the previous section, the Hamiltonian F^{**} does not contain an angular variable. This is attributed to the fact that we take only P_2 perturbational contributions into consideration. In other words, if we include higher P_i terms (in practice, only the even numbers of i contribute intermediate or long periodic perturbations), F^{**} contains trigonometric functions of y_2. For example, if we follow up till P_6 terms,

$$
\begin{aligned}
F_0^{**} &= n_{Tri}x_3 \\
F_1^{**} &= \frac{\mu^2}{2x_1^2} \\
F_2^{**}(P_2) &= \mu\frac{Mm_{Tri}}{(M+m_{Tri})^2}\frac{1}{\eta^3}\frac{a_{Tri}^2}{a^3}\frac{1}{8}(-1+3\theta^2) \\
F_2^{**}(P_4) &= \mu C_4\frac{1}{\eta^7}\frac{a_{Tri}^4}{a^5}\left[\frac{9}{1024}(3-30\theta^2+35\theta^4)(2+3e^2)\right. \\
&\quad \left.-\frac{45}{512}(1-\theta^2)(1-7\theta^2)e^2\cos(2y_2)\right] \\
F_2^{**}(P_6) &= \mu C_6\frac{1}{\eta^{11}}\frac{a_{Tri}^6}{a^7}\left[\frac{25}{32768}(-5+105\theta^2-315\theta^4+231\theta^6)(8+40e^2+15e^4)\right. \\
&\quad +\frac{2625}{32768}(1-\theta^2)(1-18\theta^2+33\theta^4)e^2(2+e^2)\cos(2y_2) \\
&\quad \left.+\frac{1575}{65536}(1-\theta^2)^2(-1+11\theta^2)e^4\cos(4y_2)\right],
\end{aligned}
$$

where,

$$C_4 \equiv \frac{M m_{Tri}(M^3 + m_{Tri}^3)}{(M + m_{Tri})^5}$$
$$C_6 \equiv \frac{M m_{Tri}(M^5 + m_{Tri}^5)}{(M + m_{Tri})^7}$$

Now we rewrite the above expression into:

$$\begin{aligned} F_0^{**} &= n_{Tri} x_3 \\ F_1^{**} &= \frac{\mu^2}{2x_1^2} \\ F_2^{**} &= F_2^{**}(P_2) \\ F_3^{**} &= F_2^{**}(P_4) + F_2^{**}(P_6) + F_2^{**}(\text{for higher} P_i), \end{aligned}$$

i.e. the old F_2^{**} are divided into two groups, the new F_2^{**} and the new F_3^{**}.

In this process, we consider the new F_2^{**} as an unperturbed Hamiltonian for a canonical transformation

$$F^{**}(y_2, x_2) \longrightarrow F^{***},$$

and eliminate y_2 from F^{**}. Canonical equations for an artificial time t^{***} are:

$$\begin{aligned} \frac{dx^{***}}{dt^{***}} &= \frac{\partial F_2^{**}}{\partial y^{***}} \\ \frac{dy^{***}}{dt^{***}} &= -\frac{\partial F_2^{**}}{\partial x^{***}}, \end{aligned}$$

therefore,

$$dt^{***} = \frac{dy_2^{***}}{(-\frac{\partial F_2^{**}}{\partial x_2^{***}})}.$$

Since the Hamiltonian F^{**} only depends on y_2, equations of motion are reduced to

$$\begin{aligned} \frac{dx_1^{**}}{dt} = 0 &\longrightarrow x_1^{**} = const. \\ \frac{dx_3^{**}}{dt} = 0 &\longrightarrow x_3^{**} = const., \end{aligned}$$

therefore, only the manipulation of $\frac{\partial F_2^{**}}{\partial x_2^{***}}$ is meaningful for obtaining dt^{***}.

Using Hori's canonical perturbation method and neglecting $O((\frac{m}{M+m_{Tri}})^2)$, the new Hamiltonian $F^{***} = \sum_i F_i^{***}$ and the generating function $S^{**} = \sum_i S_i^{**}$ are:

$$\begin{aligned} F_0^{***} &= F_0^{**} \\ F_1^{***} &= F_1^{**} \\ F_2^{***} &= F_2^{**}(\text{UNPERTURBED}) \\ F_3^{***} &= [F_3^{**}]_{sec} \end{aligned}$$

$$= \mu\left[C_4\frac{1}{\eta^7}\frac{a_{Tri}^4}{a^5}\frac{9}{1024}(3-30\theta^2+35\theta^4)(2+3e^2)\right.$$
$$\left.+C_6\frac{1}{\eta^{11}}\frac{a_{Tri}^6}{a^7}\frac{25}{32768}(-5+105\theta^2-315\theta^4+231\theta^6)(8+40e^2+15e^4)\right]$$

$$S_1^{**} = \int [F_3^{**}]_{per}\, dt^{***}$$
$$= -\frac{15}{128}B_4\frac{a_{Tri}^2}{\eta^3}\frac{n}{(-1+5\theta^2)}e^2(1-\theta^2)(1-7\theta^2)\sin(2y_2)$$
$$-\frac{175}{32768}B_6\frac{a_{Tri}^4}{a^2\eta^7}\frac{n}{(-1+5\theta^2)}\left[-20e^2(2+e^2)(1-\theta^2)(1-18\theta^2+33\theta^4)\sin(2y_2)\right.$$
$$\left.3e^4(1-\theta^2)^2(-1+11\theta^2)\sin(4y_2)\right]$$

$$F_4^{***} = O((\frac{m}{M+m_{Tri}})^2)$$

$$S_2^{**} = O((\frac{m}{M+m_{Tri}})^2),$$

where,

$$B_4 \equiv \frac{M^3+m_{Tri}^3}{(M+m_{Tri})^3}$$
$$B_6 \equiv \frac{M^5+m_{Tri}^5}{(M+m_{Tri})^5}.$$

An indefinite integral with t^{***} is replaced by

$$\int Q dt^{***} = \int Q\frac{1}{(-\frac{\partial F_2^{**}}{\partial x_2^{***}})}dy_2^{***}$$
$$= \int Q\frac{1}{-\frac{3}{8}\mu\frac{Mm_{Tri}}{(M+m_{Tri})^2}\frac{1}{na^2\eta^4}\frac{a_{Tri}^2}{a^3}(1-5\theta^2)}dy_2^{***}.$$

It is noted that S_1^{**} is $O((\frac{m}{M+m_{Tri}})^0)$ because in integrating $\int Q dt^{***}$, a quantity Q is divided by a factor of $O((\frac{m}{M+m_{Tri}})^1)$. Therefore, obtained long periodic perturbations become a lower order by $\frac{m}{M+m_{Tri}}$ than the short or intermediate one. In other words, long periodic perturbations have large amplitude, compared with shorter ones.

4.1.4 Secular perturbation

We have obtained a Hamiltonian F^{***} which does not depend on any angular variables. To summarize again, it forms :

$$F^{***} = F_0^{***} + F_1^{***} + F_2^{***} + F_3^{***}$$

where,

$$F_0^{***} = n_{Tri}x_3$$
$$F_1^{***} = \frac{\mu^2}{2x_1^2}$$

$$
\begin{aligned}
F_2^{***} &= \mu \frac{M m_{Tri}}{(M+m_{Tri})^2} \frac{1}{\eta^3} \frac{a_{Tri}^2}{a^3} \frac{1}{8}(-1+3\theta^2) \\
F_3^{***} &= \mu \left[C_4 \frac{1}{\eta^7} \frac{a_{Tri}^4}{a^5} \frac{9}{1024}(3-30\theta^2+35\theta^4)(2+3e^2) \right. \\
&\qquad \left. + C_6 \frac{1}{\eta^{11}} \frac{a_{Tri}^6}{a^7} \frac{25}{32768}(-5+105\theta^2-315\theta^4+231\theta^6)(8+40e^2+15e^4) \right]
\end{aligned}
$$

The equations of motion are:

$$
\begin{aligned}
\frac{dx^{***}}{dt} &= \frac{\partial F^{***}}{\partial y^{***}} (\equiv 0) \\
\frac{dy^{***}}{dt} &= -\frac{\partial F^{***}}{\partial x^{***}}
\end{aligned}
$$

From the first equation, we obtain

$$
x^{***} = const.,
$$

and from the second one,

$$
y^{***} = (-\frac{\partial F^{***}}{\partial x^{***}})t + const..
$$

If we calculate real values of $\frac{\partial F^{***}}{\partial x^{***}}$,

$$
\begin{aligned}
\frac{\partial F^{***}}{\partial x_1^{***}} &= -n - \frac{M m_{Tri}}{(M+m_{Tri})^2} \frac{3 n a_{Tri}^2 (-1+3\theta^2)}{8 a^2 \eta^3} \\
&\quad - \frac{135}{1024} C_4 \frac{n a_{Tri}^4}{a^4 \eta^7} e^2 (3-30\theta^2+35\theta^4) \\
&\quad - \frac{175}{32768} C_6 \frac{n a_{Tri}^6}{a^6 \eta^{11}} (-8+20e^2+15e^4)(-5+105\theta^2-315\theta^4+231\theta^6) \\
\frac{\partial F^{***}}{\partial x_2^{***}} &= \frac{M m_{Tri}}{(M+m_{Tri})^2} \frac{3 n a_{Tri}^2 (1-5\theta^2)}{8 a^2 \eta^4} \\
&\quad - \frac{45}{1024} C_4 \frac{n a_{Tri}^4}{a^4 \eta^8} [3(4+3e^2) - 18\theta^2(8+7e^2) + 7\theta^4(28+27e^2)] \\
&\quad - \frac{525}{32768} C_6 \frac{n a_{Tri}^6}{a^6 \eta^{12}} \left[-5(8+20e^2+5e^4) \right. \\
&\qquad + 5\theta^2(184+500e^2+135e^4) \\
&\qquad - 75\theta^4(40+116e^2+33e^4) \\
&\qquad \left. + 33\theta^6(72+220e^2+65e^4) \right] \\
\frac{\partial F^{***}}{\partial x_3^{***}} &= n_{Tri} + \frac{M m_{Tri}}{(M+m_{Tri})^2} \frac{3 n a_{Tri}^2 \theta}{4 a^2 \eta^4} \\
&\quad + \frac{45}{256} C_4 \frac{n a_{Tri}^4}{a^4 \eta^8} (2+3e^2)\theta(-3+7\theta^2) \\
&\quad + \frac{525}{16384} C_6 \frac{n a_{Tri}^6}{a^6 \eta^{12}} (8+40e^2+15e^4)\theta(5-30\theta^2+33\theta^4)
\end{aligned}
$$

and substitute values into them,

$$\begin{aligned} y_1^{***} &= (-\frac{\partial F^{***}}{\partial x_1^{***}})t + const. \\ y_2^{***} &= (-\frac{\partial F^{***}}{\partial x_2^{***}})t + const. \\ y_3^{***} &= (-\frac{\partial F^{***}}{\partial x_3^{***}})t + const.. \end{aligned}$$

Action variables x^{***} are constants, and angular variables y^{***} increase (or decrease) linearly with time t. This means that the action variables (the semimajor axis a^{***}, the eccentricity e^{***} and the inclination I^{***}) have no secular trend, while the angular variables (the mean anomaly l^{***}, the argument of the perihelion ω^{***} and the longitude of the ascending node Ω^{***}) have secular trends linearly with time.

4.1.5 Mean elements

Orbital elements $a^{***}, e^{***}, I^{***}, l^{***}, \omega^{***}, \Omega^{***}$ deduced from x^{***} and y^{***} are mean orbital elements. Their real values are not determined from theories, requiring the merging of results of astrometrical observations. In this work, we do not identify these values.

4.1.6 Deriving osculating elements

As we have already discussed in Chap. 3, osculating elements E for canonical variables are summed up by the following contributions:

- Mean elements E^{***}
- Contribution from long periodic perturbation δE^{**}
- Contribution from intermediate periodic perturbation δE^{*}
- Contribution from short periodic perturbation δE .

Therefore, we evaluate the following procedure: first,

$$E^{**} = E^{***} + \delta E^{**}(E^{***}),$$

then,

$$E^{*} = E^{**} + \delta E^{*}(E^{**}),$$

and finally

$$E = E^{*} + \delta E(E^{*}).$$

Old and new variables in canonical transformations are linked as

$$\begin{aligned} \delta E^{**} &= \{E^{**}, S^{**}\} + \frac{1}{2}\{\{E^{**}, S^{**}\}, S^{**}\} + \dots \\ \delta E^{*} &= \{E^{*}, S^{*}\} + \frac{1}{2}\{\{E^{*}, S^{*}\}, S^{*}\} + \dots \\ \delta E &= \{E, S\} + \frac{1}{2}\{\{E, S\}, S\} + \dots, \end{aligned}$$

and neglecting $O((\frac{m}{M+m_{Tri}})^2)$ terms, then,

$$\begin{aligned}\delta E^{**} &= \{E^{**}, S^{**}\} \\ \delta E^{*} &= \{E^{*}, S^{*}\} \\ \delta E &= \{E, S\},\end{aligned}$$

or

$$\begin{aligned}\delta x_i^{**} &= \{x_i^{**}, S^{**}\} = \frac{\partial S^{**}}{\partial y_i^{**}} \\ \delta y_i^{**} &= \{y_i^{**}, S^{**}\} = -\frac{\partial S^{**}}{\partial x_i^{**}} \\ \delta x_i^{*} &= \{x_i^{*}, S^{*}\} = \frac{\partial S^{*}}{\partial y_i^{*}} \\ \delta y_i^{*} &= \{y_i^{*}, S^{*}\} = -\frac{\partial S^{*}}{\partial x_i^{*}} \\ \delta x_i &= \{x_i, S\} = \frac{\partial S}{\partial y_i} \\ \delta y_i &= \{y_i, S\} = -\frac{\partial S}{\partial x_i}.\end{aligned}$$

If we express elements in orbital elements,

$$\begin{aligned}\delta a &= \frac{2x_1}{\mu}\delta x_1 \\ \delta e &= -\frac{1}{e}\left[\frac{x_2}{(x_1)^2}\delta x_2 - \frac{(x_2)^2}{(x_1)^3}\delta x_1\right] \\ \delta \theta &= \frac{1}{x_2}\delta x_3 - \frac{x_3}{x_2^2}\delta x_2 \\ \delta l &= \delta y_1 \\ \delta \omega &= \delta y_2 \\ \delta \Omega &= \delta y_3.\end{aligned}$$

4.2 Results for inclined problem

4.2.1 Numerical results

For the inclined problem, results of numerical integration by Bulirsch-Stoer code are in Figure 4.2. The integrational pereiod is for 15 years and Figure 4.2 (b) is zoomed up and trimmed to reveal offsets of orbital elements. Comparing results for the planar problem, shapes of elements-time plots are changed. However, offset features can be observed when Nereid approaches its pericenter.

Hereafter, we use the word 'residual range' as follows:

- **residual range** a range of residuals (analytical elements minus numerical ones) during an integration period (see Fig. 4.3)

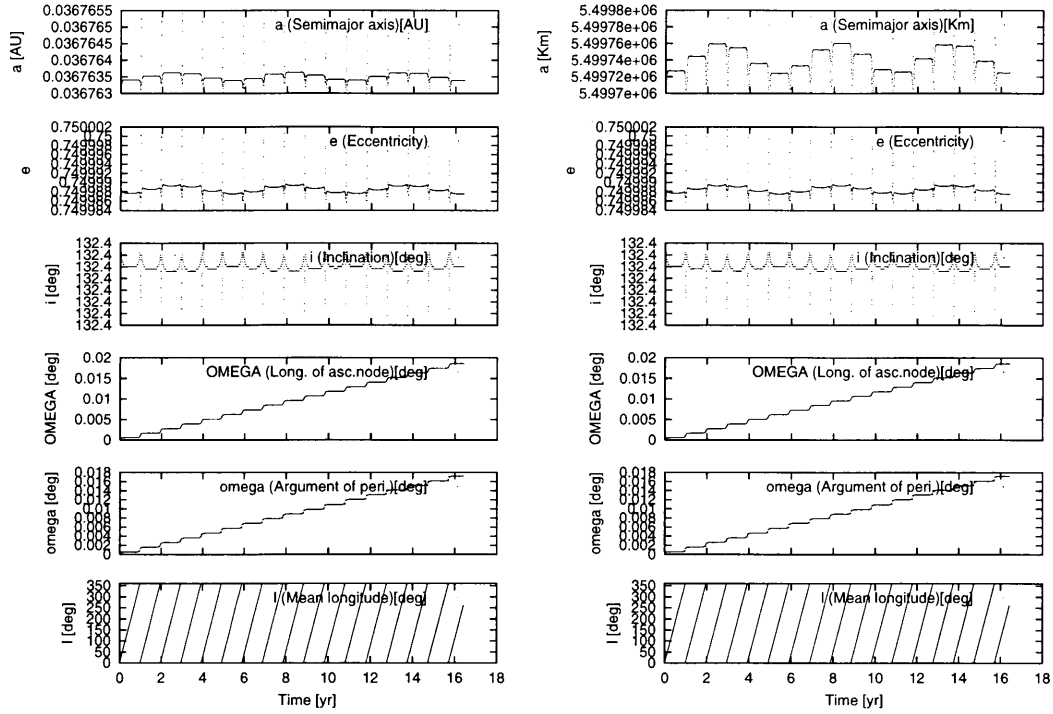

(a) (b)Trimmed for the vertical axis and zoomed up offsets

Figure 4.2: Numerical results (a)for 15 years and (b)zoomed up (Note: for panel (b), the vertical axis is trimmed to reveal offsets in semimajor axis and eccentricity). The initial values for this calculation use the mean elements.

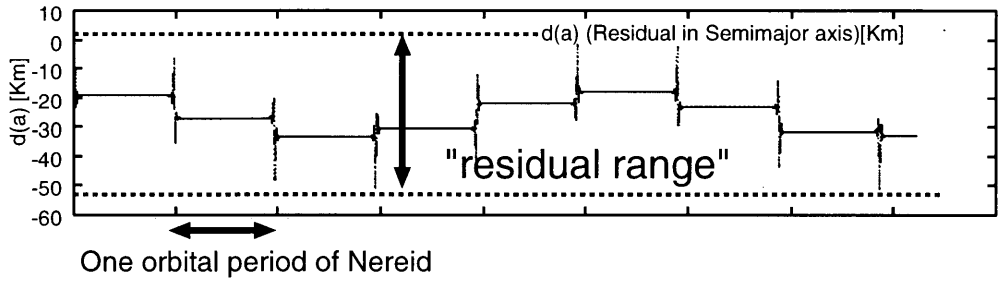

Figure 4.3: Definition of residual range in this study.

Table 4.1: Variational ranges of residuals when we take up to P_i terms of Legendre polynomials into consideration. Integration period is 400[days].

P_i	Residual ranges		
	a [Km]	e	I[deg]
P_2	73	3.4×10^{-6}	6.3×10^{-5}
P_3	18	8.2×10^{-7}	1.4×10^{-5}
P_4	6.7	3.2×10^{-7}	5.8×10^{-6}
P_5	1.1	4.9×10^{-8}	9.3×10^{-7}

4.2.2 Influence on residuals of truncation of Legendre polynomials

As seen in the experiments for the planar problem, we assess the truncational effect of Legendre polynomials in the Hamiltonian expression. Results of residuals

(Full numerical results) – (Numerical results including up to P_i Legendre polynomials)

are in Fig.4.4.

Ranges of residuals (differences between the maximum residuals and the minimum residuals) are tabulated in Table 4.1 If we expect to achieve accuracy of sub-Km on the semimajor axis, we have to take terms up to P_5 in the Hamiltonian into account.

4.2.3 Influence on residuals of truncation of generating functions

Next, we check the influence of truncational errors of short periodic generating functions S_i using residuals of

$$\left(\begin{array}{l} \text{Numerical results} \\ \text{including only } P_n \end{array} \right) - \left(\begin{array}{l} \text{Analytical results including only } P_n \text{ and} \\ \text{up to } S_i \text{ of generating functions for short periodic} \end{array} \right).$$

Their results are shown in Fig. 4.5 for the P_2-limited Hamiltonian and in Fig. 4.6 for the P_3-limited one. They are also summarized in Table 4.2.

Because there seemed to be features similar to those in the planar problem; we must take higher orders of a small parameter, $\frac{n}{n_{Tri}}$, into consideration for the property of slow-converging series.

For the P_3-limited problem, eminent offsets are observed again and they seemed to be in correlation with the longitude of Triton when Nereid passes through its pericenter.

4.3 Orbital evolution for a long timespan

We have discussed the orbital evolution of Nereid for a relatively short interval of several years. From now on, we focus on orbital evolution for a very long interval in order to observe a circulation of the pericenter of Nereid, which takes about 3.4×10^5 years.

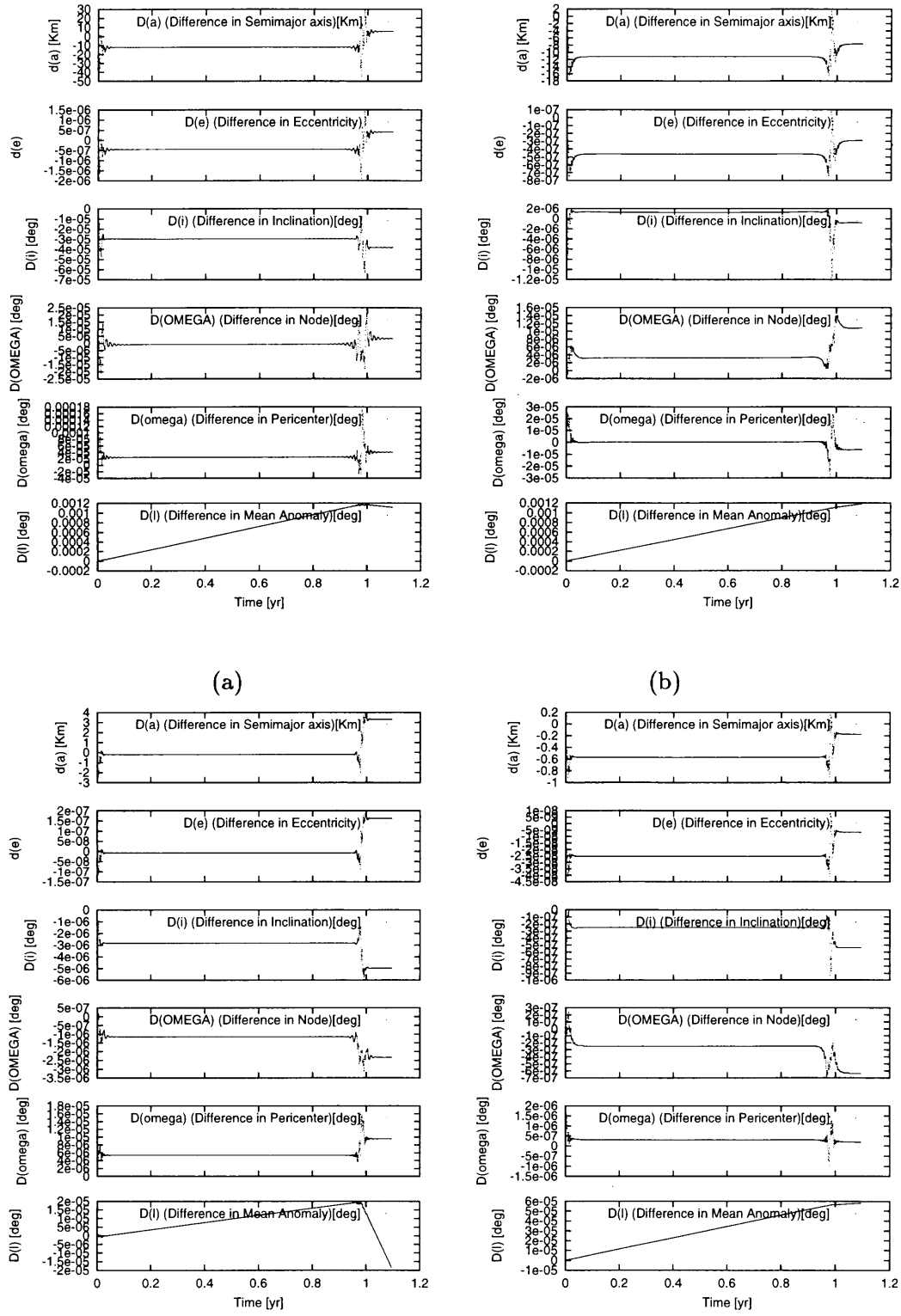

Figure 4.4: Residuals of full numerical results minus numerical results up to Legendre P_i terms in the Hamiltonian for the inclined problem. (a)up to P_2 term, (b)up to P_3 terms, (c)up to P_4 terms, (d)up to P_5 terms

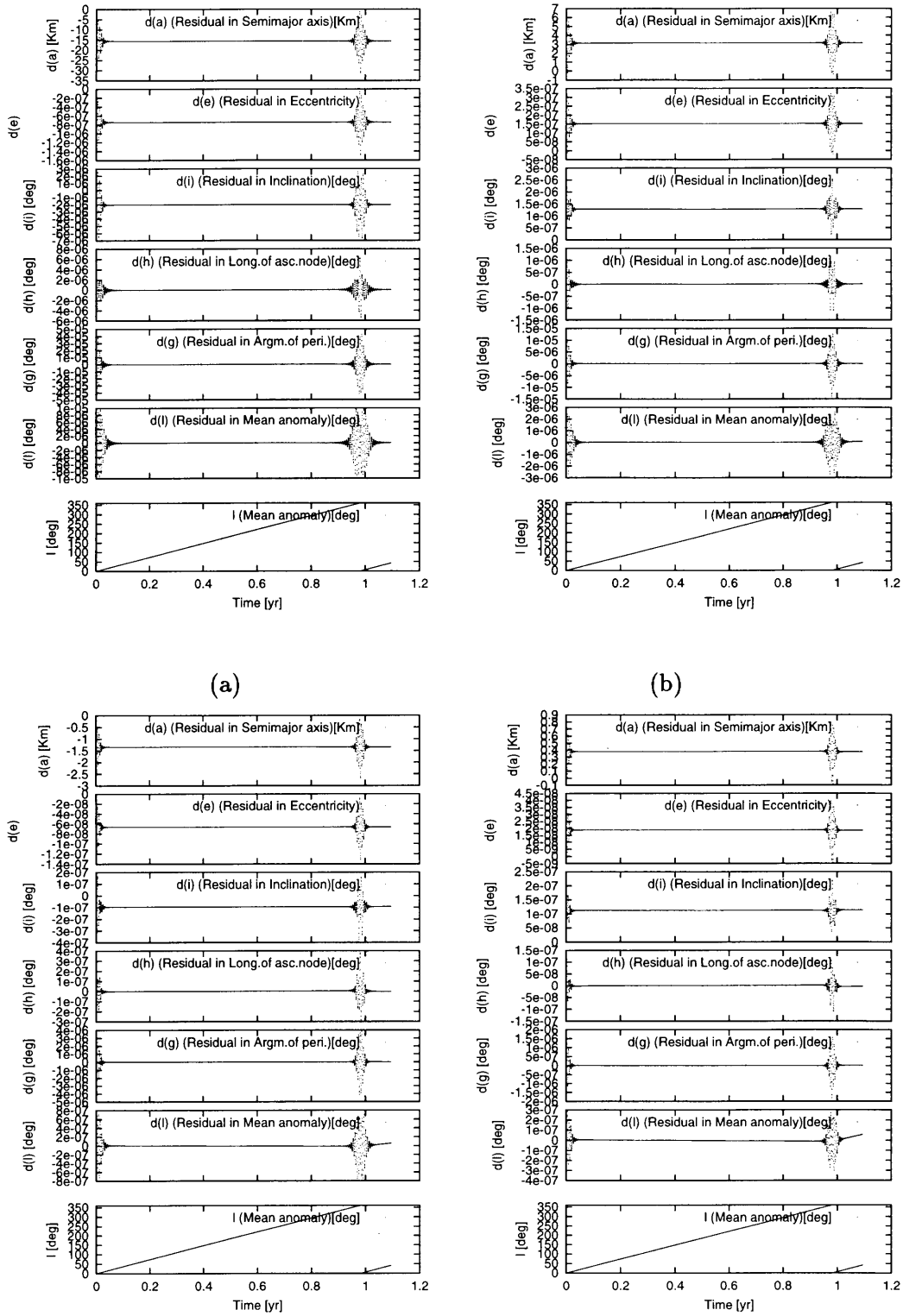

Figure 4.5: Residuals of numerical results minus truncated S_i results for a Hamiltonian limited only by a Legendre P_2 contribution. Secular trends of residuals in angular variables are subtracted. (a)up to S_2 terms, (b)up to S_3 terms, (c)up to S_4 terms, (d)up to S_5 terms

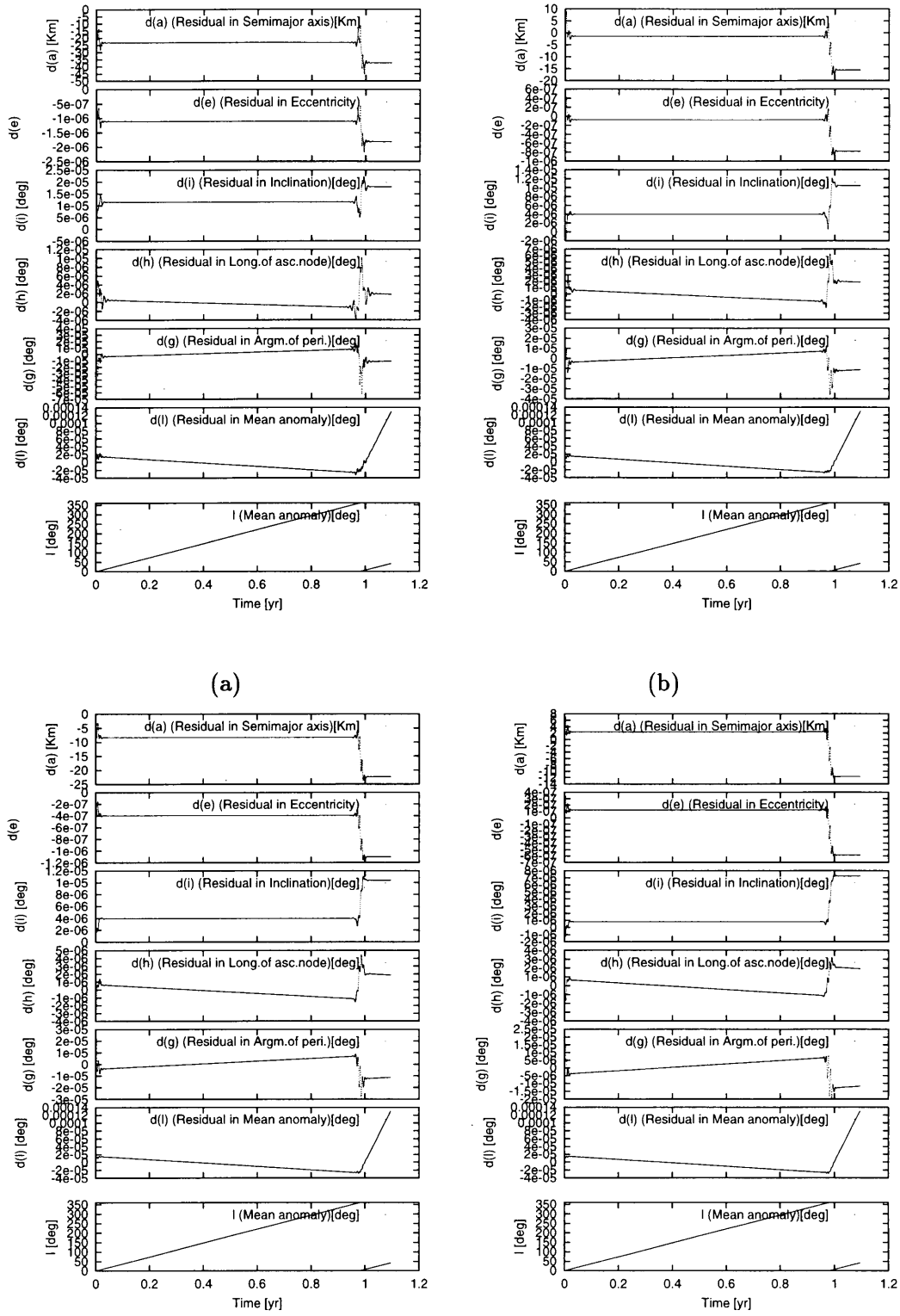

Figure 4.6: Residuals of numerical results minus truncated S_i results for a Hamiltonian limited only by a Legendre P_3 contribution. Secular trends of residuals in angular variables are subtracted. (a)up to S_2 terms, (b)up to S_3 terms, (c)up to S_4 terms, (d)up to S_5 terms

Table 4.2: Variational ranges of residuals when we take up to S_i of generating functions into consideration. Integration period is 400[days].

S_i	Residual ranges for the P_i-limited problem					
	$\boxed{P_2}$			$\boxed{P_3}$		
	a [Km]	e	I [deg]	a [Km]	e	I [deg]
S_2	31	1.5×10^{-6}	9.3×10^{-6}	45	2.2×10^{-6}	2.2×10^{-5}
S_3	7.0	3.4×10^{-7}	2.5×10^{-6}	27	1.3×10^{-6}	1.4×10^{-5}
S_4	2.7	1.3×10^{-7}	5.4×10^{-7}	24	1.2×10^{-6}	1.1×10^{-5}
S_5	0.91	4.6×10^{-8}	2.2×10^{-7}	19	9.5×10^{-7}	8.8×10^{-6}
S_i	Residual ranges for the P_i-limited problem					
	$\boxed{P_4}$			$\boxed{P_5}$		
	a [Km]	e	I [deg]	a [Km]	e	I [deg]
S_2	2.7	1.3×10^{-7}	1.2×10^{-6}	5.4	2.5×10^{-7}	3.5×10^{-6}
S_3	0.95	4.6×10^{-8}	3.3×10^{-7}	4.1	1.9×10^{-7}	2.6×10^{-6}
S_4	0.49	2.4×10^{-8}	1.5×10^{-7}	3.7	1.8×10^{-7}	2.3×10^{-6}
S_5	0.24	1.2×10^{-8}	6.0×10^{-8}	3.3	1.6×10^{-7}	2.0×10^{-6}

4.3.1 Numerical results

We numerically integrated the equations of motion for Nereid using Bulirsch-Stoer code for $\sim 4 \times 10^5$ years. The results are shown in Figure 4.7. Mean orbital elements are used for the initial values in the calculation. We can easily find that the semimajor axis a is composed of shorter periodic perturbations, while the eccentricity e and the inclination I are superimposed by longer periodic perturbations on shorter periodic ones. The longitude of ascending node Ω and the argument of pericenter ω circulate toward the prograde. Their periods are about 3.1×10^5 and 3.4×10^5 years, respectively.

Time variations in e and I are synchronized with a half period of a circulation of the pericenter.

4.3.2 Equi-potential curves

The time-independent Hamiltonian F that contains three angular variables (y_1, y_2, y_3) is the energy integral. When we averaged F over two shorter periodic terms, we can obtain F^{**}, depending only on the longest periodic angular variable. In this study, it is the argument of pericenter y_2. If we dictate F^{**} with canonical variables,

$$F^{**}(x_2, y_2).$$

It no longer depends on x_1 and x_3. Alternatively, if we express it with orbital elements,

$$F^{**}(e, I, \omega),$$

i.e. we cannot separate the contributions of the two variables of e and I.

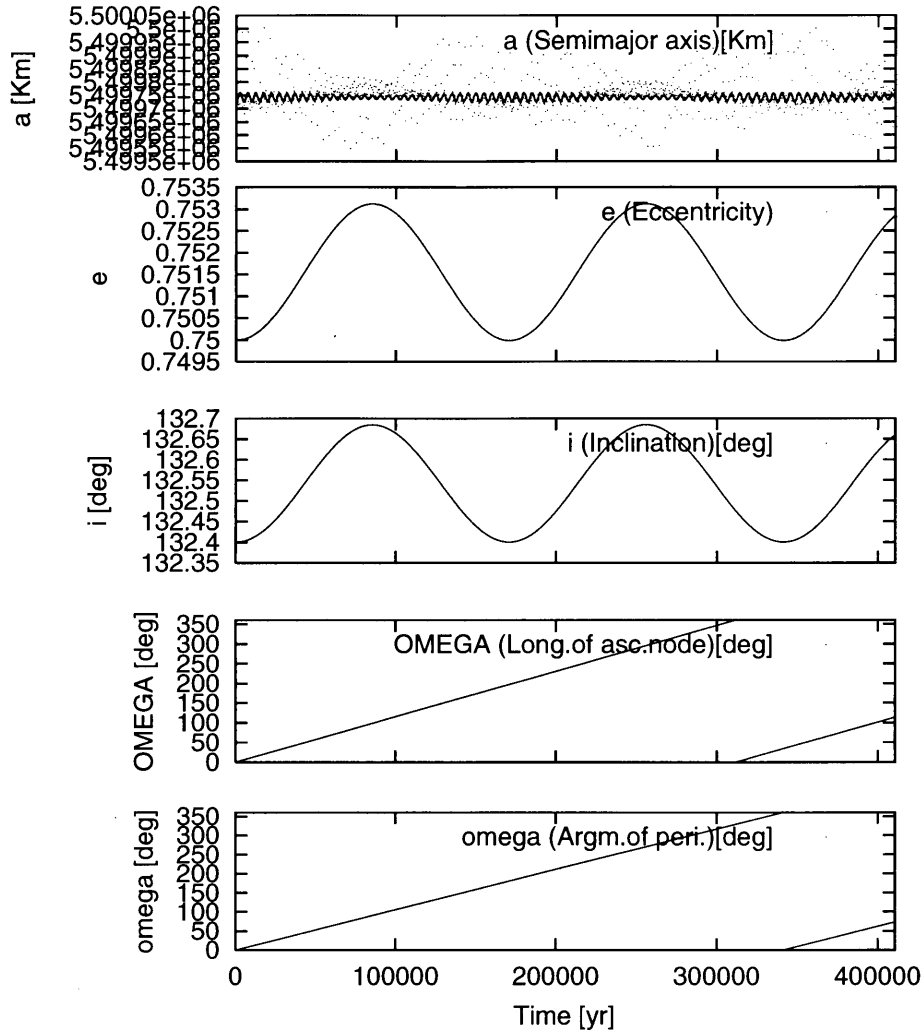

Figure 4.7: Numerical results for a long timespan. Mean elements are given as the initial values.

However, we can easily obtain the nature of variations between e and ω (or I and ω) from F^{**}. Our strategy is the following: first, F^{**} no longer depends on y_1 and y_3, then we obtain

$$\begin{aligned} x_1(\equiv \sqrt{\mu a}) &= const. \\ x_3(\equiv \sqrt{\mu a(1-e^2)}\cos I) &= const., \end{aligned}$$

or,

$$\begin{aligned} a &= const. \\ \sqrt{(1-e^2)}\cos I &= const.(\equiv (x_3)_0). \end{aligned}$$

From the last equation, we can deduce a relation

$$\cos I = \frac{(x_3)_0}{\sqrt{(1-e^2)}}.$$

This means that once we specify the value of $(x_3)_0$, or the sets of (e, I), we can eliminate the variable I from F^{**}. Namely, we substitute the above equation into $F^{**}(e, I, \omega)$, and we obtain the Hamiltonian which depends only on e and ω,

$$F^{**}(e, \omega) \qquad \text{for the initial values of } (e_0, I_0).$$

We can plot equi-F^{**} curves on the 2-D (e, ω) map.

Fortunately, we already derived the expression of $F^{**} = F_0^{**} + F_1^{**} + F_2^{**}$ as

$$\begin{aligned} F_0^{**} &= n_{Tri}x_3(\equiv const.) \\ F_1^{**} &= \frac{\mu^2}{2x_1^2}(\equiv const.) \\ F_2^{**}(P_2) &= \mu\frac{Mm_{Tri}}{(M+m_{Tri})^2}\frac{1}{\eta^3}\frac{a_{Tri}^2}{a^3}\frac{1}{8}(-1+3\theta^2) \\ F_2^{**}(P_4) &= \mu C_4\frac{1}{\eta^7}\frac{a_{Tri}^4}{a^5}\left[\frac{9}{1024}(3-30\theta^2+35\theta^4)(2+3e^2)\right. \\ &\qquad \left. -\frac{45}{512}(1-8\theta^2+7\theta^4)e^2\cos(2y_2)\right] \\ F_2^{**}(P_6) &= \mu C_6\frac{1}{\eta^{11}}\frac{a_{Tri}^6}{a^7}\left[\frac{25}{32768}(-5+105\theta^2-315\theta^4+231\theta^6)(8+40e^2+15e^4)\right. \\ &\qquad -\frac{2625}{32768}(-1+19\theta^2-51\theta^4+33\theta^6)e^2(2+e^2)\cos(2y_2) \\ &\qquad \left. +\frac{1575}{65536}(-1+\theta^2)^2(-1+11\theta^2)e^4\cos(4y_2)\right], \end{aligned}$$

where,

$$\begin{aligned} C_4 &\equiv \frac{Mm_{Tri}(M^3+m_{Tri}^3)}{(M+m_{Tri})^5} \\ C_6 &\equiv \frac{Mm_{Tri}(M^5+m_{Tri}^5)}{(M+m_{Tri})^7}. \end{aligned}$$

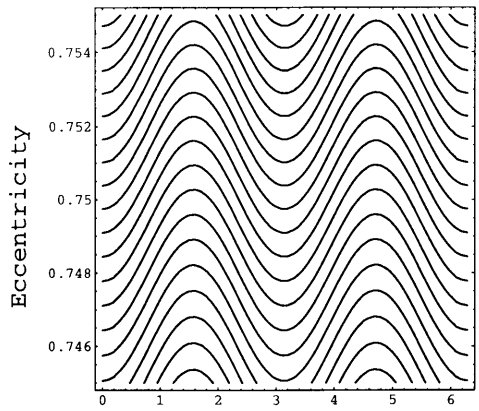

(a)

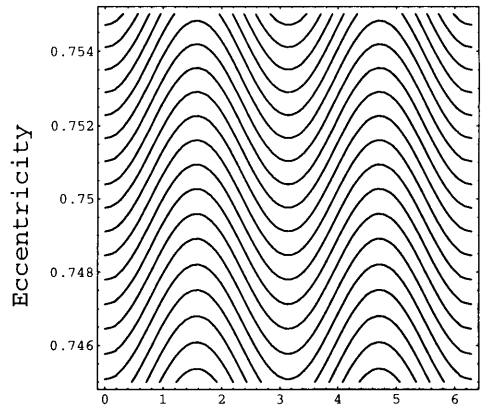

(b)

Figure 4.8: Equi-potential curves of F^{**} for $e_0 = 0.75$ and $I_0 = 132.4$[deg]. (a) The Hamiltonian contains up to P_4 perturbations and (b) up to P_6 ones.

Table 4.3: Secular circulation rates of ω and Ω in the analytical model.

Analytical	ω		Ω	
Model	Rate [deg/yr]	Period [yr]	Rate [deg/yr]	Period [yr]
up to P_2	1.072×10^{-3}	3.358×10^5	1.136×10^{-3}	3.170×10^5
up to P_4	1.034×10^{-3}	3.481×10^5	1.139×10^{-3}	3.160×10^5
up to P_6	1.033×10^{-3}	3.485×10^5	1.138×10^{-3}	3.164×10^5

The equi-potential curves of Nereid's F^{**} for $e_0 = 0.75$ and $I_0 = 132.4$[deg] are shown in Fig. 4.8. They show a circulation nature of the argument of pericenter. We cannot see a clear difference in these curves between Figs. 4.8 (a) and (b) that take the Hamiltonian up to P_4 and P_6 into consideration, respectively. This fact indicates long periodic contributions from P_6 terms are small enough compared with those from P_4.

The eccentricity shows a bimodal variation with its amplitude of ~ 0.003 during a circulation of the argument of pericenter ω. It agrees with numerical results.

4.3.3 Secular circulation rates of ω and Ω

Secular circulation rates of ω and Ω in the analytical model are calculated from $-\frac{\partial F^{***}}{\partial x_2^{***}}$ and $-\frac{\partial F^{***}}{\partial x_3^{***}} + n_{Tri}$, as we derived in Section 4.1.4. These values are listed in Table 4.3. The secular rates are mainly explained by P_2 perturbation.

4.3.4 Comparison with numerical results

As seen in the previous sections, we calculate residuals between analytical and numerical results. In this section, we include P_2 and P_4 perturbations in the analytical theory and neglect the intermediate and short periodic perturbations. Namely,

$$\text{(Analytical model)} = \left(\begin{array}{l} \text{Secular perturbations:} \\ \text{Non-perturbing terms } + P_2 + P_4 \end{array} \right) + \left(\begin{array}{l} \text{Long periodic perturbations} \\ \text{from } P_4 \text{ terms} \end{array} \right),$$

and

$$\text{(Residuals)} = \text{(Numerical results)} - \text{(Analytical results)}.$$

We note that there is no contribution from long periodic P_2 terms when we neglect $O((\frac{m}{M+m_{Tri}})^2)$. Of course, the initial values for numerical integration use osculating elements produced by an analytical model.

The analytical results compared with numerical ones are shown in Fig. 4.9 (a) and (b). Both agree in global perspective. Next, we extract only long periodic terms and compare both models. They are shown in Fig. 4.9 (c) and (d). Analytical extracted data are equal to δE^{**} contributions in Section 4.1.6, while numerical ones only subtract secular trends from the angular variables ω and Ω by fitting regression lines. Both results agree.

Now we check residuals. We subtracted secular trends from the angular variables residuals in order to easily observe periodic misfits. They are shown in Fig. 4.10.

In e, I and Ω, misfits of $\cos 2\omega$ or $\sin 2\omega$ terms dominate. They come from the higher order terms of $(\frac{m}{M+m_{Tri}})^2$ that we have neglected in our construction of a theory. In residuals of ω, $\cos 4\omega$ or $\sin 4\omega$ terms are also seen.

Residuals in mean anomaly l remain quadratic trends. They are due to growth of numerical round-off errors in longitude (or position) with time. I.e., they are attributed to the errors in numerical integration, not to those in our analytical theory.

4.4 Combined analytical model

4.4.1 Combined analytical theory

Finally, we combine all P_i-limited analytical theories and, from this point on, call it a 'combined analytical theory'. First, for each periodic component, we sum up net contributions of P_2 to P_5, and then sum up periodic components from the longer one to the shorter.

Therefore, the procedure is the following:

1. Secular perturbations:

$$\begin{aligned} x_i^{***} &= \text{(mean elements)} \\ y_i^{***} &= -(\frac{\partial F(P_2+P_4)^{***}}{\partial x_i^{***}})t + const. \end{aligned}$$

2. Long periodic perturbations:

$$\delta E^{**} = \{E^{**}, S_1^{**}(P_2 + P_4)\}$$

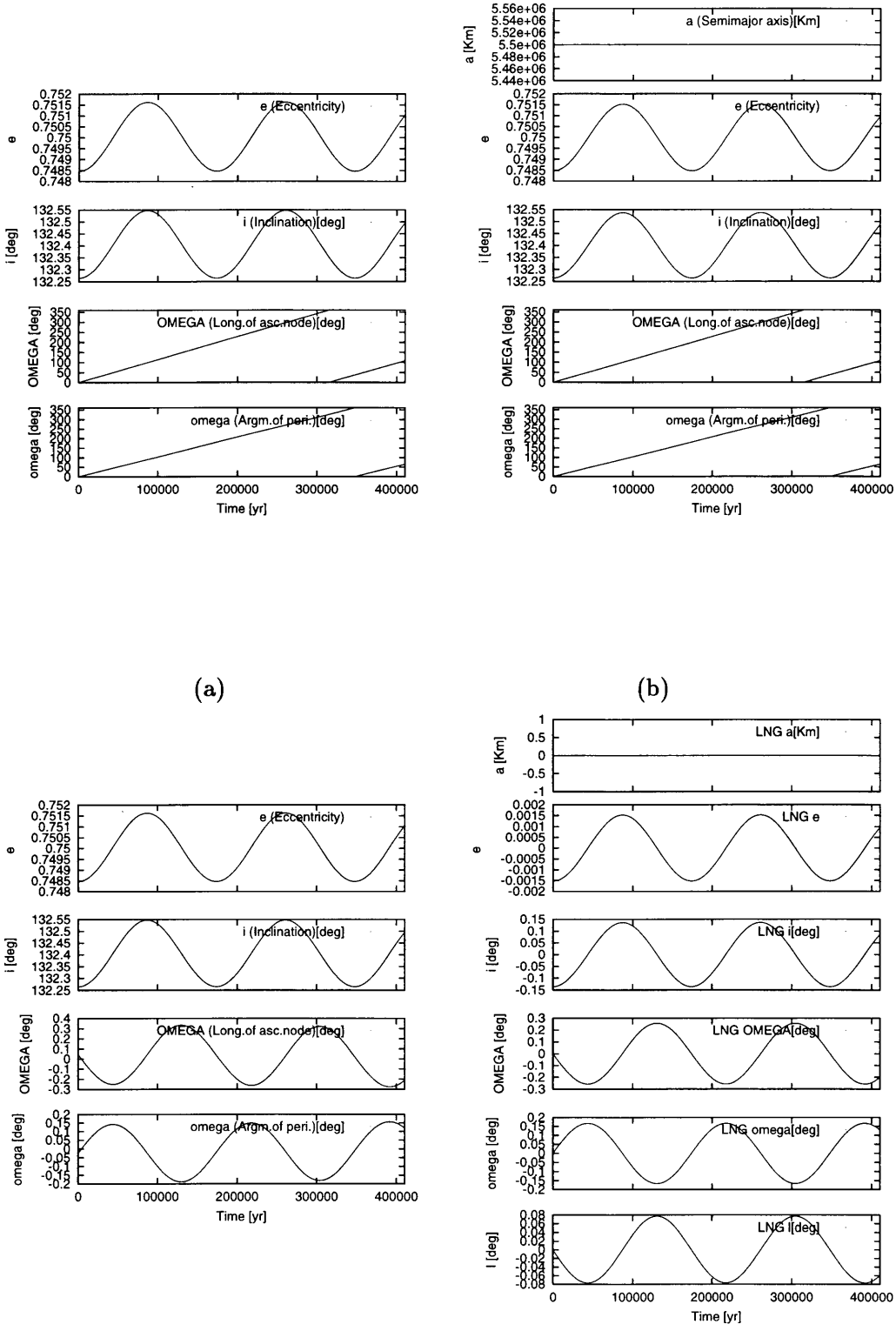

Figure 4.9: Long periodic orbital evolution. Kepler, P_2 and P_4 terms are included in the equations of motion. (a)Numerical results. (b)Analytical results. (c)Numerical results. Secular trends in angular variables are subtracted from the results by applying regression lines. (d)Only long periodic perturbations are extracted from the analytical results.

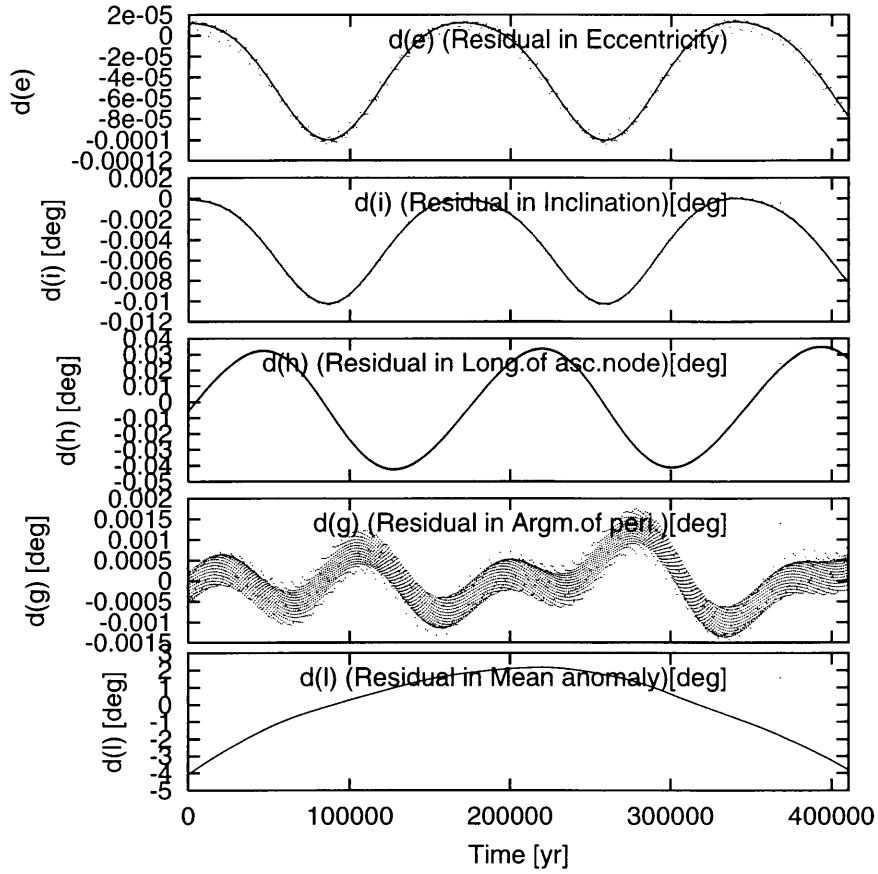

Figure 4.10: Residuals for a long timespan. Kepler, P_2 and P_4 terms are included in the model. Secular trends in the angular variables are subtracted.

Table 4.4: Combined analytical theory. The listed contribution is taken into account.

Period	P_2	P_3	P_4	P_5
Short	S_2, S_3, S_4, S_5	S_2, S_3, S_4, S_5	S_2, S_3, S_4, S_5	S_2, S_3, S_4, S_5
Intermediate	S_1^*	–	S_1^*	–
Long	–	–	S_1^{**}	–
Secular	y^{***}	–	y^{***}	–

then,

$$E^{**} = E^{***} + \delta E^{**}.$$

3. Intermediate periodic perturbations:

$$\delta E^* = \{E^*, S_1^*(P_2)\} + \{E^*, S_1^*(P_4)\}$$

then,

$$E^* = E^{**} + \delta E^*.$$

4. Short periodic perturbations:

$$\delta E = \sum_{i=2}^{5}\{E, S_i(P_2)\} + \sum_{i=2}^{5}\{E, S_i(P_3)\} + \sum_{i=2}^{5}\{E, S_i(P_4)\} + \sum_{i=2}^{5}\{E, S_i(P_5)\}$$

then,

$$E = E^* + \delta E.$$

Finally we obtain osculating elements E. (See also Table 4.4.)

By virtue of neglecting $O((\frac{m}{M+m_{Tri}})^2)$ terms, all we have to evaluate is the single Poisson brackets written above. (Because S is the order of $O(\frac{m}{M+m_{Tri}})$.) It is noted that we can add each P_i-contribution linearly because the Poisson bracket satisfies the distributive law:

$$\{X, (Y+Z)\} = \{X, Y\} + \{X, Z\}.$$

4.4.2 Results

We calculate residuals to give the full numerical results and show them in Fig. 4.11.

We can easily interpret that the residuals are dominated by offsets. These are mainly explained by the P_3 and P_5 terms.

Short periodic variations, which are trigonometric functions of y_3, are almost entirely removed from the profile (only slightly remain near the offset corners!). Therefore, we conclude that the combined analytical theory represents the true Nereid system fairly well, except for offsets.

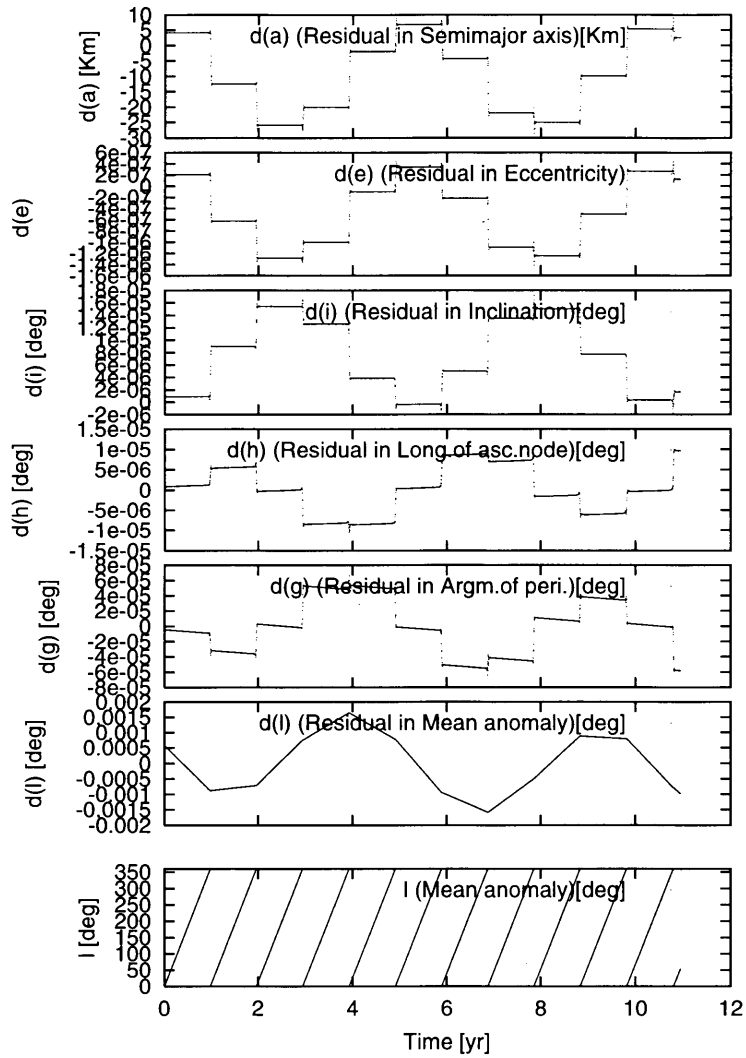

Figure 4.11: Residual of full numerical results minus 'combined analytical' ones.

Chapter 5

Accuracy of Our Analytical Theory

In Chapters 3 and 4, we have discussed the accuracy of our theory for the problem of Nereid ($a = 5.5 \times 10^6$[Km], $e = 0.75$). In this chapter, we assess accuracy of our analytical theory for other orbital parameters.

5.1 Normalized residual range

Before assessing accuracy, we will define the term 'normalized residual range':

- **whole range** a range of the orbital elements during an integration period (see Fig. 5.1; the orbital data are based on the numerical results.)
- **normalized residual range** a value of the residual range (defined in Section 4.2.) normalized by a value of the whole range

The reason for introducing the normalized residual range is the following: if we change orbital parameters of the outer body, such as a or e, the magnitudes of perturbation are also changed (see Fig. 5.2). The absolute magnitude of the residual depends on one of the perturbations. Therefore, we adopt the normalized values using the absolute magnitude of perturbations.

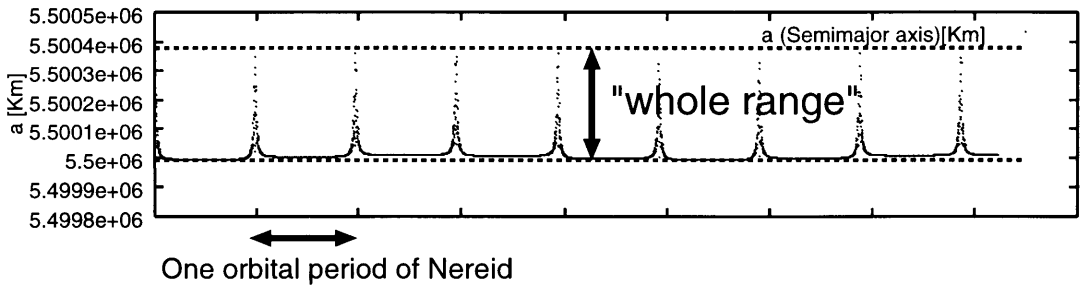

Figure 5.1: Definition of the whole range in this study.

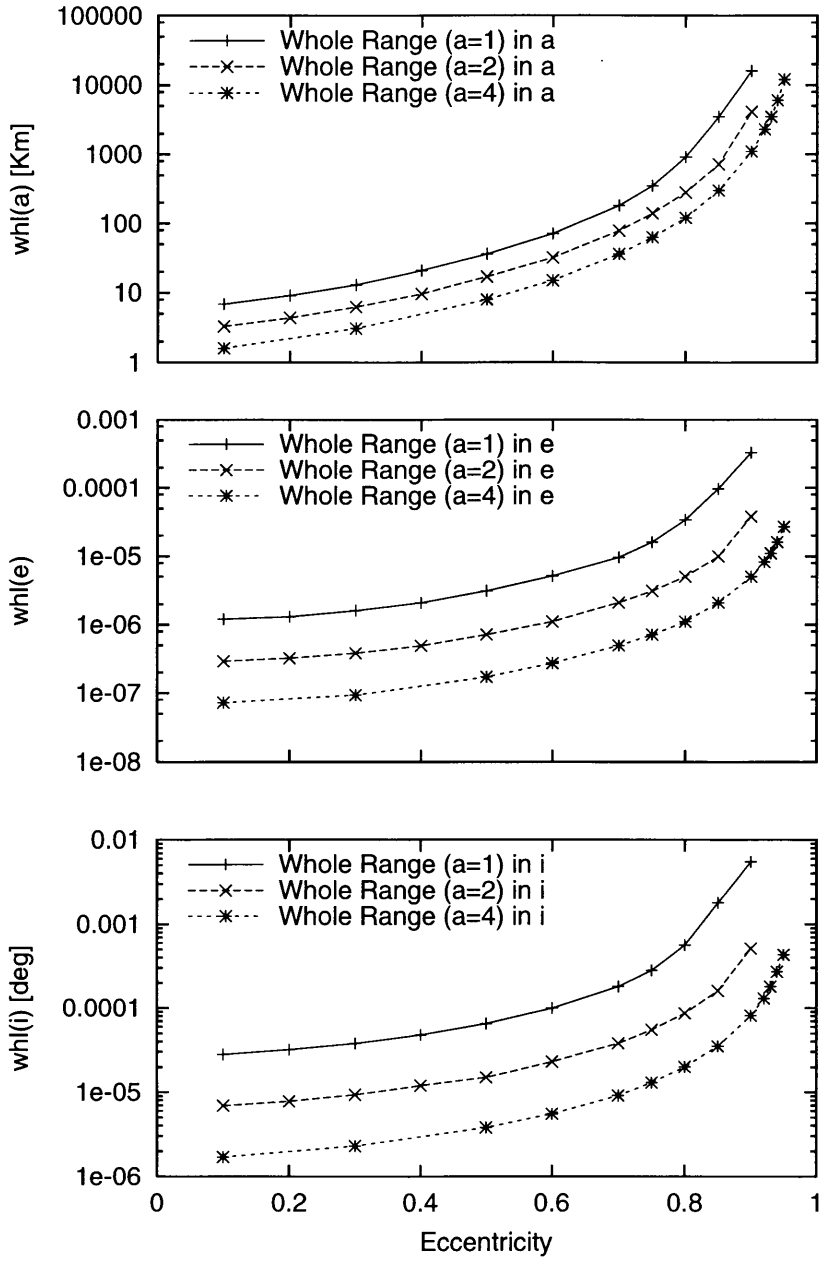

Figure 5.2: The growth of the whole range with the eccentricity. Each curve shows the values for the same semimajor axis. (From the upper panel to the lower) Whole ranges in the semimajor axis, the eccentricity and the inclination.

Table 5.1: Initial values for numerical integrations. The inclination of the outer body refers to the orbital plane of the inner one. We use the same parameters as in the Nereid problem except for those of the semimajor axis and the eccentricity.

Item	Model
Mass of the primary body [$M_\odot$]	5.1514×10^{-5}
Mass of the inner body	$(2.89 \times 10^{-4}) \times$ (Mass of Primary)
Mass of the outer body	0. (test particle)
Semimajor axis [Km]	variable (Integer multiples of 5.5×10^6)
Eccentricity	variable
Inclination [deg]	132.4
Longitude of ascending node [deg]	0.0
Argument of pericenter [deg]	0.0
Initial longitude of the outer body [deg]	0.0
Semimajor axis of the inner body [Km]	14.15×24764
Eccentricity of the inner body	0.0
Inclination of the inner body [deg]	0.0
Integration period [day]	40000.

5.2 Initial values and models

In this chapter, we adopted the initial values as shown in Table 5.1. We vary the values of a and e and check the normalized residual ranges. We used the same values as in the problem of Nereid for other parameters for the sake of convenience, to allow comparison with data in the previous chapters.

From here on, we assess the accuracy of the 'Combined analytical model' (See Section 4.4).

5.3 Comparing accuracy of the 'Combined analytical theory' with the 'full numerical model'

First, we compare the accuracy of the 'Combined analytical theory' with the 'full numerical model'.

The growth of the normalized residual ranges with the eccentricity is shown in Fig. 5.3. Our theory maintains a high degree of accuracy for a wide range of eccentricity, especially for a larger semimajor axis. The normalized residual range on the order of $\sim 10^{-5}$ is a machine precision limit for calculating residuals. Therefore, our theory perfectly agrees with numerical results.

However, for a larger eccentricity or for a smaller semimajor axis, the combined analytical model degrades accurately. This is due to the following:

- Offset growth
  (Discussed in detail in Chapter 6.)

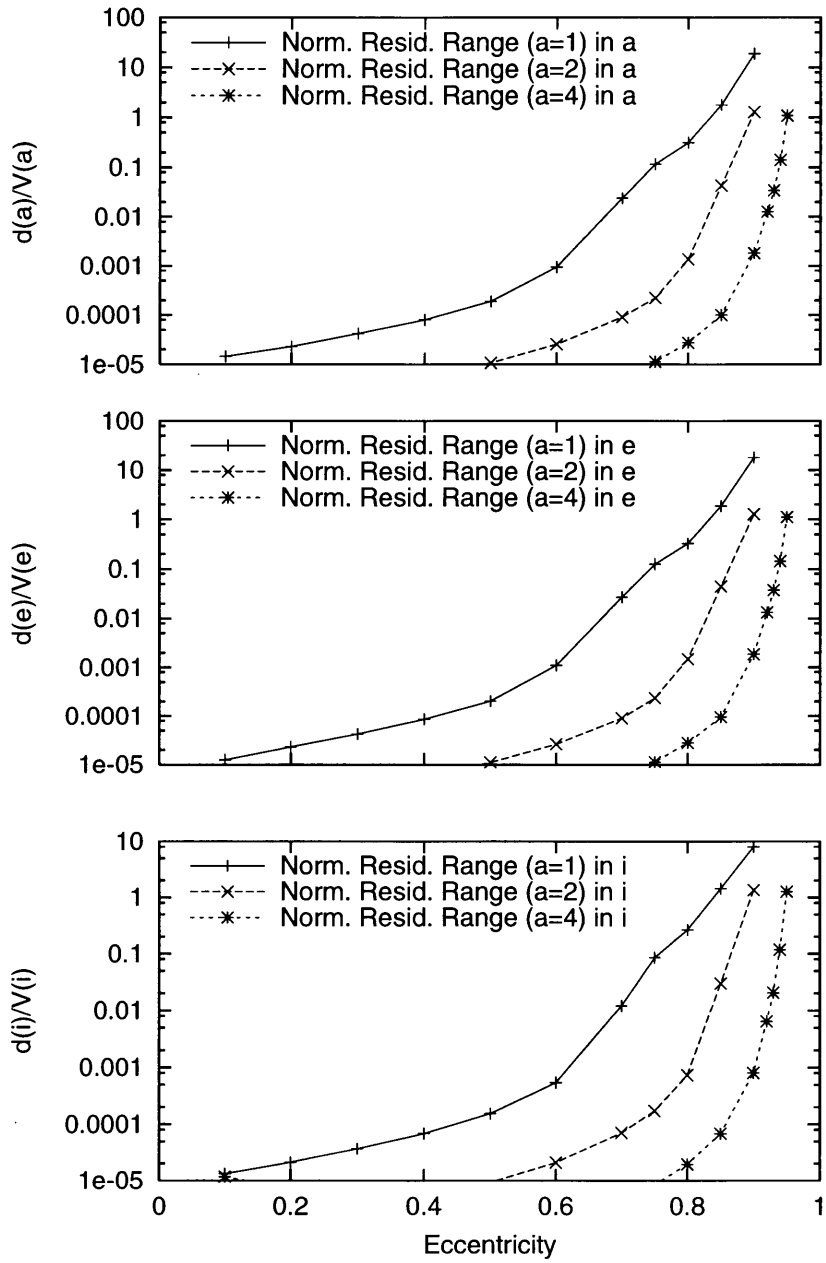

Figure 5.3: The growth of the normalized residual ranges with the eccentricity. Each curve shows the values for the same semimajor axis. (From the upper panel to the lower) Normalized residual ranges in the semimajor axis, the eccentricity and the inclination.

Table 5.2: The values of the factors (a) $\frac{n}{n_{In}}$ and (b) $\frac{(1+e)^2}{\eta^3}$.

(a)

Semimajor axis a		$\frac{n}{n_{In}}$
a_{Nereid}	$(= 5.5 \times 10^6$[Km])	1.61×10^{-2}
$2 \times a_{Nereid}$	$(= 1.1 \times 10^7$[Km])	5.69×10^{-3}
$4 \times a_{Nereid}$	$(= 2.2 \times 10^7$[Km])	2.01×10^{-3}

(b)

Eccentricity	$\frac{(1+e)^2}{\eta^3}$
0.1	1.23
0.5	3.46
0.7	7.93
0.75	10.6
0.8	15.0
0.85	23.4
0.9	43.6

- Ill-convergent series of S_i
  For short periodic perturbations, the series of S_i converges by a factor of $\frac{n}{n_{In}}$. However, S_i is calculated as follows:

$$\begin{aligned} S_i &= \int \{F_1, S_{i-1}\} dt^* \\ &= -\frac{n}{n_{In}} \int \frac{\partial S_{i-1}}{\partial y_1} dy_2 \\ &= -\frac{n}{n_{In}} \int \frac{\partial f}{\partial y_1} \frac{\partial S_{i-1}}{\partial f} dy_2 \\ &= -\frac{n}{n_{In}} \frac{(1+e\cos f)^2}{\eta^3} \int \frac{\partial S_{i-1}}{\partial f} dy_2. \end{aligned}$$

  The factor of $\frac{(1+e\cos f)^2}{\eta^3}$ becomes a larger value for a large eccentricity, especially at the pericenter, $\frac{(1+e)^2}{\eta^3}$. Therefore it prevents S_i from converging. When we vary the values of a and e, these factors change as shown in Table 5.2.

- Truncational error of Legendre polynomials
  Our theory is truncated by the P_5 terms of Legendre polynomials. Thus, the accuracy of our theory is decreased when the outer body approaches the pericenter.

- Truncational error of canonical transformation
  Our theory is truncated by the S_5 terms for short periodic perturbations and neglects terms of the order of $(\frac{m_{In}}{M+m_{In}})$. It cannot fully explain all of the perturbations.

5.4 Comparing accuracy of the 'Combined analytical theory up to P_i terms' with the 'numerical model up to P_i terms'

Next, we compare the accuracy of the 'Combined analytical theory' with the 'numerical model up to P_i terms'. Both models contain up to P_i Legendre polynomials, i.e. we use the model of $\sum_{j=2}^{i} P_j$.

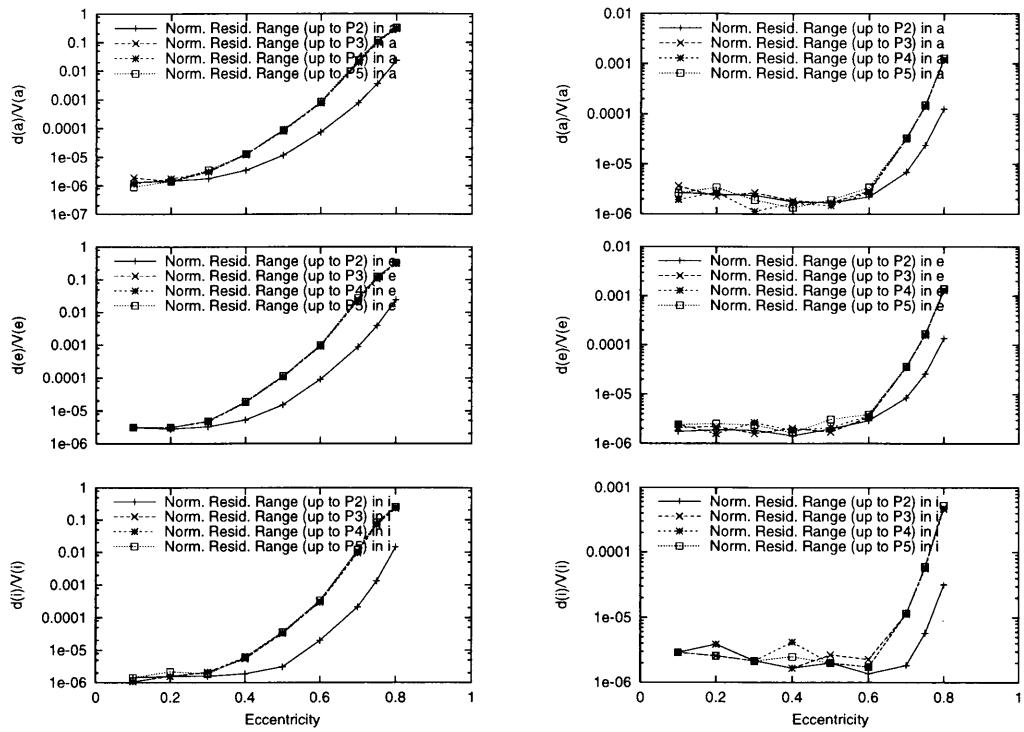

(a) (b)

Figure 5.4: Normalized residual range for the model up to P_i Legendre polynomials. (a)For $a = a_{Nereid}$ (b)for $a = 2 \times a_{Nereid}$.

The results are shown in Fig. 5.4. They show the P_3 terms decrease the accuracy of our analytical theory. In other words, the accuracy of the analytical theory is determined by one of the P_3 terms.

Chapter 6

Offset Phenomena

6.1 Some remarkable aspects of abrupt changes in orbital elements (Offset phenomena)

As we have already seen in the previous chapter, offsets in the orbital elements are observed when Nereid passes its pericenter. In this chapter, we discuss the phenomena in detail. Hereafter, we use the following terminologies (see also Fig. 6.1):

- **offset:** ΔE a difference of the values of an orbital element between the successive revolutional periods
- **offset range** a range of offset levels of an orbital element during an integration period

An offset is designated by ΔE for brevity. ΔEs are computed from the results of numerical integrations (the same model that we called "full numerical" in the previous chapters). However, the magnitude of offset cannot be measured accurately at the Nereid's pericenter passage, because it is superimposed by large fluctuations of the orbital elements caused by perturbations of Triton. Instead, we take ΔEs as differences of averaged orbital elements near Nereid's apocenter between the successive orbital revolutions.

In this chapter, we use initial values in Table 6.1. An integration period is 40000 [days] ($\sim$ 110 [yrs]).

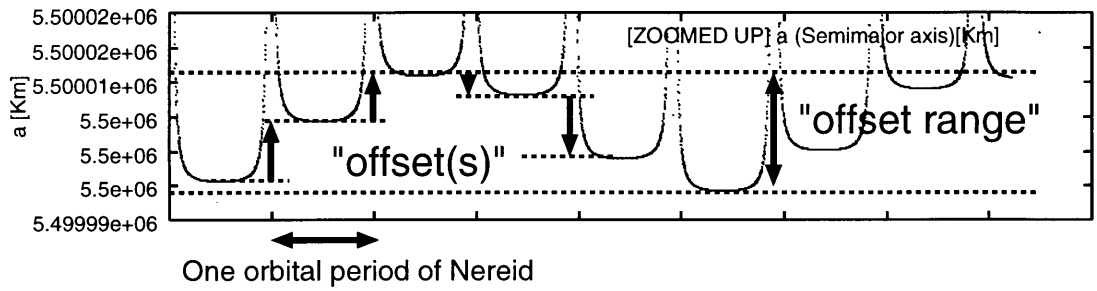

Figure 6.1: Definition of offset and range in this study.

Table 6.1: Initial values for numerical integrations. The inclination of Nereid refers to the orbital plane of Triton. [R_{Nep}] is Neptune's radius, 24764[Km]. (*) Two cases (prograde and retrograde) are considered for the planar model.

Item	Planar model	Inclined model
Semimajor axis [Km]	5.5×10^6	5.5×10^6
Eccentricity	0.75	0.75
Inclination [deg]	0.0	132.4
Longitude of ascending node [deg]	-	0.0
Argument of pericenter [deg]	0.0	0.0
Initial longitude of Nereid [deg]	0.0	0.0
Semimajor axis of Triton [R_{Nep}]	14.15	14.15
Eccentricity of Triton	0.0	0.0
Inclination of Triton [deg]	0.0/180.0 (*)	0.0

6.2 Longitude of Triton at the time of Nereid's pericenter passage

Firstly, we observe the raw result of numerical integration for the inclined problem for a long timespan (nearly 100 [yrs]) and show it in Fig. 6.2. This reveals that osculating elements a, e and I do NOT increase with time, i.e. they do not have secular trends, but they stay in fixed ranges, fluctuating with a periodicity of several revolutions of Nereid.

In our numerical calculations, Triton moves

62.18 revolutions

in one orbital period of Nereid. (If we use mostly accepted values of orbital elements or constants, Triton revolves about $61\frac{1}{4}$ times per one orbital period of Nereid.) Thus, when Nereid returns to the pericenter, the longitude of Triton proceeds about 66 degrees. The longitude of Triton at the time of Nereid's pericenter passage have the same period as the fluctuations in ΔE. It seems that Triton's phase at the Nereid's pericenter passage affects the offset phenomena. To ensure this hypothesis, we will continue to observe offsets in more detail.

6.3 Some remarks on numerical results

To clarify the relation of ΔE to Triton's phase, we depict ΔE versus the longitude of Triton at the time of Nereid's pericenter passage λ^0_{Tri}. Hereafter, we refer to this as "ΔE-λ^0_{Tri} plot." The results are shown in Fig. 6.3. We can easily show a strong correlation between ΔE and λ^0_{Tri}.

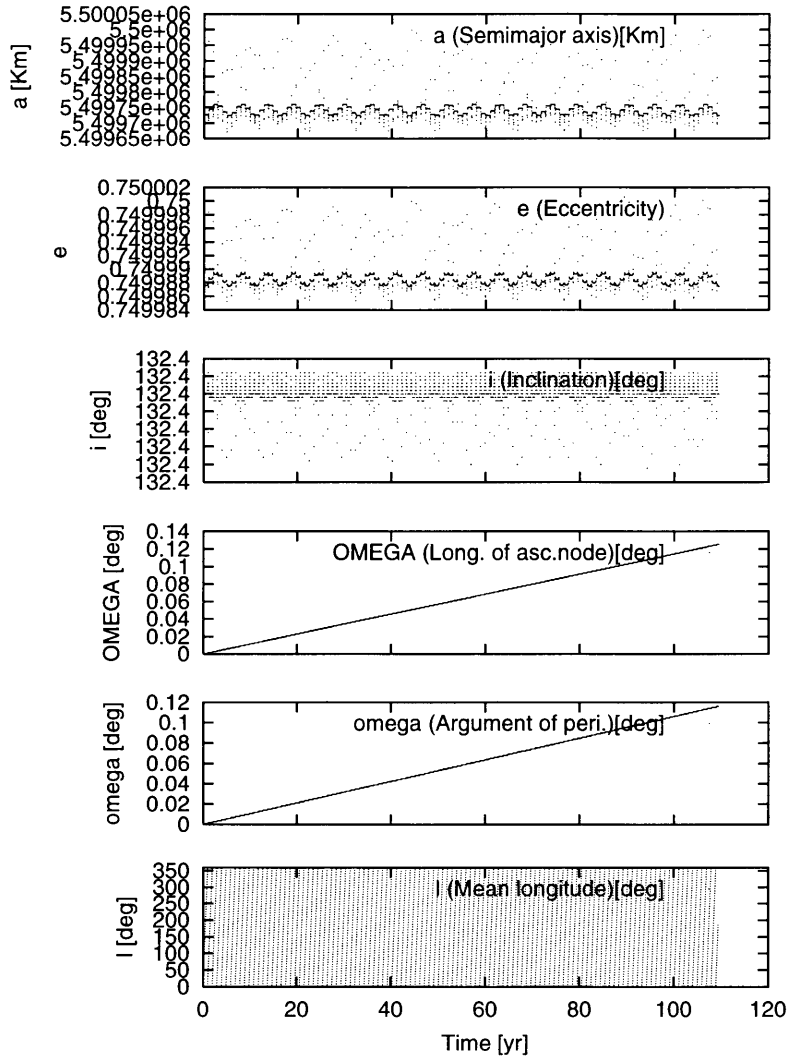

Figure 6.2: Time variations of the orbital elements for the inclined problem.

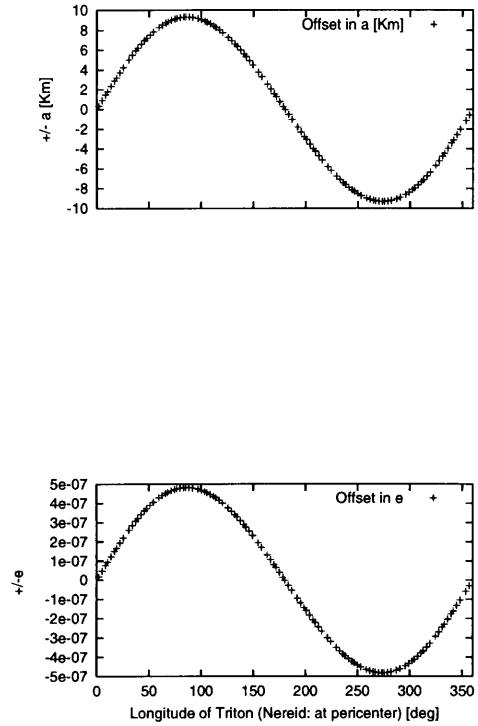

(a) (Planar, Prograde)

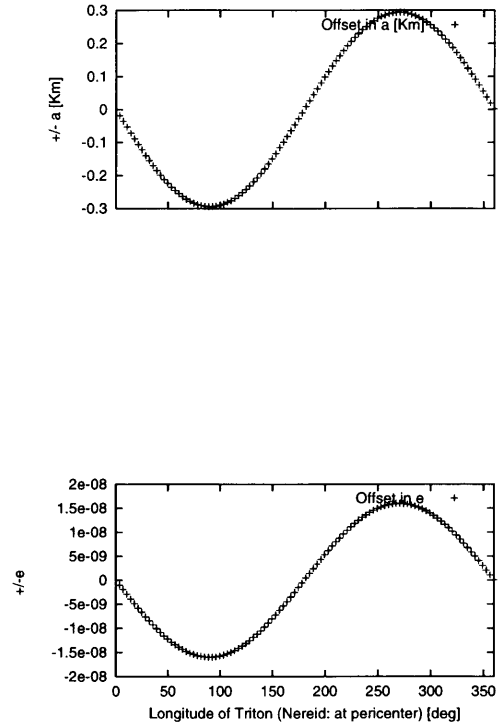

(b) (Planar, Retrograde)

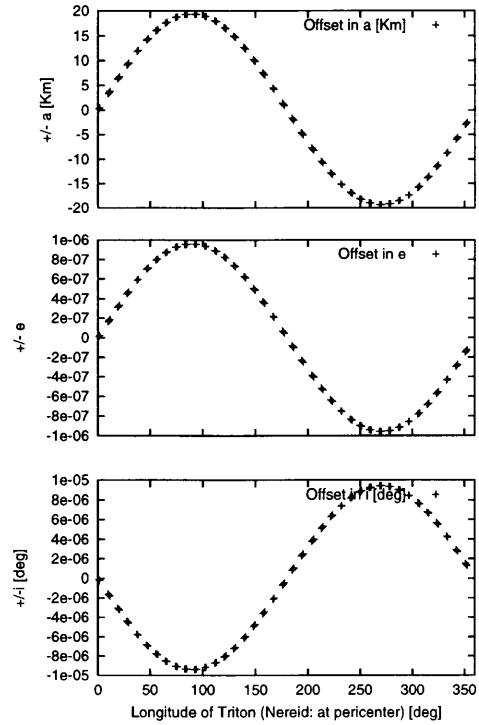

(c) (Inclined)

Figure 6.3: Offsets ΔE versus the longitude of Triton at the time of Nereid's pericenter passage λ^0_{Tri}. For the planar problem, Nereid orbits (a)in direct (b)in retrograde. (c)For the inclined problem.

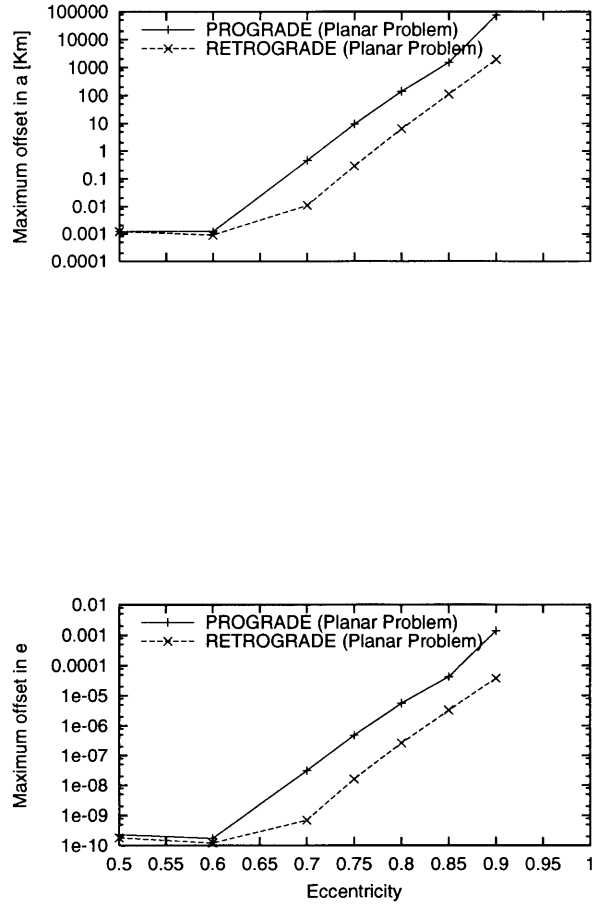

Figure 6.4: Maximum offsets $\Delta E_{\max}$ versus the eccentricity (the planar case).

6.3.1 Growth of offsets with eccentricity

If we change the initial values of Nereid's eccentricity, the offsets are vastly altered (see Figs. 6.5 and 6.6 for the planar problem and Fig. 6.7 for the inclined problem). Results are summarized in Table 6.2 and Fig. 6.4. Generally speaking, as the eccentricity of Nereid increases, ΔEs increase drastically. For $e \geq 0.6$, $\Delta E_{\max}$ exponentially increases with eccentricity.

The shapes of ΔE-λ^0_{Tri} plot show sinusoid-like curves, but they are severely distorted due to the high eccentricity for Nereid.

We notice that the shape of the Δa-λ^0_{Tri} plot is similar to that of the Δe-λ^0_{Tri} plot. Interestingly, that of the ΔI-λ^0_{Tri} is in antiphase to the former two plots.

6.3.2 Growth of offsets with mutual velocity between Nereid and Triton

In the previous section, initial conditions of the eccentricity of Nereid are varied, however, it is not so clear to what these offsets can be attributed whether, as the eccentricity increases, (1) the orbital velocity of Nereid at its pericenter increases or (2) the disturbing force from Triton

Table 6.2: Offsets in orbital elements when the eccentricity is changed. Since offsets vary with λ^0_{Tri}, $\Delta E_{\max}$ is taken as the maximum value of ΔE among λ^0_{Tri}s.

(a) Planar problem (Prograde)

Eccentricity	Offset range		Maximum offset	
	a [Km]	e	$\Delta a_{\max}$ [Km]	$\Delta e_{\max}$
0.1	4.1×10^{-3}	1.2×10^{-9}	4.0×10^{-3}	1.2×10^{-9}
0.3	2.5×10^{-3}	5.7×10^{-10}	2.2×10^{-3}	5.2×10^{-10}
0.5	1.4×10^{-3}	2.6×10^{-10}	1.2×10^{-3}	2.3×10^{-10}
0.6	1.4×10^{-3}	2.0×10^{-10}	1.2×10^{-3}	1.7×10^{-10}
0.7	8.7×10^{-1}	5.6×10^{-8}	4.7×10^{-1}	3.1×10^{-8}
0.75	1.7×10	8.8×10^{-7}	9.3	4.8×10^{-7}
0.8	2.2×10^{2}	8.9×10^{-6}	1.4×10^{2}	5.6×10^{-6}
0.85	1.6×10^{3}	4.6×10^{-5}	1.5×10^{3}	4.3×10^{-5}
0.9	3.9×10^{5}	7.4×10^{-3}	7.5×10^{4}	1.4×10^{-3}

(b) Planar problem (Retrograde)

Eccentricity	Offset range		Maximum offset	
	a [Km]	e	$\Delta a_{\max}$ [Km]	$\Delta e_{\max}$
0.1	3.1×10^{-3}	1.1×10^{-9}	2.4×10^{-3}	9.9×10^{-10}
0.3	1.9×10^{-3}	4.6×10^{-10}	1.9×10^{-3}	4.0×10^{-10}
0.5	1.3×10^{-3}	1.9×10^{-10}	1.2×10^{-3}	1.8×10^{-10}
0.6	9.8×10^{-4}	1.3×10^{-10}	9.0×10^{-4}	1.2×10^{-10}
0.7	1.9×10^{-2}	1.3×10^{-9}	1.1×10^{-2}	7.0×10^{-10}
0.75	5.5×10^{-1}	3.0×10^{-8}	2.9×10^{-1}	1.6×10^{-8}
0.8	1.2×10	5.1×10^{-7}	6.3	2.6×10^{-7}
0.85	2.4×10^{2}	7.5×10^{-6}	1.1×10^{2}	3.3×10^{-6}
0.9	4.9×10^{3}	9.8×10^{-5}	1.9×10^{3}	3.8×10^{-5}

(c) Inclined problem

Eccentricity	Offset range			Maximum offset		
	a [Km]	e	I [deg]	$\Delta a_{\max}$ [Km]	$\Delta e_{\max}$	$\Delta I_{\max}$ [deg]
0.1	8.6×10^{-3}	2.4×10^{-9}	5.6×10^{-8}	8.2×10^{-3}	2.3×10^{-9}	5.4×10^{-8}
0.3	2.3×10^{-3}	1.0×10^{-9}	3.0×10^{-8}	2.1×10^{-3}	8.9×10^{-10}	2.7×10^{-8}
0.5	5.3×10^{-4}	8.9×10^{-10}	3.4×10^{-8}	4.3×10^{-4}	3.5×10^{-10}	1.5×10^{-8}
0.6	4.6×10^{-3}	1.9×10^{-9}	8.6×10^{-8}	2.6×10^{-3}	4.2×10^{-10}	1.4×10^{-8}
0.7	2.8	1.8×10^{-7}	1.7×10^{-6}	1.5	9.3×10^{-8}	7.2×10^{-7}
0.75	3.6×10	1.8×10^{-6}	1.8×10^{-5}	1.9×10	9.6×10^{-7}	9.4×10^{-6}
0.8	3.2×10^{2}	1.2×10^{-5}	1.6×10^{-4}	1.7×10^{2}	6.5×10^{-6}	8.4×10^{-5}
0.85	2.1×10^{3}	5.8×10^{-5}	1.1×10^{-3}	1.1×10^{3}	3.1×10^{-5}	5.5×10^{-4}
0.9	3.2×10^{4}	6.0×10^{-4}	1.5×10^{-2}	9.7×10^{3}	1.8×10^{-4}	4.5×10^{-3}

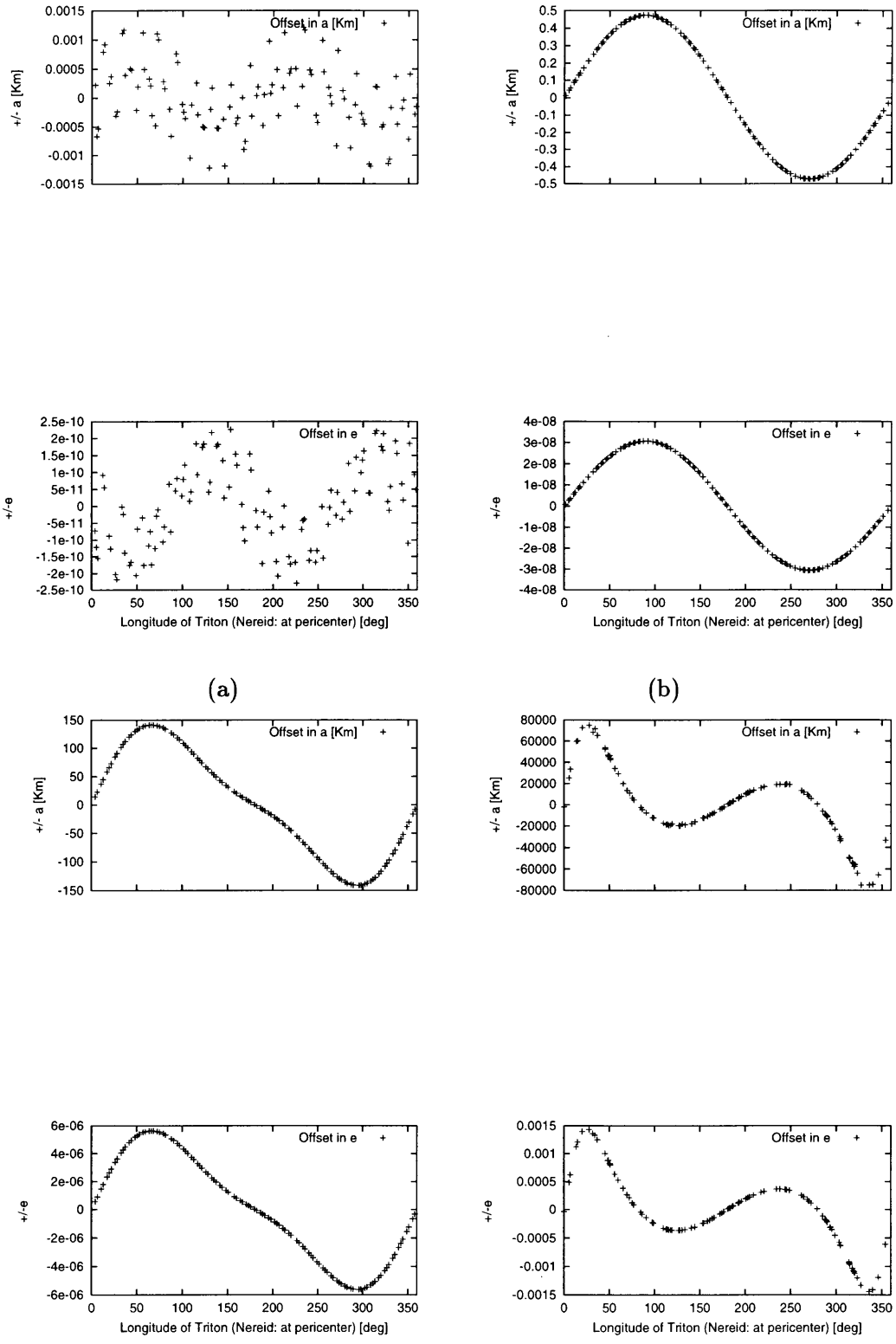

Figure 6.5: Offsets ΔE versus the longitude of Triton at the time of Nereid's pericenter passage λ^0_{Tri} when the eccentricity of Nereid changes (the planar prograde case). (a)$e = 0.5$, (b)$e = 0.7$, (c)$e = 0.8$, (d)$e = 0.9$.

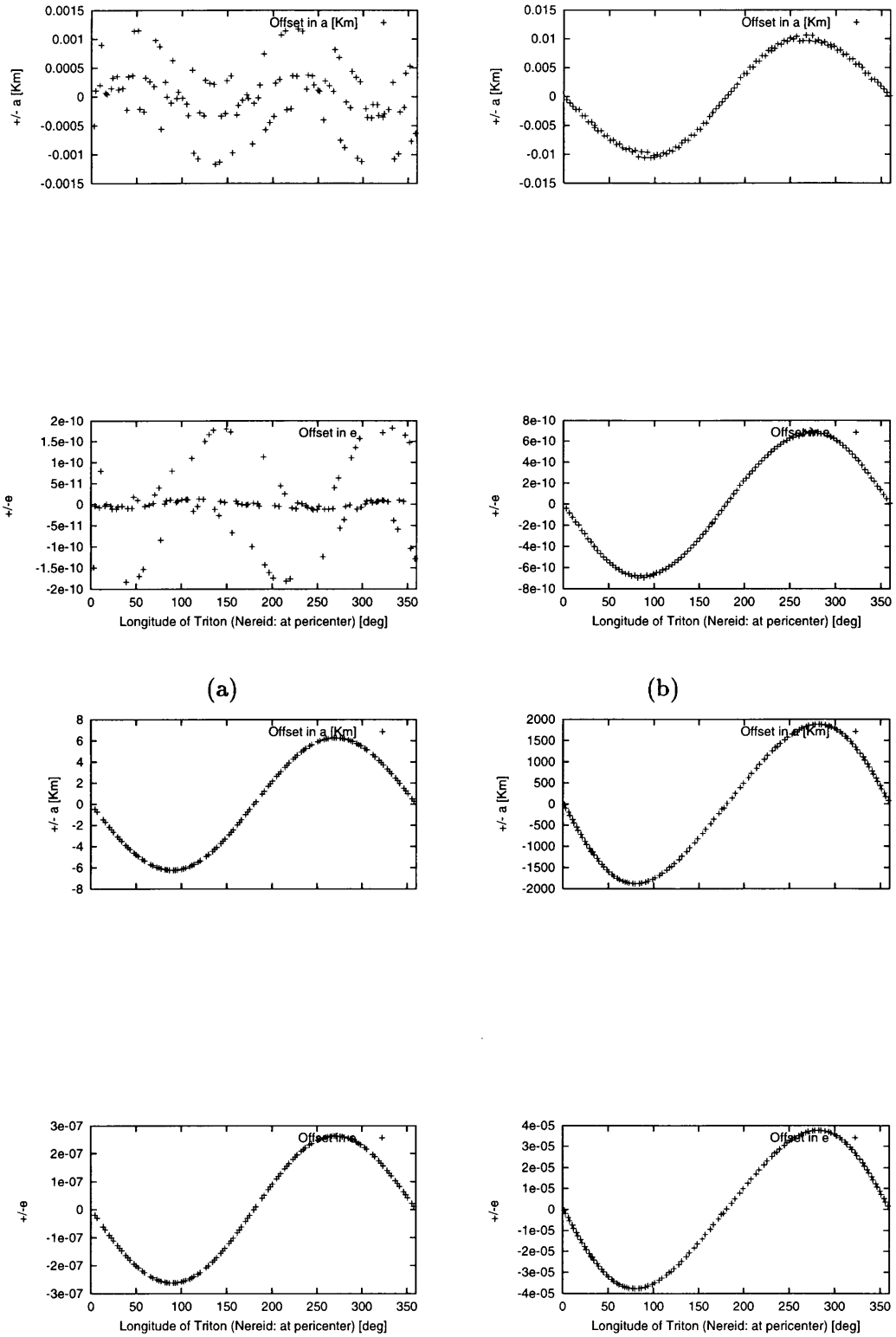

Figure 6.6: Offsets ΔE versus the longitude of Triton at the time of Nereid's pericenter passage λ^0_{Tri} when the eccentricity of Nereid changes (the planar retrograde case). (a)$e = 0.5$, (b)$e = 0.7$, (c)$e = 0.8$, (d)$e = 0.9$.

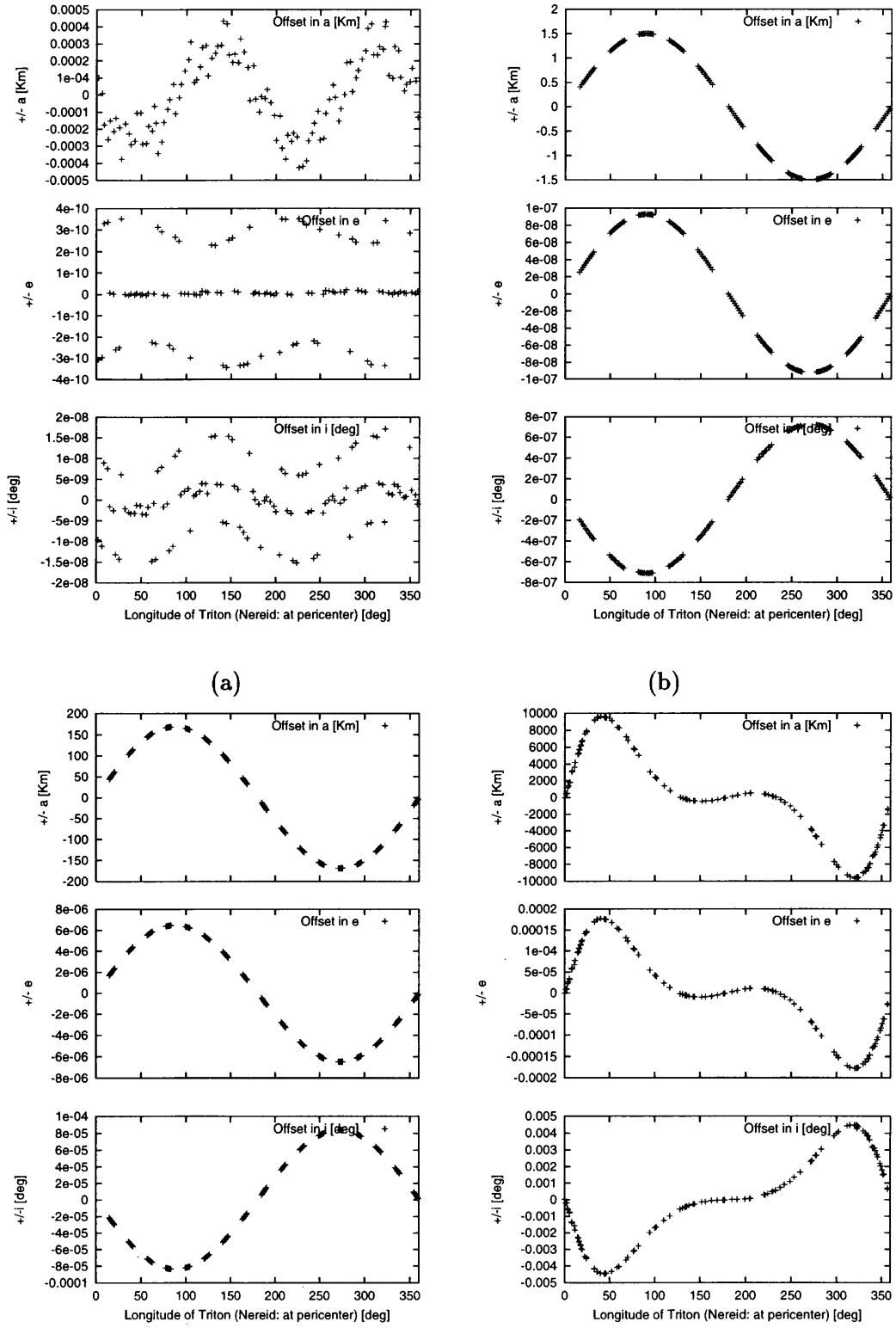

Figure 6.7: Offsets ΔE versus the longitude of Triton at the time of Nereid's pericenter passage λ^0_{Tri} when the eccentricity of Nereid changes (the inclined case). (a)$e = 0.5$, (b)$e = 0.7$, (c)$e = 0.8$, (d)$e = 0.9$.

(or Neptune) increases since Nereid approaches to Triton more closely, etc.

Here, the orbital velocity of Triton (or Neptune) is changed, while the initial value of the eccentricity of Nereid is fixed at 0.75. This is equivalent to the mutual velocity of Nereid to Triton being changed.

The models are listed in Table 6.3, and ΔE-λ^0_{Tri} plots are shown in Fig. 6.8.

For the sake of brevity, we discuss only the planar case from here on.

If the mean motion of Triton is large enough ($2n_{Tri}$), large offsets are not observed for any λ^0_{Tri} (Fig. 6.8 (a)). However, as n_{Tri} decreases, the magnitude of offsets is increased, and their ΔE-λ^0_{Tri} plots show profiles highly distorted from sinusoidal curves (Fig. 6.8 (b) and (c)). Rather, they seem to be double-sinusoidals. The direction of the orbital motion of Triton is reversed (i.e. in retrogradal motion), offsets are decreased, and the plots exhibit (reversed) sinusoids again (Fig. 6.8 (d)). Through these numerical experiments, large offsets are observed when the mean motion of Triton is near $\frac{1}{4}n_{Tri}$.

Now, we estimate the orbital angular velocity of Nereid at its pericenter. The angular orbital velocity to its focus (Neptune) is equivalent to $\frac{df}{dt}$. The value is derived as:

$$\begin{aligned} \frac{df}{dt} &= \frac{a^2 n\eta}{r^2} \\ &= \frac{n}{\eta^3}(1+e\cos f)^2, \end{aligned}$$

and at its pericenter, $f = 0$,

$$\begin{aligned} \left.\frac{df}{dt}\right|_{f=0} &= \frac{(1+e)^2}{\eta^3} n \\ &\sim 10.583n. \end{aligned}$$

In the case of the Neptunian system, $\frac{n}{n_{Tri}} \sim \frac{1}{60}$, therefore, the angular velocity of Nereid is:

$$\left.\frac{df}{dt}\right|_{f=0} \sim \frac{1}{6} n_{Tri}.$$

When the angular velocity of Nereid at its pericenter is close to that of Triton, the maximum offsets are observed.

6.4 Summary of observed offsets

We have seen the observational aspects of offsets. If we summarize the facts:

- The magnitude of offsets varies with the spatial configuration of Triton and Nereid.
- The magnitude of offsets varies with the mutual velocity of Triton and Nereid.
- A Δa-λ^0_{Tri} plot has a similar shape to a Δe-λ^0_{Tri} plot and exhibits an antiphased shape compared with a ΔI-λ^0_{Tri} plot.
- For the case of λ^0_{Tri} =0[deg] or 180[deg], no offset is observed. ΔE-λ^0_{Tri} plots exhibit antisymmetric feature against λ^0_{Tri} =0[deg] or 180[deg].

Table 6.3: Offsets in orbital elements when the mean motion of Triton is changed, i.e. the mutual velocity of Triton and Nereid is changed. Offsets are taken as the maximum values since offsets vary with λ^0_{Tri}.

(a) Planar problem

Model	Mean motion of Triton	Offset range		Maximum offset	
		a [Km]	e	$\Delta a_{\max}$ [Km]	$\Delta e_{\max}$
(A)	$2n_{Tri}$	1.4×10^{-2}	7.3×10^{-10}	1.3×10^{-2}	6.6×10^{-10}
(B)	n_{Tri} (prograde)	1.7×10	8.8×10^{-7}	9.3	4.8×10^{-7}
(C)	$\frac{1}{2}n_{Tri}$	5.8×10^{2}	2.9×10^{-5}	3.0×10^{2}	1.5×10^{-5}
(D)	$\frac{1}{4}n_{Tri}$	5.9×10^{3}	2.8×10^{-4}	2.6×10^{3}	1.2×10^{-4}
(E)	$\frac{1}{8}n_{Tri}$	3.2×10^{3}	1.4×10^{-4}	3.1×10^{3}	1.3×10^{-4}
(F)	$-\frac{1}{8}n_{Tri}$	5.4×10	3.4×10^{-6}	3.8×10	2.4×10^{-6}
(G)	$-\frac{1}{4}n_{Tri}$	2.7×10	1.6×10^{-6}	2.7×10	1.6×10^{-6}
(H)	$-\frac{1}{2}n_{Tri}$	2.8×10	1.6×10^{-6}	7.7	4.3×10^{-7}
(I)	$-n_{Tri}$ (retrograde)	5.5×10^{-1}	3.0×10^{-8}	2.9×10^{-1}	1.6×10^{-8}

(b) Inclined problem

Model	Mean motion of Triton	Offset range			Maximum offset		
		a [Km]	e	I [deg]	$\Delta a_{\max}$ [Km]	$\Delta e_{\max}$	$\Delta I_{\max}$ [deg]
(A)	$2n_{Tri}$	1.0×10^{-1}	1.6×10^{-8}	1.1×10^{-6}	9.4×10^{-2}	4.9×10^{-9}	$- - -$
(B)	n_{Tri}	3.6×10	1.8×10^{-6}	1.8×10^{-5}	1.9×10	9.6×10^{-7}	9.4×10^{-6}
(C)	$\frac{1}{2}n_{Tri}$	3.9×10^{2}	1.9×10^{-5}	3.2×10^{-4}	1.1×10^{2}	5.3×10^{-6}	8.9×10^{-5}
(D)	$\frac{1}{4}n_{Tri}$	5.1×10^{2}	2.5×10^{-5}	5.1×10^{-4}	2.2×10^{2}	1.1×10^{-5}	2.5×10^{-4}
(E)	$\frac{1}{8}n_{Tri}$	3.3×10^{2}	1.6×10^{-5}	5.8×10^{-4}	3.3×10^{2}	1.6×10^{-5}	5.7×10^{-4}
(F)	$-\frac{1}{8}n_{Tri}$	2.3×10^{3}	1.0×10^{-4}	1.3×10^{-3}	2.2×10^{3}	9.9×10^{-5}	1.2×10^{-3}
(G)	$-\frac{1}{4}n_{Tri}$	4.5×10^{3}	2.2×10^{-4}	1.0×10^{-3}	1.8×10^{3}	8.5×10^{-5}	3.4×10^{-4}
(H)	$-\frac{1}{2}n_{Tri}$	8.3×10^{2}	3.8×10^{-5}	3.0×10^{-4}	3.6×10^{2}	1.7×10^{-5}	9.5×10^{-5}
(I)	$-n_{Tri}$	1.2×10^{2}	5.8×10^{-6}	2.5×10^{-5}	6.5×10	3.2×10^{-6}	1.3×10^{-5}

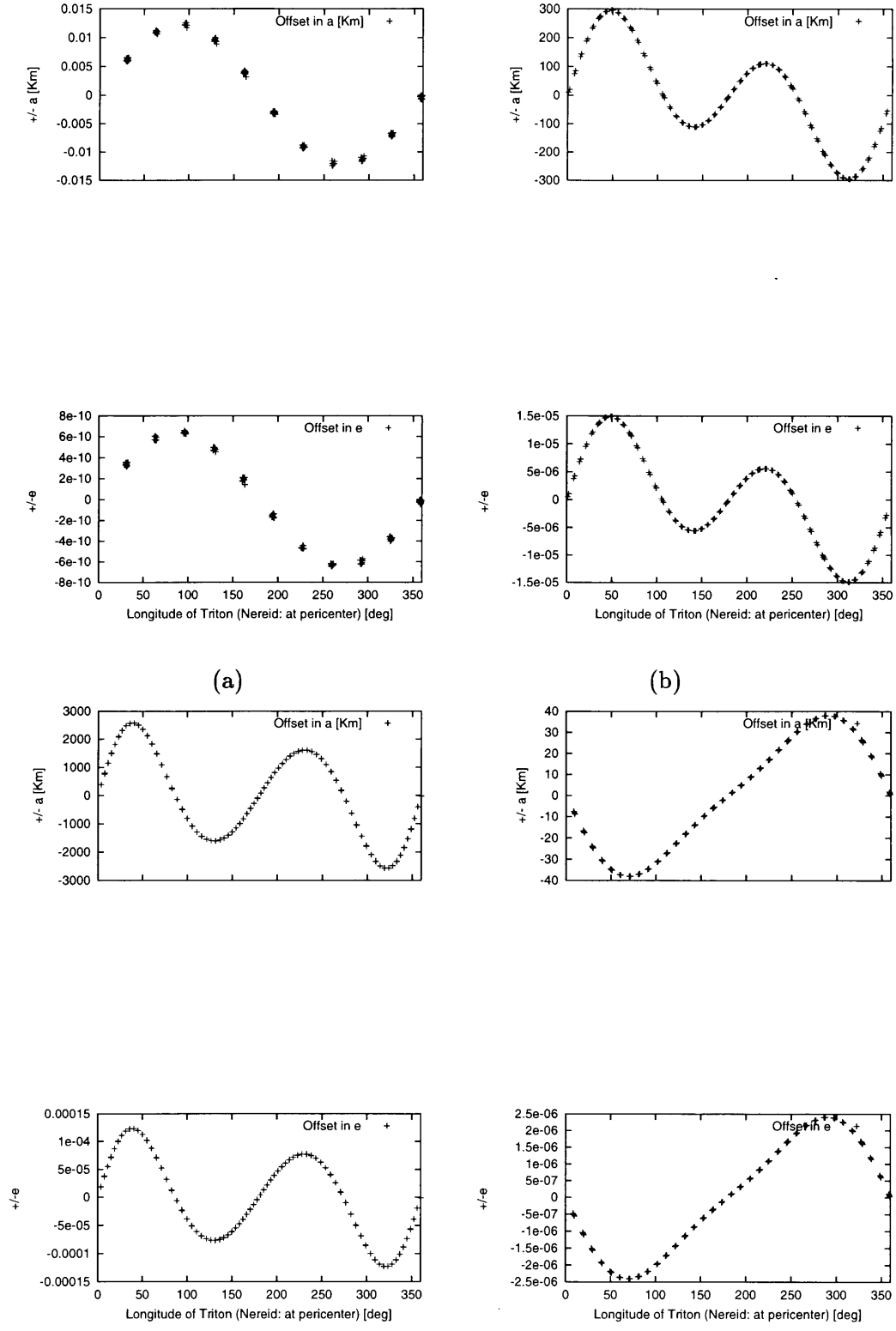

Figure 6.8: Offsets ΔE versus the longitude of Triton at the time of Nereid's pericenter passage λ^0_{Tri} when the mean motion of Triton is changed (the planar case). (a)$2n_{Tri}$, (b)$\frac{1}{2}n_{Tri}$, (c)$\frac{1}{4}n_{Tri}$, (d)$-\frac{1}{8}n_{Tri}$.

6.5 Theoretical interpretation of offsets

6.5.1 Jacobi integral and Tisserand criterion

Now we introduce the Jacobi integral or the Tisserand criterion. The primary and the secondary bodies (whose mass m_1 and m_2 respectively, and the mutual distance a_c) orbit circularly around a common barycenter with the common angular velocity n_c. A mass-less body (apart r_1 from the primary and r_2 from the secondary) moves around them (i.e. restricted three body problem). If we ride on the corotating coordinate system of (X, Y, Z) with the primary and the secondary, the motion of the third body can be described as follows:

$$\frac{1}{2}[(\dot{X})^2 + (\dot{Y})^2 + (\dot{Z})^2] + U^* = const.,$$

where

$$U^* = -n_c^2 \left[\frac{m_1}{m_1 + m_2} \frac{a_c^3}{r_1} + \frac{m_2}{m_1 + m_2} \frac{a_c^3}{r_2} \right] - \frac{1}{2} n_c^2 (X^2 + Y^2).$$

This invariant is called the Jacobi integral.

If $m_2 \ll m_1$, the value of $\frac{m_2}{m_1}$ is negligible, then, in the inertial coordinate system, the third body's orbital elements a, e and I are satisfied the following equation,

$$\frac{a_c}{2a} + \sqrt{\frac{a}{a_c}(1 - e^2)} \cos I \sim const.$$

which is called the Tisserand criterion.

In the prograde planar problem, $\cos I = 1$, the Tisserand criterion is reduced to

$$\frac{a_c}{2a} + \sqrt{\frac{a}{a_c}(1 - e^2)} \sim const..$$

We take variations in a and e,

$$\frac{1}{2} \left[-\frac{a_c}{a^2} + \sqrt{\frac{1 - e^2}{a a_c}} \right] \delta a \sim \left[\sqrt{\frac{a}{a_c}} \frac{1}{1 - e^2} \right] e \delta e$$

is derived.

In the Neptunian system, substituting numerical values for them,

$$\delta a[\mathrm{Km}] \sim 1.93 \times 10^7 \delta e$$

which means offsets in a are proportional to those in e, which is true in our results as we have seen in the previous sections.

In the case of retrograde motion ($\cos I = -1$), then

$$\delta a[\mathrm{Km}] \sim 1.84 \times 10^7 \delta e$$

is obtained.

We estimate $\delta a_{\max}^{Est}$ from the observed $\Delta e_{\max}$ in Table 6.4. These agree with the observed $\delta a_{\max}^{Obs}$.

These facts show that offset phenomena occur in the theoretical framework of restricted three-body problems. Offsets are NOT the products of numerical errors.

Table 6.4: Estimated offsets in semimajor axis from those in eccentricity.

(a) Planar problem (Prograde)

Eccentricity	Estimation by Tisserand criterion			Observation
	$\Delta e_{\max}^{Obs}$	Factor	$\Delta a_{\max}^{Est}$ [Km]	$\Delta a_{\max}^{Obs}$ [Km]
0.1	1.2×10^{-9}	1.12936×10^{6}	1.4×10^{-3}	4.0×10^{-3}
0.3	5.2×10^{-10}	3.68855×10^{6}	1.9×10^{-3}	2.2×10^{-3}
0.5	2.3×10^{-10}	7.47208×10^{6}	1.7×10^{-3}	1.2×10^{-3}
0.6	1.7×10^{-10}	1.05241×10^{7}	1.8×10^{-3}	1.2×10^{-3}
0.7	3.1×10^{-8}	1.54459×10^{7}	4.8×10^{-1}	4.7×10^{-1}
0.75	4.8×10^{-7}	1.93270×10^{7}	9.3	9.3
0.8	5.6×10^{-6}	2.51177×10^{7}	1.4×10^{2}	1.4×10^{2}
0.85	4.3×10^{-5}	3.47547×10^{7}	1.5×10^{3}	1.5×10^{3}
0.9	1.4×10^{-3}	5.41012×10^{7}	7.6×10^{4}	7.5×10^{4}

(b) Planar problem (Retrograde)

Eccentricity	Estimation by Tisserand criterion			Observation
	$\Delta e_{\max}^{Obs}$	Factor	$\Delta a_{\max}^{Est}$ [Km]	$\Delta a_{\max}^{Obs}$ [Km]
0.1	9.9×10^{-10}	1.09344×10^{6}	1.1×10^{-3}	2.4×10^{-3}
0.3	4.0×10^{-10}	3.56625×10^{6}	1.4×10^{-3}	1.9×10^{-3}
0.5	1.8×10^{-10}	7.19964×10^{6}	1.3×10^{-3}	1.2×10^{-3}
0.6	1.2×10^{-10}	1.01093×10^{7}	1.2×10^{-3}	9.0×10^{-4}
0.7	7.0×10^{-10}	1.47655×10^{7}	1.0×10^{-2}	1.1×10^{-2}
0.75	1.6×10^{-8}	1.84096×10^{7}	2.9×10^{-1}	2.9×10^{-1}
0.8	2.6×10^{-7}	2.38064×10^{7}	6.2	6.3
0.85	3.3×10^{-6}	3.26956×10^{7}	1.1×10^{2}	1.1×10^{2}
0.9	3.8×10^{-5}	5.02513×10^{7}	1.9×10^{3}	1.9×10^{3}

6.5.2 Gauss' planetary equations

A perturbing force F is applied to Nereid, and its orbital elements never remain in constant values. Changes in the orbital elements are expressed by Gauss' planetary equations. They state: if we decompose F into the three components of (T, N, W), where

- T : a component tangential to the orbit
- N : a component perpendicular to T and on the orbital plane
- W : a component perpendicular to the orbital plane .

Then, changes in the orbital elements are:

$$\begin{aligned}
\frac{da}{dt} &= \frac{2A}{n\eta}T \\
\frac{de}{dt} &= \frac{\eta}{naA}[\{2(e+\cos f)\}T - \{\frac{r}{a}\sin f\}N] \\
\frac{dI}{dt} &= \frac{r}{na^2\eta}\{\cos(f+\omega)\}W,
\end{aligned}$$

and $A = \sqrt{1+2e\cos f+e^2}$.

Hereafter, we discuss offset phenomena with use of these equations.

6.5.3 Impulsive perturbing force model at pericenter

Now we suppose that an impulsive force $\mathrm{F}_{Imp}(T_{Imp}, N_{Imp}, W_{Imp})$ acts on Nereid at the instant of pericenter passage. Substituting $f = 0$ in Gauss' planetary equations, then

$$\begin{aligned}
\frac{da}{dt} &= \frac{2A_0}{n\eta}T_{Imp} \\
\frac{de}{dt} &= 2\frac{\eta}{na}T_{Imp} \\
\frac{dI}{dt} &= \frac{r}{na^2\eta}\{\cos\omega\}W_{Imp},
\end{aligned}$$

and $A_0 = 1 + e$. If the presumption is true,

$$\Delta a \propto T_{Imp}$$

is satisfied.

However, as we have already seen in the previous sections, results show that Δa for the direct motion is different from that for the retrograde motion. Thus T_{Imp} for the direct motion differs from the one for the retrograde model in spite of having the same spatial configuration of the three bodies at the time. Therefore, this model does not work well in describing offset phenomena in general.

6.5.4 Cumulative effect of perturbing force

Next, we consider cumulative effects of the orbital change during Nereid stays near pericenter. That is, we sum up the variation during a pericenter passage over an orbital period.

$$\mathcal{D}_E \equiv \int_{-\frac{P}{2}}^{\frac{P}{2}} \frac{dE}{dt} dt,$$

where P is the orbital period of Nereid and the time is measured from the pericentral passage time of Nereid. $\frac{dE}{dt}(t)$ is given by Gauss' planetary equations. In other words, $\mathcal{D}_E$ is the net gain of the orbital element E per Nereid revolution.

First, for the planar model, we evaluate the value of

$$\mathcal{D}_a = \int_{-\frac{P}{2}}^{\frac{P}{2}} \frac{da}{dt} dt$$

$$\mathcal{D}_e = \int_{-\frac{P}{2}}^{\frac{P}{2}} \frac{de}{dt} dt,$$

for a fixed value of λ^0_{Tri}. Then we change λ^0_{Tri} and plot a $\mathcal{D}_E$-λ^0_{Tri} diagram. These are shown in Figs. 6.9 and 6.10. In this calculation, we adopt $P = 360$[day]. The values of $\frac{da}{dt}$ versus time t ($\frac{da}{dt}$-t plot) for some λ^0_{Tri} are also paneled. The total area enclosed by the curve $\frac{da}{dt}(t)$ (including its sign) and the time axis gives $\mathcal{D}_a$.

Now we compare the results in Section 5.3. $\mathcal{D}_E$-λ^0_{Tri} curve is almost identical to that in ΔE-λ^0_{Tri} ! This means that observed offsets are represented by the net gains of the orbital elements per one pericenter passage of Nereid.

$\frac{da}{dt}$-t plots (only extracted in -25[day] $\leq t \leq +25$[day] for drawing) show that if the Nereid's eccentricity is high enough (for example, $e = 0.9$), an impulsive force is applied to Nereid at the instant of $t = 0$. For these models, we can deal with the offsets using an impulsive force model as discussed in the previous section.

When large offsets are observed, the $\frac{da}{dt}$-t plot shows an asymmetric feature in relation to the pericenter passage time ($t = 0$).

From these results, we convince ourselves again of the accuracy of numerical integrations by Bulirsch-Stoer in the previous chapters.

6.6 Descriptive explanation of offset phenomena — Analogy to mean motion resonance

We introduce Peale(1976)'s description of the mechanism of the mean motion resonance, because his explanation can be applied to the offset mechanism.

If the system is trapped in the mean motion resonance, the repetitious perturbing force is applied to a perturbed body in the same direction at the same location. Its orbital elements evolve in the direction such that the system is in a stable configuration. Thenafter the system librates around it.

Peale(1976) explained the mean motion resonance descriptively. For his large eccentric model, he considered two bodies orbiting about the primary: a perturbed body moving in an outer

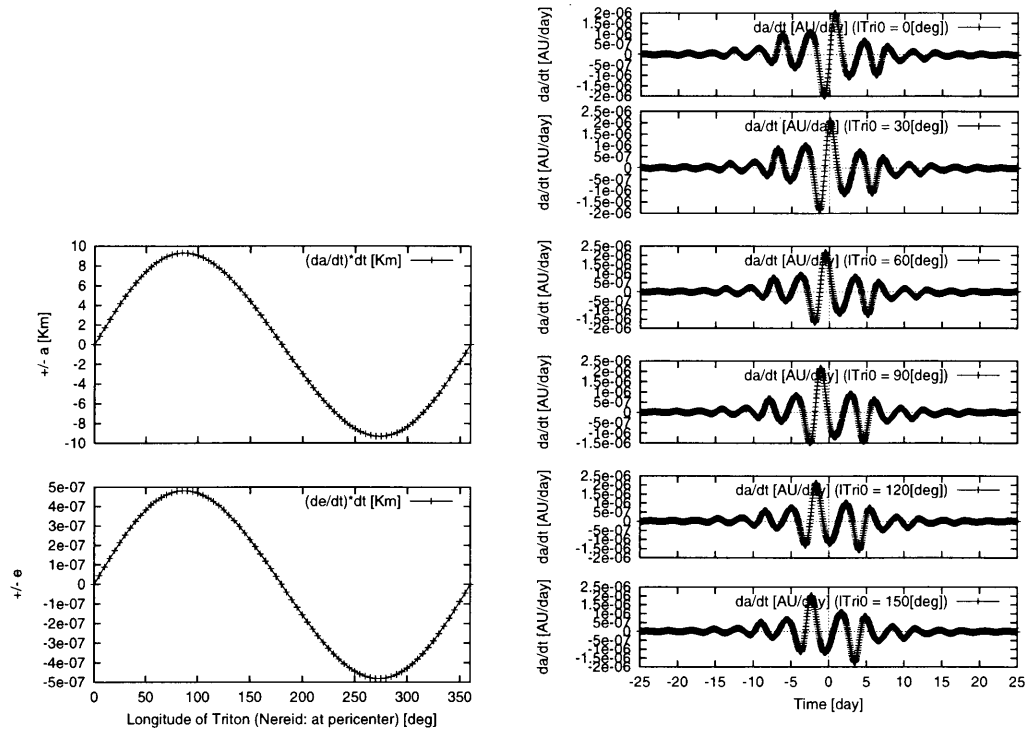

(a)

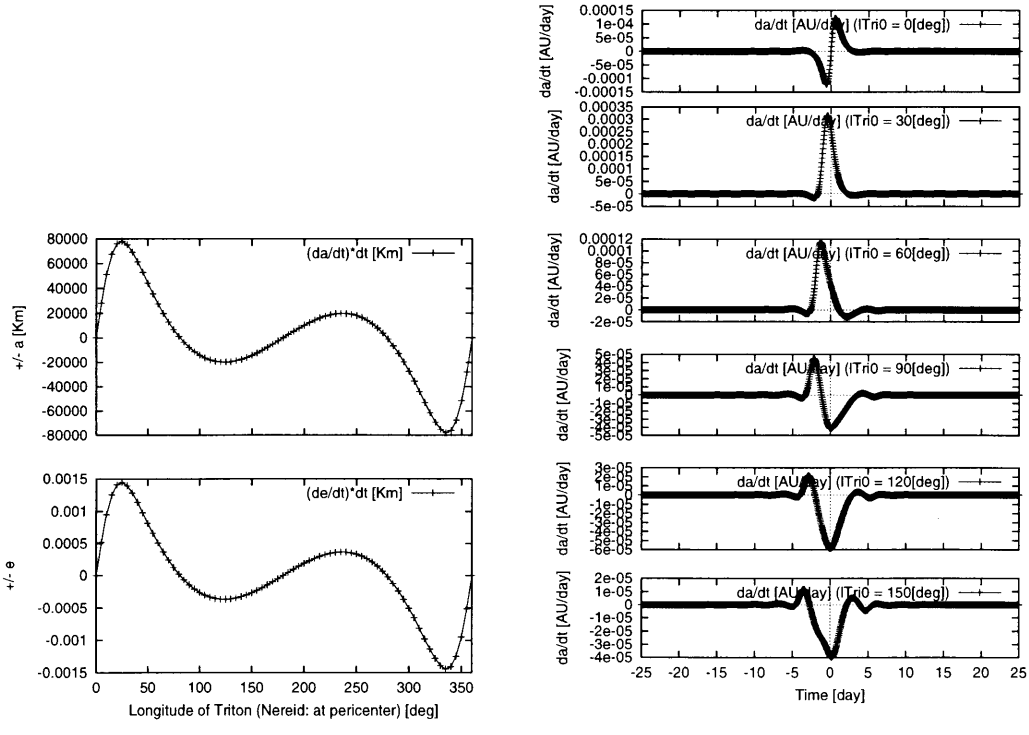

(b)

Figure 6.9: $\mathcal{D}_E$ versus the longitude of Triton at the time of Nereid's pericenter passage λ^0_{Tri} when the eccentricity of Nereid changes (planar prograde case). We define the time of pericenter passage as $Time = 0$. $\frac{da}{dt}(t)$ is also shown. (a)$e = 0.75$, (b)$e = 0.9$.

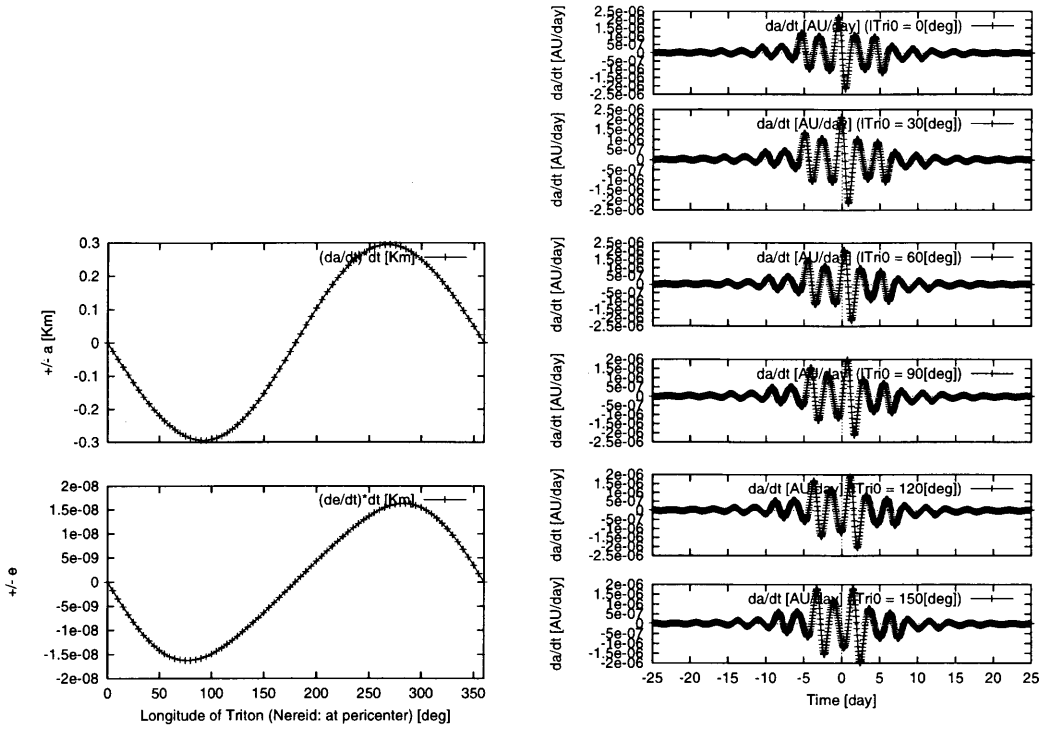

(a)

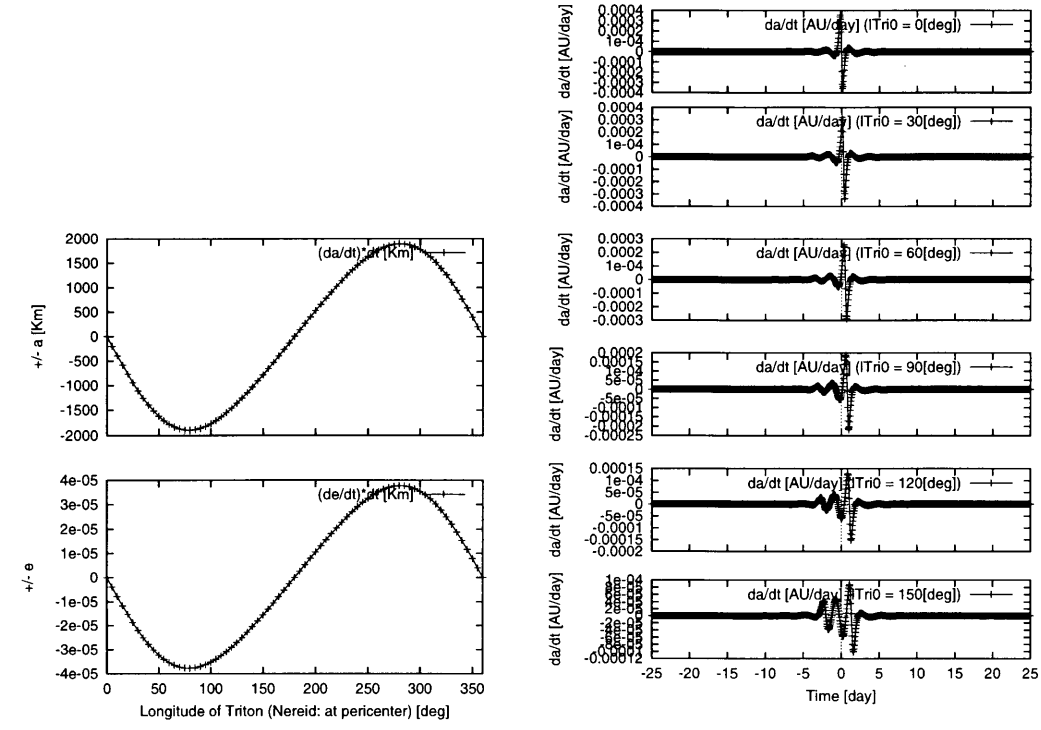

(b)

Figure 6.10: $\mathcal{D}_E$ versus the longitude of Triton at the time of Nereid's pericenter passage λ^0_{Tri} when the eccentricity of Nereid changes (planar retrograde case). We define the time of pericenter passage as $Time = 0$. $\frac{da}{dt}(t)$ is also shown. (a)$e = 0.75$, (b)$e = 0.9$.

eccentric orbit and an inner perturbing body moving in a circular orbit (see Fig. 1 of Peale (1976)). This is the same orbital configuration as in this study.

He discussed the net gain (or loss) of the outer body's angular velocity and angular momentum during the conjunction of two bodies. He showed the relation between their net gains and the longitude of the conjunction. Total amounts of the angular velocity and angular momentum will not cancel to zero except when the conjunction occurs at its pericenter or apocenter.

In the case of the mean motion resonance, the gained angular velocity and angular momentum will drive the system to a stable configuration so that the conjunction occurs at the apocenter.

In the case of Nereid, Triton and Nereid are not in resonant configuration. However, the same discussion can apply to the Nereid system. Nereid's angular velocity and angular momentum can change during the conjunction with Triton. An increase in the angular velocity means a decrease in the semimajor axis ($-\Delta a$). Similarly, an increase in the angular momentum equals a decrease in the eccentricity ($-\Delta e$). Therefore, offsets in the orbital elements are observed.

Since they are not in mean motion resonance, changes in orbital elements do not accumulate in one direction. Therefore, the orbital elements stay in some ranges. In other words, the inner and the outer bodies meet at points along their orbits. However, conjunctions occur at different longitudes at each recursion, so that successive conjunctions don't happen at the same longitude.

6.7 Study of the evolution of cometary orbits

From the ancient era onward, many comets have been recorded or observed, and after the study of Halley, their periodical appearances have attracted a great deal of attention for astronomers. However, since some comets are greatly perturbed by the giant planet, Jupiter, they do not return back to the Sun in fixed periods. Some also change their periodicities by small amounts because non-gravitational effects influence their motions.

Today, chaotic periodicity in the orbital period for long periodic comets is indicated, including Halley's Comet. A change in the orbital period directly reflects a change in the semimajor axis through $n^2a^3 = \mu$.

Carusi et.al. (1985a, 1985b, 1987) showed the results of numerical integrations of known comets and pointed out that sudden changes in orbital elements are NOT due to the close approach to giant planets, but rather, caused by indirect perturbations from giant planets (in the heliocentric coordinate system). They stated that the cometary motion is well written in the heliocentric coordinates in the neighborhood of the Sun while it refers to the barycentric system (the barycenter of the Sun and Jupiter) far from the Sun. Chirikov and Vecheslavov (1989) discussed the fact that time intervals of the perihelion passage for Halley's Comet are strongly correlated to Jupiter's phase.

Recently, Chambers (1995) pointed out that offset phenomena observed in the semimajor axis of Comet Swift-Tuttle are caused by the combined effect of (1) the displacement of the Sun from the barycenter of the Solar System and (2) the relative velocity of the Sun and the barycenter. They showed its dependency as

$$\Delta a \propto M_p \sin(\psi_p - \theta),$$

where M_p is the mass of a perturbing body (mainly explained by Jupiter), ψ_p is its longitude when the comet passes its perihelion and θ is a parameter of orbital configurations.

These models are similar to our study in the sense that offsets in orbital elements are observed for a body moving in a highly eccentric orbit. The analogous configurations are:

Primary:	Neptune	$\leftrightarrow$	Sun
Inner:	Triton	$\leftrightarrow$	Jupiter
Outer:	Nereid	$\leftrightarrow$	Comet.

However, in these cometary studies, a comet comes inside the perturbing body's orbit, while in our model, Nereid does not enter the orbit.

Chapter 7

Discussion

7.1 Validity of neglecting higher order terms of $(\frac{m_{In}}{M+m_{In}})$

In this paper, we deal with the small factor of the order $(\frac{m_{In}}{M+m_{In}})^2$ or higher terms as negligible parameters. Here, we discuss the validity of this simplification.

From the beginning, we consider a system of a primary body with two objects orbiting around it. Therefore, the mass of the primary is large enough compared with the others, i.e.

$$\text{Mass of the primary} \gg \text{Mass of the inner (or outer)}.$$

This makes the small parameter of $\frac{m_{In\ (or\ Out)}}{M}$ such that

$$\frac{m_{In\ (or\ Out)}}{M} \ll 1.$$

Therefore, its square can be negligible.

In practice, this simplification is valid for the system that the theory is applicable to. For the Nereid system,

$$\frac{m_{Tri}}{M} \sim 2.89 \times 10^{-4},$$

the squared value is approximately of the order of 10^{-7}. This is comparable to higher degrees of Legendre expansion of the Hamiltonian or higher orders of small parameters in canonical transformations for the short periodical variable. We only have to include the factor of $(\frac{m_{In}}{M+m_{In}})^2$ terms in the problem when we take higher small parameters in the Hamiltonian or in the canonical transformations into consideration.

For the extrasolar planetary system, it depends on each system. In the Solar System, the mass ratio of Jupiter to the sun is approximately $\sim 10^{-3}$. The typical mass for the primary star is listed in Table 7.1. The spectral type of the primary star is estimated from spectroscopic observations. On the other hand, the upper limit of the planetary mass is bounded by 13 Jupiter masses. (This is the lower limit of the mass for brown dwarfs. Recently, this classification has come to be accepted among astronomers. See Martin et.al.(1999) or Oppenheimer et.al.(2000).)

It is noted that today's search for an extrasolar planetary system is mainly directed at the sun-like stars (with spectral types of F,G,K) located in the neighborhood of our Solar System. Hence, this selectional effect biases the distribution of characters which these planetary systems have.

Table 7.1: Spectral type and its mass. The data is extracted from Allen (1973).

Spectral type	Mass $[M_\odot]$
O5	40
A0	3
F0	1.7
G0	1.1
K0	0.8
M0	0.5

If we consider a planet with Jupiter-mass around a sun-like star, the mass ratio is $\frac{m_{In}}{M+m_{In}} \sim 10^{-3}$. The upper limit of the ratio for a system in which the most massive planet revolves around a sun-like star is $\frac{m_{In}}{M+m_{In}} \sim 10^{-2}$. Therefore, it is valid to neglect the square of the mass ratio. When other extrasolar planetary systems are discovered in future, it is hoped that a large variety of the mass ratio and orbital configurations will be found.

7.2 Differences between the perturbations of Triton and Sun when constructing an analytical theory

When we build an analytical theory for Nereid under the influence of the Sun's perturbations, its perturbed Hamiltonians or generating functions of canonical transformations are rapidly converging for the small parameter. This feature is seen in the work of Mignard (1975) or Saad (2000). However, this characteristic feature no longer holds for a theory that takes into account Triton's perturbations.

This difference reflects the character of small parameters. Now we compare the small parameters for these two perturbations from the viewpoint of the speed of convergence.

The perturbing potential is depicted in a series of Legendre polynomials P_is. In the case of the Sun's perturbation, the value of one degree higher in terms of Legendre polynomials decreases by a factor of

$$\frac{r}{r_\odot} \sim 1.22 \times 10^{-3}.$$

On the other hand, in the case of Triton's perturbation, the one decreases by the factor of

$$\frac{r_{Tri}}{r} \sim \begin{cases} 0.255 & \text{(Nereid is at the pericenter)} \\ 0.0365 & \text{(Nereid is at the apocenter)} \end{cases},$$

i.e. the Sun's perturbations are more rapidly converging when the perturbed Hamiltonian is expanded in the Legendre polynomials.

Similarly, the slow-converging character of Triton's perturbations is also seen in short-periodic generating functions S_i when we evaluate Poisson brackets. In the case of the Sun's perturbations, the value of one order higher in terms of generating functions decreases by a factor of

$$\frac{n_\odot}{n} \sim 6. \times 10^{-3},$$

whereas in the case of Triton's perturbation, the one decreases by the factor of

$$\frac{n}{n_{Tri}} \sim \frac{1}{60}.$$

In practice, as we have already seen in the results section, we multiply $\frac{n_\odot}{n}$ by $\frac{(1+e\cos f)^2}{\eta^3} \sim 10.583$(Nereid is at the pericenter) for changing variables. This manipulation also prevents S_i from rapidly converging (or, uniformly converging).

Slow converging series directly bring large truncational errors. In other words, we have to take the problem up to a higher degree of small parameters into consideration to achieve a fixed accuracy.

Triton's perturbation has unwanted effects on the construction of an analytical theory of Nereid. However, there are some pleasant affects. The mass coefficient in the perturbed Hamiltonian $\frac{m_{Tri}}{M_0}$ acts as a preferable small parameter.

In the case of the Sun's perturbation,

$$\frac{m_\odot}{M_0} \sim 19412.2,$$

the value is far from the small parameter. In the case of Triton's, the value is

$$\frac{m_{Tri}}{M_0} \sim 2.89 \times 10^{-4},$$

therefore, the square of the value can be treated as negligible. If we leave out the $(\frac{m_{Tri}}{M_0})^2$ terms, the number of Poisson brackets to be evaluated can be reduced.

7.3 Configuration of celestial bodies at the time of close approach

During Nereid's orbiting near the pericenter, there is a risk of coming into close approach with Triton. Here, we introduce some introductive indicators and assess the closest distance. For a close-approaching property, two characteristic lengths are widely used.

- **Hill radius** r_H **:** The radius in which a celestial body stays forever nearby a perturbing body.
- **The sphere of action** r_{act} **:** The radius in which the ratio of tidal force to Keplerian force for a perturbing body is larger than that for the central main body. Inside this radius, a celestial body is considered to be moving about the perturbing body.

If we denote masses of central body and perturbing body as M and m, respectively, these two radii r_H and r_{act} measured from the perturbing body are expressed as follows:

$$\begin{aligned} r_H &= (\frac{m}{3M})^{\frac{1}{3}} R \\ r_{act} &= (\frac{m}{M})^{\frac{2}{5}} R, \end{aligned}$$

where R is the distance between the central and perturbing body.

Table 7.2: The closest distance between Nereid and Triton in the case that they revolve on the common plane (i.e. the planar case, $I = 0$). We adopt Nereid's semimajor axis for 222.1 $[R_{Nep}]$ ($\sim 5.5 \times 10^6$ [Km])

Eccentricity	Pericenter distance of Nereid $[R_{Nep}]$	Closest Distance $[R_{Nep}]$
0.75	55.5	41.4
0.9	22.2	8.06

Now we apply them for the Nereid system. If we adopt the values $m = 2.89 \times 10^{-4} M$ and $R = 14.15[R_{Nep}]$ (R_{Nep} is a radius of Neptune, 24,764[Km]),

$$\begin{aligned} r_H &= 0.649 R_{Nep} \quad (1.61 \times 10^4 [\text{Km}]) \\ r_{act} &= 0.534 R_{Nep} \quad (1.32 \times 10^4 [\text{Km}]), \end{aligned}$$

respectively. On the other hand, the closest mutual distance of Triton and Nereid varies with Nereid's eccentricity (see Table 7.2). Therefore, the closest distance between Nereid and Triton studied in the previous chapter is far from r_H or r_{act}, and there is no danger of falling into a close approach.

7.4 Reliability of Numerical Integration

We have checked the accuracy of our analytical theory by comparing it with the numerical results integrated by Bulirsch-Stoer. Results of numerical integrations are degraded by numerical errors, like a 'round-off'. They occur in a round-off process at the smallest digit throughout calculation. For a long-interval calculation, the result suffers severely from these errors; therefore, 'good' integration codes are for the purpose.

The Bulirsch-Stoer code used in this study is widely admitted as a highly accurate integration code for a relatively short interval (which means that it is not suited for the age of the Solar system). Murison (1989) discussed the usefulness of the code for keeping a Jacobi integral value, which is the integral for the restricted three-body problem in the corotating coordinate system with a perturbing body, throughout his numerical integration.

For its good numerical accuracy, the code is widely utilized in dynamical studies of the solar system (for example, Nakamura and Yoshikawa (1991)).

Chapter 8

Further Application of This Study

8.1 Application to the Nereid system

8.1.1 Brief description of the Nereid satellite

Nereid, a satellite of Neptune, moves on the most eccentric orbit of known satellites in the Solar system. It was discovered by Kuiper in 1949 to be the second satellite of Neptune, and has an orbital period of nearly one year.

Nereid is observed as a 19th-magnitude object close to the bright image of Neptune. Its faintness and its long orbital period have prevented astronomers from acquiring precise astrometric data, necessary for estimating orbital elements of Nereid. The semimajor axis of the orbit is about 5.5×10^6 [Km] ($\sim$ 220 radii of Neptune). However, its orbital eccentricity reaches 0.75, Nereid approaches Neptune in 1.4×10^6 [Km].

Before investigation by the spacecraft Voyager II, only two satellites were known to be orbiting Neptune. Triton, the first one discovered, by Lassell in 1846, orbits in a nearly circular but retrograde orbit once every six days.

Since the inner satellite Triton revolves in a nearly circular retrograde orbit, where the outer satellite Nereid has a large eccentric orbit and direct motion, many astronomers have been attracted to the problem of the satellites' origins after the discovery of Nereid.

During the Voyager II mission, six new satellites were found. All of them are in the vicinity of Neptune, and their semimajor axes are spread from 1.94 to 4.75 in the radius of Neptune, since Voyager II passed Neptune at a close distance. For Nereid, large amounts of astrometric positional data and some images were taken by the mission.

8.1.2 Ephemerides of Nereid

After the discovery of Nereid, many astronomers reported its osculating elements, such as van Biesbroeck (1951,1957), Rose(1974) and Veillet(1982). Due to its long orbital period (nearly 1 year), astrometric observations for a long span are required to obtain orbital elements accurately. Besides, its faintness (19th magnitude) has obstructed the acquisition of clear images of Nereid from ground-based telescopes.

Mignard (1975) first studied the motion of Nereid, and built an ephemeris (Mignard (1981))

Table 8.1: Some approximate values related to the spatial configuration of the Neptunian system. α and δ mean the right ascension and the declination referring to the Earth's equator and equinox.

Item	α[deg]	δ[deg]
Neptune's pole	298.0±1.3	40.7±1.2
Triton's orbital ANTIPOLE	295.2	20.4
Nereid's orbital pole	263.1	62.6

Table 8.2: Some approximate values of the mutual inclinations.

Item			Mutual Inclination [deg]
Nereid's orbital plane	$\leftrightarrow$	Triton's orbital plane	132.4
Nereid's orbital plane	$\leftrightarrow$	Sun's orbital plane	6.7

analytically. He used canonical transformations and took only the solar perturbation (P_2 and P_3 terms) into account.

For the Voyager II mission's flight program, it is necessary to get precise ephemerides of satellites, and for this purpose, Jacobson(1990, 1991) constructed a precise numerical ephemeris of Neptunian satellites.

In an analytical approach, Oberti (1990) showed periodic and secular perturbation terms of Nereid using a canonical perturbation method of Deprit type. In this work, the solar perturbation (P_2 to P_4 terms) and that of Triton (P_2 and P_3 terms) were included in his Hamiltonian and set the origin at the Neptune-Triton barycenter. Segerman and Richardson (1997) also studied the motion of Nereid. They took the solar perturbation (P_2 and P_3 terms), that of Triton (P_2 and P_3 terms) and the J_2 effect of Neptune into consideration.

Saad(2000) studied the motion of Nereid using a canonical perturbation method of Hori type. He considered only the solar perturbation (P_2 term only). The secular perturbation he solved analytically, based on Kinoshita and Nakai(1999)'s work.

8.1.3 Today's orbital configuration of the Neptunian system

Jacobson (1990) not only reported a numerical ephemeris of the two Neptunian satellites, but also summarized the astronomical constants of Neptune and the satellites (e.g. orbital planes of satellites or the rotational axis of Neptune, etc.). Now we consider the spatial configuration of the Neptunian system (Table 8.1). Orbital elements are recalculated from Cartesian positions and velocities in Table.2 of Jacobson(1990)'s paper, since the epoch (JD 2447080.5) is not far from the one (JD 2447763.5) in his Table.3.

Visualizing this configuration, we adopt a stereograophic projection. These values are plotted on the stereonet, projected onto the northern (upper) hemisphere of the celestial sphere and referred to the Earth's equatorial plane. The diagram is shown in Fig. 8.1.

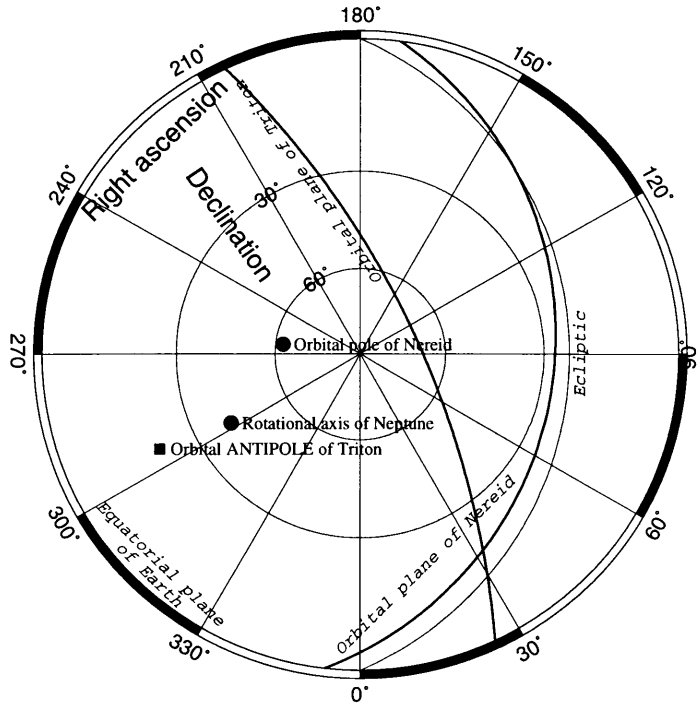

Figure 8.1: A stereographic projection map of the spatial configuration of the Neptunian system. The data are projected onto the northern hemisphere of the celestial sphere and referred to the Earth's equatorial plane. The border circle indicates the equatorial plane of the Earth, and the angles indicate the right ascension of the coordinate in degrees.

Table 8.3: The ratios of the magnitude of the main perturbing potential to that of Kepler potential.

Ratio	Nereid stays at		
	pericenter	mean distance	apocenter
Sun/Kepler	$6. \times 10^{-7}$	$4. \times 10^{-5}$	$2. \times 10^{-4}$
Triton/Kepler	$2. \times 10^{-5}$	$1. \times 10^{-6}$	$4. \times 10^{-7}$
J_2/Kepler	$1. \times 10^{-6}$	$7. \times 10^{-8}$	$2. \times 10^{-8}$

8.1.4 Perturbations on the motion of Nereid

Nereid is revolving around Neptune, but its Kepler motion is disturbed incessantly by the Sun, Triton and other disturbers.

The magnitude of perturbation is roughly estimated by taking a ratio of a perturbing force and a Kepler force. Now, we designate the masses of Sun, Neptune and Triton as $M_\odot, M, m_{Tri}$, and distances from Nereid to those as $r_\odot, r, r_{Tri}$, respectively. The universal gravitational constant is written as k^2, and the dynamical oblateness coefficient and the equatorial radius of Neptune is written by J_2 and R_{Nep}. Then, the main part of (perturbational) potential are estimated as follows:

$$\begin{aligned} \text{Kepler} &= k^2 \frac{M}{r} \\ \text{Sun} &= k^2 \frac{M_\odot r^2}{r_\odot^3} \\ \text{Triton} &= k^2 \frac{m_{Tri} r_{Tri}^2}{r^3} \\ J_2 &= k^2 \frac{M R_{Nep}^2}{r^3} J_2 \end{aligned}$$

The values of ratios $\frac{\text{perturbational potential}}{\text{Kepler potential}}$ are summarized in Table 8.3.

The table shows that the Sun's perturbation is dominant among these perturbations. Therefore, the Sun plays an important role in the time-variation of orbital elements of Nereid. The pioneering work of Mignard (1975) contained only the effect of the Sun's perturbation up to P_3 terms.

However, the table also indicates that when Nereid is near its pericenter, other perturbations are not neglected in magnitude. Next, it is necessary to include Triton's perturbation in the theory. That is the goal of the analytical theory on the motion of Nereid.

For a long time period, planetary satellites have been classified into two categories according to the predominant perturbing body. Brouwer and Clemence (1961b) categorized as follows:

- TYPE A ..... A perturbation from the oblateness of the mother planet plays an important role.
- TYPE B ..... The attraction by the Sun plays an important role.

Table 8.4: The corresponding length to the angle of 0.1[arcsec] at some distances from ground-based telescopes.

At the mean distance of	Corresponding distance[Km]
Jupiter	380
Saturn	690
Uranus	1400
Neptune	2200
Pluto	2900
Pluto (at aphelion)	3600

- TYPE C ..... The attraction by other satellites plays an important role.

A TYPE A satellite orbits in the vicinity of a planet, while a TYPE B one orbits far from a planet. A TYPE C satellite orbits near massive satellites or in mean motion resonance with other satellites. Nereid is classified as a TYPE B satellite.

8.1.5 Accuracy of astrometric observation from ground-based telescopes

The positions of satellites have been observed from ground-based telescopes (including meridian circles) for a few hundred years. Accuracy of positional observation is bounded by atmospheric conditions (e.g. seeing). Some planetary spacecraft missions have recorded positions of satellites from close distances, free from atmospheric disturbance. However, these data cover only a short timespan.

The accuracy of ground-based positional astrometry (by meridian circles) is about 0.1[arcsec]. It corresponds to the length of about 2200[Km] at the mean distance of the Neptune. The corresponding lengths of the angle 0.1[arcsec] at some distances are summarized in Table 8.4.

8.2 Application to newly discovered outer satellites

Gladman et.al. (1997) discovered two satellites of Uranus on CCD-images using the Hale 5-meter telescope at Mount Palomar. Some successive observations revealed that these satellites orbit far from Uranus in retrograde. Today, they are named Caliban (semimajor axis $\sim$ 280 radii of Uranus) and Sycorax ($\sim$ 480 radii of Uranus).

After this discovery, satellites orbiting the outer region have been reported one after another for Jupiter, Saturn and Uranus. These newly discovered satellites tend to have slightly more eccentric orbits (eccentricity $\sim$ 0.5). For Jovian and Saturnian outer satellites, perturbation by the Sun is predominant. However, satellites of the farther revolving planet from the Sun have the same spatial configuration (the planet + the inner orbiting satellite + the outer orbiting satellite) as those in this study. Further discovery of satellites may be applicable to this theory.

8.3 Application to extrasolar planetary systems

8.3.1 Brief history of discovery

In the mid-1990's, Mayor and Queloz (1995) reported the presence of a Jupiter-mass companion to 51 Pegasi through observations of its radial velocity. This discovery opens our eyes to the real existence of extra-solar planets. Many observers are eager to detect other candidates through catching variations in radial velocities or using other techniques.

Fortunately, as of 2001, several tens of extra-solar planets have been detected. It is hoped that, in the near future, more extra-solar planets will be discovered and the existence of planets may be common for sun-like stars.

Table 1 shows the planetary candidates discovered as of July, 2001. (This list is duplicated from the website of University of California Planet Search Project. URL is `http://exoplanets.org`.)

8.3.2 Their observational characters

On the study of extrasolar planets, some review papers have already been published (for example, Marcy and Butler(1998) or Marcy et.al.(2000)). Today's findings are mainly due to radial velocity observation. Since an orbiting planet drifts the central star around a common barycenter, we can detect radial velocity from spectral data of the primary star.

In the study of binary dynamics, the orbital inclination I is referred to the celestial sphere, which is perpendicular to the line of sight. We cannot get information on the orbital inclination from velocity data except for some eclipsing binaries. If $I = 0$, no Doppler shift is detected.

The orbital period P and the radial velocity are measured from observational data, we can get information on the total mass of the binary system M_{Total}. However, observed radial velocity is multiplied by the factor of $\sin I$, and all we can estimate is the value of $M_{Total} \sin I$. In other words, we can give the lower limit of the M_{Total}.

The amplitude of radial velocity K directly relates to the $P^{-\frac{1}{3}}$ with a factor of $\frac{m_P}{(M_* + m_P)^{\frac{2}{3}}} \sin I$; i.e.,

$$K \propto P^{-\frac{1}{3}} \frac{m_P}{(M_* + m_P)^{\frac{2}{3}}} \sin I,$$

where M_* and m_P are the masses of the primary and the planet, respectively. This factor enables us to estimate the planetary mass when the mass of the primary star is estimated from its spectral type.

The distribution of $M \sin I$ for the known extrasolar planets is highly concentrated in the mass lower than several Jupiter masses. This means that slightly more massive planets than Jupiter are orbiting around the sun-like stars. From the study of stellar evolution, stars with mass greater than $0.08 M_\odot (\sim 83.8 M_{Jup})$ ignite their hydrogen cores and burn by themselves. A celestial object with a mass larger than $13 M_{Jup}$ is regarded as a 'planet' in recent studies. (A body with a mass between $13 M_{Jup}$ and $0.08 M_\odot$ is called a 'brown dwarf'. See Martin et.al.(1999) or Oppenheimer et.al.(2000).) This is the upper limit of mass for a planet.

Although the formation theory of the Solar System indicates that giant planets were born far from the central star (i.e. the Sun), some extrasolar giant planets have been detected in the neighborhood of the primary stars.

Table 8.5: Masses and Orbital Characteristics of Extrasolar Planets. (Duplicated from the website of University of California Planet Search Project.) Stellar masses are derived from spectral types, metallicity, and stellar evolution. Column $M \sin i$ is the companion mass (with ambiguity of orbital inclination) in Jupiter mass, P is the orbital period and K is the velocity semiamplitude.

No.	Star name	$M \sin i$ $[M_{Jup}]$	P [day]	a [AU]	e	K [m/sec]
1	HD83443	0.34	3.0	0.038	0.08	57.0
2	HD46375	0.25	3.0	0.041	0.02	35.2
3	HD179949	0.93	3.1	0.045	0.00	112.0
4	HD187123	0.54	3.1	0.042	0.01	72.0
5	τBoo	4.14	3.3	0.047	0.02	474.0
6	BD-103166	0.48	3.5	0.046	0.05	60.6
7	HD75289	0.46	3.5	0.048	0.00	54.0
8	HD209458	0.63	3.5	0.046	0.02	82.0
9	51Peg	0.46	4.2	0.052	0.01	55.2
10	υAnd b	0.68	4.6	0.059	0.02	70.2
11	HD168746	0.24	6.4	0.066	0.00	28.0
12	HD217107	1.29	7.1	0.072	0.14	139.7
13	HD162020	13.73	8.4	0.072	0.28	1813.0
14	HD130322	1.15	10.7	0.092	0.05	115.0
15	HD108147	0.35	10.9	0.098	0.56	37.0
16	HD38529	0.77	14.3	0.129	0.27	53.6
17	55Cnc	0.93	14.7	0.118	0.03	75.8
18	HD13445=GJ86	4.23	15.8	0.117	0.04	379.0
19	HD195019	3.55	18.2	0.136	0.01	271.0
20	HD6434	0.48	22.1	0.154	0.30	37.0
21	HD192263	0.81	24.4	0.152	0.22	68.2
22	HD83443 c	0.17	29.8	0.174	0.42	14.0
23	GJ876 c	0.56	30.1	0.130	0.27	81.0
24	ρCrB	0.99	39.8	0.224	0.07	61.3
25	HD74156 b	1.55	51.6	0.276	0.65	108.0
26	HD168443 b	7.64	58.1	0.295	0.53	470.0
27	GJ876 b	1.89	61.0	0.207	0.10	210.0
28	HD121504	0.89	64.6	0.317	0.13	45.0
29	HD178911 B	6.46	71.5	0.326	0.14	343.0
30	HD16141	0.22	75.8	0.351	0.28	10.8

Table 8.4: (Continued)

No.	Star name	$M \sin i$ [M_{Jup}]	P [day]	a [AU]	e	K [m/sec]
31	HD114762	10.96	84.0	0.351	0.33	615.0
32	HD80606	3.43	111.8	0.438	0.93	414.0
33	70Vir	7.42	116.7	0.482	0.40	316.2
34	HD52265	1.14	119.0	0.493	0.29	45.4
35	HD1237	3.45	133.8	0.505	0.51	164.0
36	HD37124	1.13	154.8	0.547	0.31	48.0
37	HD82943 c	0.88	221.6	0.728	0.54	34.0
38	HD8574	2.23	228.8	0.756	0.40	76.0
39	HD169830	2.95	230.4	0.823	0.34	83.0
40	υAnd c	2.05	241.3	0.828	0.24	58.0
41	HD12661	2.84	250.5	0.795	0.19	89.1
42	HD89744	7.17	256.0	0.883	0.70	257.0
43	HD202206	14.68	258.9	0.768	0.42	554.0
44	HD134987	1.58	260.0	0.810	0.24	50.2
45	HD17051= ιHor	2.98	320.0	0.970	0.16	80.0
46	HD92788	3.88	337.0	0.969	0.28	113.0
47	HD28185	5.59	385.0	1.000	0.06	168.0
48	HD177830	1.24	391.0	1.10	0.40	34.0
49	HD27442	1.42	426.0	1.18	0.02	34.0
50	HD210277	1.29	436.6	1.12	0.45	39.1
51	HD82943 b	1.63	444.6	1.16	0.41	46.0
52	HD19994	1.83	454.2	1.26	0.20	42.0
53	HD222582	5.18	576.0	1.35	0.71	179.6
54	HD141937	9.69	658.8	1.48	0.40	247.0
55	HD160691	1.99	743.0	1.65	0.62	54.0
56	HD213240	3.75	759.0	1.60	0.31	91.0
57	16Cyg B	1.68	796.7	1.69	0.68	50.0
58	HD10697	6.08	1074.0	2.12	0.11	114.0
59	47UMa b	2.54	1089.0	2.09	0.06	49.3
60	HD190228	5.01	1127.0	2.25	0.43	96.0
61	HD50554	4.91	1279.0	2.38	0.42	95.0
62	υAnd d	4.29	1308.5	2.56	0.31	70.4
63	HD106252	6.81	1500.0	2.61	0.54	139.0
64	HD168443 c	16.96	1770.0	2.87	0.20	289.0
65	14Her	4.05	2000.0	3.17	0.45	70.4
66	HD74156 c	7.46	2300.0	3.47	0.40	121.0
67	ϵEri	0.88	2518.0	3.36	0.60	19.0
68	47UMa c	0.76	2594.0	3.73	0.10	11.1

Some primary stars with planets show high metalicity (high [Fe/H] ratio). Many astronomers try to explain the relation theoretically.

8.3.3 Their orbital characters and applicability of our theory

For the discovered extrasolar planets listed in Table 8.5, we are going to discuss orbital characters.

Fig. 8.2 shows their individual characters among the parameters of the semimajor axis, the eccentricity and the planetary mass (the value of $m_P \sin I$). The original idea of such plottings appeared in Russell and Boss(1998)' article. Fig. 8.2 is newly reproduced from the all data in Table 8.5, and does not contain companions classified as brown dwarfs or binaries.

The extrasolar planets are distributed from the lower-left to the upper-right in the figure; however, this is due to an observational bias. Since we detect the radial velocity K of the central star drifted by the companion, it must be larger than the observational detection limit K_0, i.e.,

$$K_0 \leq K \propto P^{-\frac{1}{3}} m_P \sin I.$$

We rewrite P into the semimajor axis of a planet a, then

$$K \propto a^{-\frac{1}{2}} m_P \sin I.$$

The constant value of K lies on a linear line in the $\log(m_P \sin I)$-$\log a$ plot like Fig. 8.2, thus $K \geq K_0$ occupies the upper region of the constant K_0 line. In other words, some undiscovered planets can exist in the lower region of the line.

The figure tells us that the orbital eccentricity of extrasolar planet seems to become larger as the distance from the central star is further. Some astronomers try to explain the near-zero eccentricity in the vicinity of the central star by tidal dissipation. This is an analogy to binary stars studied by Duquennoy and Mayor(1991).

This property supports the expectation that a more highly eccentric planet revolves further from the known extrasolar planets. Our theory can be applied to such a system.

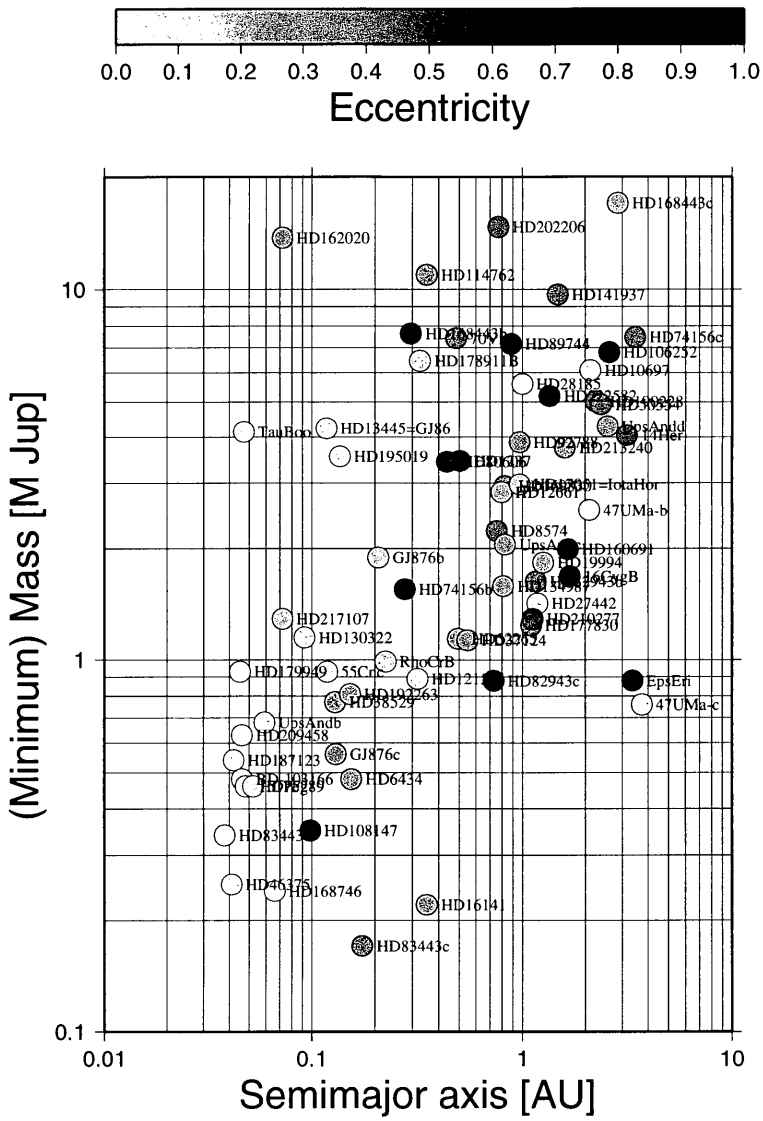

Figure 8.2: Orbital properties of the discovered extrasolar planets. The (Minimum) mass means the value of $m_P \sin I$. The eccentricity is indicated by the gray-scale-filled plot circle.

Chapter 9

Conclusions

We have developed an analytical theory on the motion of a celestial body orbiting in a highly eccentric orbit. The body is perturbed by an inner celestial body which revolves in a circular orbit around the main star. Our theory is constructed using Hori's canonical perturbation method without expanding the Hamiltonian in eccentricity. In order to check the accuracy of our theory, we compared the analytical results with numerically integrated ones.

We ascertained that our theory provides the orbital elements with high accuracy. The semi-major axis ratio of the outer body to the inner one is larger, and our theory maintains its high degree of accuracy in the case of a higher eccentricity.

We also found that both results diverge in the case of a very large eccentricity. This is mainly due to the following: (1) The series of the generating function S_i for the short periodic perturbations becomes less convergent, or more diverse. (2) The offset phenomena: abrupt changes in the orbital elements take place when the outer body passes through its pericenter. The magnitude of the offset relates to a spatial configuration of the two revolving satellites. They are not represented in the analytical theory.

We assessed errors due to truncational effects of the Legendre series in the Hamiltonian. We also discussed truncational errors of the generating functions when we calculated short periodic perturbations.

We tried to apply our theory to the Neptunian satellite Nereid that orbits in a highly eccentric orbit ($e = 0.75$) perturbed by the inner revolving satellite, Triton. Our theory maintains a good degree of accuracy, yielding results better than 30Km in the osculating semimajor axis of Nereid.

Our analytical theory can also be applied to other highly eccentric orbits. Some extrasolar planets are known as "Hot Jupiters", which revolve around their primary stars in circular orbits at small distances from them. Another new planet may exist in the outer field. The motion of such a new planet can be described by our theory.

Acknowledgements

I sincerely appreciate Professor Hiroshi Kinoshita for his constant support throughout this study. He introduced to me a way of studying dynamics of natural satellites. Without his guidance, I could not have accomplished this doctoral thesis successfully. Although I was majoring in geology or geophysics until enrolling in the doctoral course of this graduate university, I have completed my course here.

I wish to express my deepest thanks to the people who encouraged me in my stay in Mitaka, Tokyo.

I express my thanks to the attendants of the seminars related to celestial mechanics, held weekly at the National Astronomical Observatory of Japan. Discussions there enlarged my knowledge and widened my academic view.

I appreciate my colleagues who study in the Division of Celestial Mechanics at the observatory. I also express thanks to the members who spent the same time with me in the Prefabricated Building for Graduates at the observatory site. They constantly eased my mind and supported me mentally in my daily research life.

Finally, I am gratefully indebted to my parents, Masanori and Takako, for cherishing and feeding me. They have given my life a good direction.

References

Allen, C.W., 1973, Astrophysical Quantities (3rd. ed.), The Athlone Press, University of London.

Brouwer, D. and Clemence, G.M., 1961a, Methods of Celestial Mechanics, Academic Press.

Brouwer, D. and Clemence, G.M., 1961b, Orbits and Masses of Planets and Satellites, in *Planets and Satellites* (Kuiper, G.P. and Middlehurst, B.M. eds.), The University of Chicago Press, 31.

Carusi, A., Kresák, Ľ., Perozzi, E. and Valsecchi, G.B., 1985a, Long-term Evolution of Short-period Comets, Adam Hilger Ltd..

Carusi, A., Kresák, L., Perozzi, E. and Valsecchi, G.B., 1985b, First Results of the Integration of Motion of Short-period Comets over 800 Years, in *Dynamics of Comets: Their Origin and Evolution* (Carusi, A. and Valsecchi, G.B. eds.), D.Reidel Publishing Company, 319.

Carusi, A., Kresák, L., Perozzi, E. and Valsecchi, G.B., 1987, High-order Librations of Halley-type Comets, *Astron. Astrophys.*, **187**, 899.

Chambers, J.E., 1995, The Long-term Dynamical Evolution of Comet Swift-Tuttle, *Icarus*, **114**, 372.

Chirikov, B.V. and Vecheslavov, V.V., 1989, Chaotic Dynamics of Comet Halley, *Astron. Astrophys.*, **221**, 146.

Deprit, A., 1968, Canonical Transformations Depending on a Small Parameter, *Cele. Mech. Dyn. Astron.*, **1**, 12.

Duquennoy, A. and Mayor, M., 1991, Multiplicity among Solar-type Stars in the Solar Neighbourhood - II. Distribution of the Orbital Elements in an Unbiased Sample, *Astron. Astrophys.*, **248**, 485.

Gladman, B.J., Nicholson, P.D., Burns, J.A. and Kavelaars, J.J., 1997, reported in IAUC 6764 (Marsden, B.G. ed.).

Hori, G., 1966, Theory of General Perturbations with Unspecified Canonical Variables, *Publ. Astron. Soc. Japan*, **18**, 287.

Jacobson, R.A., 1990, The orbits of the satellites of Neptune, *Astron. Astrophys.*, **231**, 241.

Jacobson, R.A., 1991, Triton and Nereid astrographic observations from Voyager 2, *Astron. Astrophys. Suppl. Ser.*, **90**, 541.

Kinoshita, H. and Nakai, H., 1999, Analytical Solution of the Kozai Resonance and its Application, *Cele. Mech. Dyn. Astron.*, **75**, 125.

Marcy, G.W. and Butler, R.P., 1998, Detection of Extrasolar Giant Planets, *Annu. Rev. Astron. Astrophys.*, **36**, 57.

Marcy, G.W., Cochran, W.D. and Mayor, M., 2000, Extrasolar Planets around Main-sequence Stars, in *Protostars and Planets IV* (Mannings, V., Boss, A.P. and Russell, S.S. eds.), The University of Arizona Press, 1285.

Martin, E.L., Brandner, W. and Basri, G., 1999, A Search for Companions to Nearby Brown Dwarfs: The Binary DENIS-P J1228.2-1547, *Science*, **283**, 1718.

Mayor, M. and Queloz, D., 1995, A Jupiter-mass Companion to a Solar-type Star, *Nature*, **378**, 355.

Mignard, F., 1975, Satellite à forte excentricité. Application à Néréide, *Astron. Astrophys*, **43**, 359.

Mignard, F., 1981, The Mean Elements of Nereid, *Astron. J.*, **86**, 1728.

Murison, M.A., 1989, On an Efficient and Accurate Method to Integrate Restricted Three-body Orbits, *Astron. J.*, **97**, 1496.

Nakamura, T. and Yoshikawa, M., 1991, Cosmo-dice: Dynamical Investigation of Cometary Evolution, *Publ. Natl. Astron. Obs. Japan*, **2**, 293.

Oberti, P., 1990, An accurate solution for Nereid's motion I. Analytical modeling, *Astron. Astrophys.*, **239**, 381.

Oppenheimer, B.R., Kulkarni, S.R. and Stauffer, J.R., 2000, Brown Dwarfs, in *Protostars and Planets IV* (Mannings, V., Boss, A.P. and Russell, S.S. eds.), The University of Arizona Press, 1313.

Rose, L.E., 1974, Orbit of Nereid and the mass of Neptune, *Astron. J.*, **79**, 489.

Russell, S.S. and Boss, A.P., 1998, Protostars and Planets, *Science*, **281**, 932.

Saad, A.S., 2000, The Theory of Motion and Ephemerides of the Second Neptunian Satellite Nereid, Doctoral thesis, The Graduate University for Advanced Studies.

Segerman, A.M. and Richardson,D.L., 1997, An Analytical Theory for the Orbit of Nereid, *Cele. Mech. Dyn. Astron.*, **66**, 321.

van Biesbroeck, 1951, The Orbit of Nereid, Neptune's Second Satellite, *Astron. J.*, **56**, 110.

van Biesbroeck, 1957, The Mass of Neptune from a New Orbit of its Second Satellite Nereid, *Astron. J.*, **62**, 272.

Veillet, C., 1982, Orbital Elements of Nereid from New Observations, *Astron. Astrophys.*, **112**, 277.

von Zeipel, H., 1916, Recherches sur le mouvement des petites planètes. Première partie., *Arkiv för Matematik, astronomi och fysik*, **11**, *No. 1*, 1.

Appendix A

Analytical Expressions (The Planar Problem)

We use the following descriptions in this paper.

M	Mass of the primary body
m_{In}	Mass of the inner body
m	($\equiv 0$) Mass of the outer body
μ	$k^2(M + m_{In} + m) \equiv n^2 a^3$
a	Semimajor axis of the outer body
a_{In}	Semimajor axis of the inner body
n	Mean motion of the outer body
n_{In}	Mean motion of the inner body
e	Eccentricity of the outer body
η	$\sqrt{1-e^2}$
f	True anomaly of the outer body
r	Radius of the outer body
ϖ	Longitude of pericenter of the outer body
λ_{In}	Longitude of the inner body
y_2	$\varpi - \lambda_{In}$

$$C_2 \equiv \frac{M m_{In}}{(M + m_{In})^2}$$
$$C_3 \equiv \frac{M m_{In}(M^2 - m_{In}^2)}{(M + m_{In})^4}$$

Hereafter, we neglect $O((\frac{m}{M+m_{In}})^2)$ or higher order terms.

A.1 Hamiltonians

Original Hamiltonian

$$\begin{aligned} F &= n_{In}x_2 + \frac{\mu^2}{2x_1^2} \\ &\quad +\mu C_2 \frac{a_{In}^2}{a^3}(\frac{a}{r})^3 \frac{1}{4}[1 + 3\cos(2f + 2y_2)] \\ &\quad +\mu C_3 \frac{a_{In}^3}{a^4}(\frac{a}{r})^4 \frac{1}{8}[5\cos(3f + 3y_2) + 3\cos(f + y_2)] \\ &\quad +\ldots \end{aligned}$$

Hamiltonians F^* and F^{**}

$$\begin{aligned} F^* &= n_{In}x_2 + \frac{\mu^2}{2x_1^2} + \frac{1}{4}\mu C_2 \frac{a_{In}^2}{r^3} + \ldots \\ F^{**} &= n_{In}x_2 + \frac{\mu^2}{2x_1^2} + \frac{1}{4}\mu C_2 \frac{a_{In}^2}{a^3\eta^3} + \ldots \end{aligned}$$

A.2 P_2-limited generating functions

For short periodic terms

$$\begin{aligned} S_1 &= 0 \\ S_2 &= -\frac{3}{8}\mu C_2 \frac{1}{n_{In}} \frac{a_{In}^2}{r^3} \sin(2f + 2y_2) \\ S_3 &= -\frac{3}{32}\mu C_2 \frac{na}{\eta n_{In}^2} \frac{a_{In}^2}{r^4} \\ &\quad [-e\sin(f + 2y_2) \\ &\quad +4\sin(2f + 2y_2) \\ &\quad +5e\sin(3f + 2y_2)] \\ S_4 &= -\frac{3}{128}\mu C_2 \frac{(na)^2}{\eta^2 n_{In}^3} \frac{a_{In}^2}{r^5} \\ &\quad [+3e^2\sin(2y_2) \\ &\quad -10e\sin(f + 2y_2) \\ &\quad +(16 - 10e^2)\sin(2f + 2y_2) \\ &\quad +54e\sin(3f + 2y_2) \\ &\quad +35e^2\sin(4f + 2y_2)] \\ S_5 &= -\frac{3}{512}\mu C_2 \frac{(na)^3}{\eta^3 n_{In}^4} \frac{a_{In}^2}{r^6} \\ &\quad [+15e^3\sin(f - 2y_2) \\ &\quad +40e^2\sin(2y_2) \\ &\quad +(-68e + 45e^3)\sin(f + 2y_2) \end{aligned}$$

$$
\begin{aligned}
&+(64-208e^2)\sin(2f+2y_2)\\
&+(436e-105e^3)\sin(3f+2y_2)\\
&+712e^2\sin(4f+2y_2)\\
&+315e^3\sin(5f+2y_2)]
\end{aligned}
$$

$$
\begin{aligned}
S_6 &= -\frac{3}{2048}\mu C_2\frac{(na)^4}{\eta^4 n_{In}^5}\frac{a_{In}^2}{r^7}\\
&\quad[-105e^4\sin(2f-2y_2)\\
&\quad+210e^3\sin(f-2y_2)\\
&\quad+(340e^2-300e^4)\sin(2y_2)\\
&\quad+(-392e+1162e^3)\sin(f+2y_2)\\
&\quad+(256-2616e^2+630e^4)\sin(2f+2y_2)\\
&\quad+(3128e-3718e^3)\sin(3f+2y_2)\\
&\quad+(9620e^2-1260e^4)\sin(4f+2y_2)\\
&\quad+10270e^3\sin(5f+2y_2)\\
&\quad+3465e^4\sin(6f+2y_2)]
\end{aligned}
$$

$$
\begin{aligned}
S_7 &= -\frac{3}{8192}\mu C_2\frac{(na)^5}{\eta^5 n_{In}^6}\frac{a_{In}^2}{r^8}\\
&\quad[+945e^5\sin(3f-2y_2)\\
&\quad-1260e^4\sin(2f-2y_2)\\
&\quad+(1960e^3-2625e^5)\sin(f-2y_2)\\
&\quad+(2352e^2-8232e^4)\sin(2y_2)\\
&\quad+(-2064e+17784e^3-5250e^5)\sin(f+2y_2)\\
&\quad+(1024-26112e^2+26688e^4)\sin(2f+2y_2)\\
&\quad+(21072e-74712e^3+9450e^5)\sin(3f+2y_2)\\
&\quad+(108240e^2-67800e^4)\sin(4f+2y_2)\\
&\quad+(208520e^3-17325e^5)\sin(5f+2y_2)\\
&\quad+164820e^4\sin(6f+2y_2)\\
&\quad+45045e^5\sin(7f+2y_2)]
\end{aligned}
$$

$$
\begin{aligned}
S_8 &= -\frac{3}{32768}\mu C_2\frac{(na)^6}{\eta^6 n_{In}^7}\frac{a_{In}^2}{r^9}\\
&\quad[-10395e^6\sin(4f-2y_2)\\
&\quad+6930e^5\sin(3f-2y_2)\\
&\quad+(-12600e^4+28350e^6)\sin(2f-2y_2)\\
&\quad+(14896e^3-68166e^5)\sin(f-2y_2)\\
&\quad+(14448e^2-138208e^4+55125e^6)\sin(2y_2)\\
&\quad+(-10272e+211056e^3-236484e^5)\sin(f+2y_2)\\
&\quad+(4096-228384e^2+640368e^4-94500e^6)\sin(2f+2y_2)
\end{aligned}
$$

$$
\begin{aligned}
&+(136672e - 1142352e^3 + 594780e^5)\sin(3f + 2y_2) \\
&+(1097712e^2 - 1989792e^4 + 155925e^6)\sin(4f + 2y_2) \\
&+(3384080e^3 - 1316490e^5)\sin(5f + 2y_2) \\
&+(4688600e^4 - 270270e^6)\sin(6f + 2y_2) \\
&+2938110e^5\sin(7f + 2y_2) \\
&+675675e^6\sin(8f + 2y_2)]
\end{aligned}
$$

$$
\begin{aligned}
S_9 &= -\frac{3}{131072}\mu C_2\frac{(na)^7}{\eta^7 n_{In}^8}\frac{a_{In}^2}{r^{10}} \\
&\quad [+135135e^7\sin(5f - 2y_2) \\
&\quad +(97020e^5 - 363825e^7)\sin(3f - 2y_2) \\
&\quad +(-98560e^4 + 609840e^6)\sin(2f - 2y_2) \\
&\quad +(100240e^3 - 1195740e^5 + 694575e^7)\sin(f - 2y_2) \\
&\quad +(82176e^2 - 1807616e^4 + 2437200e^6)\sin(2y_2) \\
&\quad +(-49216e + 2150832e^3 - 6199416e^5 + 1157625e^7)\sin(f + 2y_2) \\
&\quad +(16384 - 1836288e^2 + 11526144e^4 - 6311520e^6)\sin(2f + 2y_2) \\
&\quad +(865088e - 14854896e^3 + 20561688e^5 - 1819125e^7)\sin(3f + 2y_2) \\
&\quad +(10421760e^2 - 43162880e^4 + 13650720e^6)\sin(4f + 2y_2) \\
&\quad +(48111056e^3 - 53097996e^5 + 2837835e^7)\sin(5f + 2y_2) \\
&\quad +(103640320e^4 - 27550320e^6)\sin(6f + 2y_2) \\
&\quad +(111462540e^5 - 4729725e^7)\sin(7f + 2y_2) \\
&\quad +57820560e^6\sin(8f + 2y_2) \\
&\quad +11486475e^7\sin(9f + 2y_2)]
\end{aligned}
$$

For long periodic terms

$$
\begin{aligned}
S_1^* &= \frac{1}{4}\mu C_2\frac{a_{In}^2}{a^3}\frac{1}{\eta^3 n}(f - y_1 + e\sin f) \\
S_2^* &= O((\frac{m}{M + m_{In}})^2)
\end{aligned}
$$

A.3 P_3-limited generating functions

For short periodic terms

$$
\begin{aligned}
S_1 &= 0 \\
S_2 &= -\frac{1}{24}\mu C_3\frac{1}{n_{In}}\frac{a_{In}^3}{r^4} \\
&\quad [+9\sin(f + y_2)
\end{aligned}
$$

$$
\begin{aligned}
&\quad +5\sin(3f+3y_2)]\\
S_3 &= -\frac{1}{144}\mu C_3\frac{na}{\eta n_{In}^2}\frac{a_{In}^3}{r^5}\\
&\quad [-81e\sin(y_2)\\
&\quad +54\sin(f+y_2)\\
&\quad +135e\sin(2f+y_2)\\
&\quad -5e\sin(2f+3y_2)\\
&\quad +30\sin(3f+3y_2)\\
&\quad +35e\sin(4f+3y_2)]\\
S_4 &= -\frac{1}{864}\mu C_3\frac{(na)^2}{\eta^2 n_{In}^3}\frac{a_{In}^3}{r^6}\\
&\quad [-1215e^2\sin(f-y_2)\\
&\quad -648e\sin(y_2)\\
&\quad +(324-2430e^2)\sin(f+y_2)\\
&\quad +2592e\sin(2f+y_2)\\
&\quad +2835e^2\sin(3f+y_2)\\
&\quad +15e^2\sin(f+3y_2)\\
&\quad -80e\sin(2f+3y_2)\\
&\quad +(180-70e^2)\sin(3f+3y_2)\\
&\quad +520e\sin(4f+3y_2)\\
&\quad +315e^2\sin(5f+3y_2)]\\
S_5 &= -\frac{1}{5184}\mu C_3\frac{(na)^3}{\eta^3 n_{In}^4}\frac{a_{In}^3}{r^7}\\
&\quad [+25515e^3\sin(2f-y_2)\\
&\quad -4374e^2\sin(f-y_2)\\
&\quad +(-4860e+54675e^3)\sin(y_2)\\
&\quad +(1944-57348e^2)\sin(f+y_2)\\
&\quad +(37908e-76545e^3)\sin(2f+y_2)\\
&\quad +113238e^2\sin(3f+y_2)\\
&\quad +76545e^3\sin(4f+y_2)\\
&\quad -75e^3\sin(3y_2)\\
&\quad +350e^2\sin(f+3y_2)\\
&\quad +(-860e+315e^3)\sin(2f+3y_2)\\
&\quad +(1080-2100e^2)\sin(3f+3y_2)\\
&\quad +(5780e-945e^3)\sin(4f+3y_2)\\
&\quad +8350e^2\sin(5f+3y_2)\\
&\quad +3465e^3\sin(6f+3y_2)]
\end{aligned}
$$

$$
\begin{aligned}
S_6 &= -\frac{1}{31104}\mu C_3 \frac{(na)^4}{\eta^4 n_{In}^5}\frac{a_{In}^3}{r^8} \\
&\quad [-688905e^4\sin(3f-y_2) \\
&\quad -201204e^3\sin(2f-y_2) \\
&\quad +(-75816e^2+1530900e^4)\sin(f-y_2) \\
&\quad +(-34992e+1110996e^3)\sin(y_2) \\
&\quad +(11664-1014768e^2+2296350e^4)\sin(f+y_2) \\
&\quad +(501552e-3653748e^3)\sin(2f+y_2) \\
&\quad +(3061800e^2-2755620e^4)\sin(3f+y_2) \\
&\quad +5234220e^3\sin(4f+y_2) \\
&\quad +2525985e^4\sin(5f+y_2) \\
&\quad -525e^4\sin(f-3y_2) \\
&\quad -2100e^3\sin(3y_2) \\
&\quad +(5000e^2-2100e^4)\sin(f+3y_2) \\
&\quad +(-7760e+12460e^3)\sin(2f+3y_2) \\
&\quad +(6480-37680e^2+5670e^4)\sin(3f+3y_2) \\
&\quad +(57040e-45260e^3)\sin(4f+3y_2) \\
&\quad +(147080e^2-13860e^4)\sin(5f+3y_2) \\
&\quad +141780e^3\sin(6f+3y_2) \\
&\quad +45045e^4\sin(7f+3y_2) \\
S_7 &= -\frac{1}{186624}\mu C_3 \frac{(na)^5}{\eta^5 n_{In}^6}\frac{a_{In}^3}{r^9} \\
&\quad [+22733865e^5\sin(4f-y_2) \\
&\quad +18436410e^4\sin(3f-y_2) \\
&\quad +(4461480e^3-51667875e^5)\sin(2f-y_2) \\
&\quad +(-384912e^2+13856832e^4)\sin(f-y_2) \\
&\quad +(-244944e+22902264e^3-80372250e^5)\sin(y_2) \\
&\quad +(69984-15956352e^2+106209468e^4)\sin(f+y_2) \\
&\quad +(6333552e-117170712e^3+103335750e^5)\sin(2f+y_2) \\
&\quad +(70158960e^2-222024240e^4)\sin(3f+y_2) \\
&\quad +(226660680e^3-113669325e^5)\sin(4f+y_2) \\
&\quad +264211470e^4\sin(5f+y_2) \\
&\quad +98513415e^5\sin(6f+y_2) \\
&\quad +4725e^5\sin(2f-3y_2) \\
&\quad -15750e^4\sin(f-3y_2) \\
&\quad +(-35000e^3+18375e^5)\sin(3y_2)
\end{aligned}
$$

$$
\begin{aligned}
&+(56560e^2 - 95760e^4)\sin(f + 3y_2) \\
&+(-63440e + 283240e^3 - 47250e^5)\sin(2f + 3y_2) \\
&+(38880 - 531840e^2 + 339660e^4)\sin(3f + 3y_2) \\
&+(527600e - 1217800e^3 + 103950e^5)\sin(4f + 3y_2) \\
&+(2155280e^2 - 965280e^4)\sin(5f + 3y_2) \\
&+(3613400e^3 - 225225e^5)\sin(6f + 3y_2) \\
&+2615550e^4\sin(7f + 3y_2) \\
&+675675e^5\sin(8f + 3y_2)]
\end{aligned}
$$

$$
\begin{aligned}
S_8 \;=\; & -\frac{1}{1119744}\mu C_3 \frac{(na)^6}{\eta^6 n_{In}^7}\frac{a_{In}^3}{r^{10}} \\
& [-886620735e^6\sin(5f - y_2) \\
& -1209323520e^5\sin(4f - y_2) \\
& +(-479084220e^4 + 2046047850e^6)\sin(3f - y_2) \\
& +(-41990400e^3 + 536164920e^5)\sin(2f - y_2) \\
& +(-4304016e^2 + 628911216e^4 - 3255076125e^6)\sin(f - y_2) \\
& +(-1679616e + 392190336e^3 - 2881591200e^5)\sin(y_2) \\
& +(419904 - 235356192e^2 + 3716202888e^4 - 4340101500e^6)\sin(f + y_2) \\
& +(78102144e - 3147600384e^3 + 8422749360e^5)\sin(2f + y_2) \\
& +(1471868496e^2 - 11262980016e^4 + 5115119625e^6)\sin(3f + y_2) \\
& +(7965578880e^3 - 13891474080e^5)\sin(4f + y_2) \\
& +(16766110620e^4 - 5319724410e^6)\sin(5f + y_2) \\
& +14643364680e^5\sin(6f + y_2) \\
& +4433103675e^6\sin(7f + y_2) \\
& -51975e^6\sin(3f - 3y_2) \\
& +138600e^5\sin(2f - 3y_2) \\
& +(-283500e^4 + 198450e^6)\sin(f - 3y_2) \\
& +(-452480e^3 + 892080e^5)\sin(3y_2) \\
& +(557200e^2 - 2489200e^4 + 496125e^6)\sin(f + 3y_2) \\
& +(-487040e + 4889600e^3 - 3184560e^5)\sin(2f + 3y_2) \\
& +(233280 - 6526880e^2 + 11242600e^4 - 1039500e^6)\sin(3f + 3y_2) \\
& +(4687360e - 24745600e^3 + 8768640e^5)\sin(4f + 3y_2) \\
& +(28411600e^2 - 36324400e^4 + 2027025e^6)\sin(5f + 3y_2) \\
& +(73534720e^3 - 21447720e^5)\sin(6f + 3y_2) \\
& +(90818700e^4 - 4054050e^6)\sin(7f + 3y_2) \\
& +52659600e^5\sin(8f + 3y_2) \\
& +11486475e^6\sin(9f + 3y_2)]
\end{aligned}
$$

For long periodic terms

$$S^* = 0$$

Appendix B

Analytical Expressions (The Inclined Problem)

We use the following descriptions in this paper.

M	Mass of the primary body
m_{In}	Mass of the inner body
m	($\equiv 0$) Mass of the outer body
μ	$k^2(M + m_{In} + m) \equiv n^2 a^3$
a	Semimajor axis of the outer body
a_{In}	Semimajor axis of the inner body
n	Mean motion of the outer body
n_{In}	Mean motion of the inner body
e	Eccentricity of the outer body
η	$\sqrt{1 - e^2}$
I	Inclination of the outer body
θ	$\equiv \cos I$
f	True anomaly of the outer body
r	Radius of the outer body
λ_{In}	Longitude of the inner body
y_2	($\equiv \omega$) Argument of pericenter of the outer body
y_3	($\equiv h - \lambda_{In}$)

$$
\begin{aligned}
C_2 &\equiv \frac{M m_{In}}{(M + m_{In})^2} \\
C_3 &\equiv \frac{M m_{In}(M^2 - m_{In}^2)}{(M + m_{In})^4} \\
C_4 &\equiv \frac{M m_{In}(M^3 + m_{In}^3)}{(M + m_{In})^5} \\
C_5 &\equiv \frac{M m_{In}(M^4 - m_{In}^4)}{(M + m_{In})^6} \\
C_6 &\equiv \frac{M m_{In}(M^5 + m_{In}^5)}{(M + m_{In})^7}
\end{aligned}
$$

Hereafter, we neglect $O((\frac{m}{M+m_{In}})^2)$ or higher order terms.

B.1 Hamiltonians

Original Hamiltonian

$$
\begin{aligned}
F &= n_{In}x_3 + \frac{\mu^2}{2x_1^2} \\
&\quad + \mu C_2 \frac{a_{In}^2}{a^3}(\frac{a}{r})^3 \left[\frac{1}{8}(-1+3\theta^2)\right. \\
&\qquad + \frac{3}{8}(1-\theta^2)\cos(2f+2y_2) \\
&\qquad + \frac{3}{16}(1-\theta)^2\cos(2f+2y_2-2y_3) \\
&\qquad + \frac{3}{8}(1-\theta^2)\cos(2y_3) \\
&\qquad \left. + \frac{3}{16}(1+\theta)^2\cos(2f+2y_2+2y_3)\right] \\
&\quad + \mu C_3 \frac{a_{In}^3}{a^4}(\frac{a}{r})^4 \left[\frac{15}{64}(1-\theta-\theta^2+\theta^3)\cos(f+y_2-3y_3)\right. \\
&\qquad + \frac{5}{64}(1-3\theta+3\theta^2-\theta^3)\cos(3f+3y_2-3y_3) \\
&\qquad + \frac{15}{64}(1+\theta-\theta^2-\theta^3)\cos(f+y_2+3y_3) \\
&\qquad + \frac{5}{64}(1+3\theta+3\theta^2+\theta^3)\cos(3f+3y_2+3y_3) \\
&\qquad + \frac{3}{64}(-1+11\theta+5\theta^2-15\theta^3)\cos(f+y_2-y_3) \\
&\qquad + \frac{15}{64}(1-\theta-\theta^2+\theta^3)\cos(3f+3y_2-y_3) \\
&\qquad + \frac{3}{64}(-1-11\theta+5\theta^2+15\theta^3)\cos(f+y_2+y_3) \\
&\qquad \left. + \frac{15}{64}(1+\theta-\theta^2-\theta^3)\cos(3f+3y_2+y_3)\right] \\
&\quad + \ldots
\end{aligned}
$$

Hamiltonians F^*, F^{**} and F^{***}

$$
\begin{aligned}
F^* &= n_{In}x_3 \\
&\quad + \frac{\mu^2}{2x_1^2} \\
&\quad + \frac{1}{8}\mu C_2 \frac{a_{In}^2}{r^3}[(-1+3\theta^2)+3(1-\theta^2)\cos(2f+2y_2)] \\
&\quad + \frac{3}{512}\mu C_4 \frac{a_{In}^4}{r^5}[3(3-30\theta^2+35\theta^4) \\
&\qquad -20(1-8\theta^2+7\theta^4)\cos(2f+2y_2) \\
&\qquad +35(1-\theta^2)^2\cos(4f+4y_2)]
\end{aligned}
$$

$$
\begin{aligned}
&+\frac{5}{8192}\mu C_6\frac{a_{In}^6}{r^7}[10(-5+105\theta^2-315\theta^4+231\theta^6)\\
&-105(-1+19\theta^2-51\theta^4+33\theta^6)\cos(2f+2y_2)\\
&+126(-1+\theta^2)^2(-1+11\theta^2)\cos(4f+4y_2)\\
&-231(-1+\theta^2)^3\cos(6f+6y_2)]\\
&+\ldots\\
F^{**} &= n_{In}x_3\\
&+\frac{\mu^2}{2x_1^2}\\
&+\frac{1}{8}\mu C_2\frac{a_{In}^2}{a^3}\frac{1}{\eta^3}(-1+3\theta^2)\\
&+\frac{9}{1024}\mu C_4\frac{a_{In}^4}{a^5}\frac{1}{\eta^7}[(3-30\theta^2+35\theta^4)(2+3e^2)-10(1-8\theta^2+7\theta^4)e^2\cos(2y_2)]\\
&+\frac{25}{65536}\mu C_6\frac{a_{In}^6}{a^7}\frac{1}{\eta^{11}}[+2(-5+105\theta^2-315\theta^4+231\theta^6)(8+40e^2+15e^4)\\
&-210(-1+19\theta^2-51\theta^4+33\theta^6)e^2(2+e^2)\cos(2y_2)\\
&+63(-1+\theta^2)^2(-1+11\theta^2)e^4\cos(4y_2)]\\
&+\ldots\\
F^{***} &= n_{In}x_3\\
&+\frac{\mu^2}{2x_1^2}\\
&+\frac{1}{8}\mu C_2\frac{a_{In}^2}{a^3}\frac{1}{\eta^3}(-1+3\theta^2)\\
&+\frac{9}{1024}\mu C_4\frac{a_{In}^4}{a^5}\frac{1}{\eta^7}(3-30\theta^2+35\theta^4)(2+3e^2)\\
&+\frac{25}{32768}\mu C_6\frac{a_{In}^6}{a^7}\frac{1}{\eta^{11}}(-5+105\theta^2-315\theta^4+231\theta^6)(8+40e^2+15e^4)\\
&+\ldots
\end{aligned}
$$

B.2 P_2-limited generating functions

For short periodic terms

$$
\begin{aligned}
S_1 &= 0\\
S_2 &= -\frac{3}{16}\mu C_2\frac{1}{n_{In}}\frac{a_{In}^2}{r^3}\\
&\quad\Big[[2\theta\sin(2f+2y_2)]\cos(2y_3)\\
&\quad+[(1-\theta^2)\\
&\quad+(1+\theta^2)\cos(2f+2y_2)]\sin(2y_3)\Big]\\
S_3 &= -\frac{3}{64}\mu C_2\frac{na}{\eta n_{In}^2}\frac{a_{In}^2}{r^4}
\end{aligned}
$$

$$
\begin{aligned}
&\Big[[-6(-1+\theta^2)e\sin(f)\\
&\quad+(1+\theta^2)\{-e\sin(f+2y_2)\\
&\quad+4\sin(2f+2y_2)\\
&\quad+5e\sin(3f+2y_2)\}]\cos(2y_3)\\
&\quad+[2\theta\{-e\cos(f+2y_2)\\
&\quad+4\cos(2f+2y_2)\\
&\quad+5e\cos(3f+2y_2)\}]\sin(2y_3)\Big]
\end{aligned}
$$

$$
\begin{aligned}
S_4 \;=\; & -\frac{3}{256}\mu C_2\frac{(na)^2}{\eta^2 n_{In}^3}\frac{a_{In}^2}{r^5}\\
&\Big[[2\theta\{3e^2\sin(2y_2)\\
&\quad-10e\sin(f+2y_2)\\
&\quad+2(8-5e^2)\sin(2f+2y_2)\\
&\quad+54e\sin(3f+2y_2)\\
&\quad+35e^2\sin(4f+2y_2)\}]\cos(2y_3)\\
&\quad+[-18e^2(1-\theta^2)\\
&\quad-12(-1+\theta^2)e\cos(f)\\
&\quad-30(-1+\theta^2)e^2\cos(2f)\\
&\quad+3(1+\theta^2)e^2\cos(2y_2)\\
&\quad-10(1+\theta^2)e\cos(f+2y_2)\\
&\quad-2(1+\theta^2)(-8+5e^2)\cos(2f+2y_2)\\
&\quad+54(1+\theta^2)e\cos(3f+2y_2)\\
&\quad+35(1+\theta^2)e^2\cos(4f+2y_2)\}]\sin(2y_3)\Big]
\end{aligned}
$$

$$
\begin{aligned}
S_5 \;=\; & -\frac{3}{1024}\mu C_2\frac{(na)^3}{\eta^3 n_{In}^4}\frac{a_{In}^2}{r^6}\\
&\Big[[(-1+\theta^2)\{6e(-4+45e^2)\sin(f)\\
&\quad-192e^2\sin(2f)\\
&\quad-210e^3\sin(3f)\}\\
&\quad+(1+\theta^2)\{15e^3\sin(f-2y_2)\\
&\quad+40e^2\sin(2y_2)\\
&\quad+e(-68+45e^2)\sin(f+2y_2)\\
&\quad-16(-4+13e^2)\sin(2f+2y_2)\\
&\quad-e(-436+105e^2)\sin(3f+2y_2)\\
&\quad+712e^2\sin(4f+2y_2)\\
&\quad+315e^3\sin(5f+2y_2)\}]\cos(2y_3)\\
&\quad+[2\theta\{-15e^3\cos(f-2y_2)\\
&\quad+40e^2\cos(2y_2)
\end{aligned}
$$

$$
\begin{aligned}
&+e(-68+45e^2)\cos(f+2y_2)\\
&-16(-4+13e^2)\cos(2f+2y_2)\\
&-e(-436+105e^2)\cos(3f+2y_2)\\
&+712e^2\cos(4f+2y_2)\\
&+315e^3\cos(5f+2y_2)\}]\sin(2y_3)\Big]
\end{aligned}
$$

For intermediate periodic terms

$$
\begin{aligned}
S_1^* &= \frac{1}{16}\mu C_2\frac{a_{In}^2}{a^3}\frac{1}{\eta^3 n}[2(-1+3\theta^2)\{(f-l)+e\sin f\}\\
&\quad +(1-\theta^2)\{3e\sin(f+2y_2)+3\sin(2f+2y_2)+e\sin(3f+2y_2)\}\\
&\quad -(1-\theta^2)\frac{1}{e^2}\{2-3e^2-2\eta(1-e^2)\}\sin(2y_2)]\\
S_2^* &= O((\frac{m}{M+m_{In}})^2)
\end{aligned}
$$

For long periodic terms

$$S^{**}=0$$

B.3 P_3-limited generating functions

For short periodic terms

$$
\begin{aligned}
S_1 &= 0\\
S_2 &= -\frac{5}{96}\mu C_3\frac{1}{n_{In}}\frac{a_{In}^3}{r^4}\\
&\quad \Big[[\theta\{-3(-1+\theta^2)\sin(f+y_2)\\
&\quad +(3+\theta^2)\sin(3f+3y_2)\}]\cos(3y_3)\\
&\quad +[-3(-1+\theta^2)\cos(f+y_2)\\
&\quad +(1+3\theta^2)\cos(3f+3y_2)\}]\sin(3y_3)\Big]\\
&\quad -\frac{3}{32}\mu C_3\frac{1}{n_{In}}\frac{a_{In}^3}{r^4}\\
&\quad \Big[[\theta\{(-11+15\theta^2)\sin(f+y_2)\\
&\quad -5(-1+\theta^2)\sin(3f+3y_2)\}]\cos(y_3)\\
&\quad +[(-1+5\theta^2)\cos(f+y_2)\\
&\quad -5(-1+\theta^2)\cos(3f+3y_2)\}]\sin(y_3)\Big]\\
S_3 &= -\frac{5}{576}\mu C_3\frac{na}{\eta n_{In}^2}\frac{a_{In}^3}{r^5}\\
&\quad \Big[[3(-1+\theta^2)\{3e\sin(y_2)\\
&\quad -2\sin(f+y_2)
\end{aligned}
$$

$$
\begin{aligned}
&-5e\sin(2f+y_2)\}\\
&+(1+3\theta^2)\{-e\sin(2f+3y_2)\\
&+6\sin(3f+3y_2)\\
&+7e\sin(4f+3y_2)\}]\cos(3y_3)\\
&+[3\theta(-1+\theta^2)\{3e\cos(y_2)\\
&-2\cos(f+y_2)\\
&-5e\cos(2f+y_2)\}\\
&+\theta(3+\theta^2)\{-e\cos(2f+3y_2)\\
&+6\cos(3f+3y_2)\\
&+7e\cos(4f+3y_2)\}]\sin(3y_3)\Big]\\
&-\frac{3}{64}\mu C_3\frac{na}{\eta n_{In}^2}\frac{a_{In}^3}{r^5}\\
&\Big[[(-1+5\theta^2)\{-3e\sin(y_2)\\
&+2\sin(f+y_2)\\
&+5e\sin(2f+y_2)\}\\
&-5(-1+\theta^2)\{-e\sin(2f+3y_2)\\
&+6\sin(3f+3y_2)\\
&+7e\sin(4f+3y_2)\}]\cos(y_3)\\
&+[\theta(-11+15\theta^2)\{-3e\cos(y_2)\\
&+2\cos(f+y_2)\\
&+5e\cos(2f+y_2)\}\\
&-5\theta(-1+\theta^2)\{-e\cos(2f+3y_2)\\
&+6\cos(3f+3y_2)\\
&+7e\cos(4f+3y_2)\}]\sin(y_3)\Big]\\
S_4 \;=\; &-\frac{5}{3456}\mu C_3\frac{(na)^2}{\eta^2 n_{In}^3}\frac{a_{In}^3}{r^6}\\
&\Big[[3\theta(-1+\theta^2)\{15e^2\sin(f-y_2)\\
&+8e\sin(y_2)\\
&+2(-2+15e^2)\sin(f+y_2)\\
&-32e\sin(2f+y_2)\\
&-35e^2\sin(3f+y_2)\}\\
&+\theta(3+\theta^2)\{3e^2\sin(f+3y_2)\\
&-16e\sin(2f+3y_2)\\
&-2(-18+7e^2)\sin(3f+3y_2)\\
&+104e\sin(4f+3y_2)\\
&+63e^2\sin(5f+3y_2)\}]\cos(3y_3)
\end{aligned}
$$

$$
\begin{aligned}
&+[3(-1+\theta^2)\{-15e^2\cos(f-y_2)\\
&+8e\cos(y_2)\\
&+2(-2+15e^2)\cos(f+y_2)\\
&-32e\cos(2f+y_2)\\
&-35e^2\cos(3f+y_2)\}\\
&+(1+3\theta^2)\{3e^2\cos(f+3y_2)\\
&-16e\cos(2f+3y_2)\\
&-2(-18+7e^2)\cos(3f+3y_2)\\
&+104e\cos(4f+3y_2)\\
&+63e^2\cos(5f+3y_2)\}]\sin(3y_3)\Big]\\
&-\frac{3}{128}\mu C_3\frac{(na)^2}{\eta^2 n_{In}^3}\frac{a_{In}^3}{r^6}\\
&\Big[[\theta(-11+15\theta^2)\{-15e^2\sin(f-y_2)\\
&-8e\sin(y_2)\\
&-2(-2+15e^2)\sin(f+y_2)\\
&+32e\sin(2f+y_2)\\
&+35e^2\sin(3f+y_2)\}\\
&+5\theta(-1+\theta^2)\{-3e^2\sin(f+3y_2)\\
&+16e\sin(2f+3y_2)\\
&+2(-18+7e^2)\sin(3f+3y_2)\\
&-104e\sin(4f+3y_2)\\
&-63e^2\sin(5f+3y_2)\}]\cos(y_3)\\
&+[(-1+5\theta^2)\{15e^2\cos(f-y_2)\\
&-8e\cos(y_2)\\
&-2(-2+15e^2)\cos(f+y_2)\\
&+32e\cos(2f+y_2)\\
&+35e^2\cos(3f+y_2)\}\\
&+5(-1+\theta^2)\{-3e^2\cos(f+3y_2)\\
&+16e\cos(2f+3y_2)\\
&+2(-18+7e^2)\cos(3f+3y_2)\\
&-104e\cos(4f+3y_2)\\
&-63e^2\cos(5f+3y_2)\}]\sin(y_3)\Big]
\end{aligned}
$$

$$
\begin{aligned}
S_5 \;=\; &-\frac{5}{20736}\mu C_3\frac{(na)^3}{\eta^3 n_{In}^4}\frac{a_{In}^3}{r^7}\\
&\Big[[3(-1+\theta^2)\{-105e^3\sin(2f-y_2)\\
&+18e^2\sin(f-y_2)
\end{aligned}
$$

$$
\begin{aligned}
&-5e(-4+45e^2)\sin(y_2)\\
&+4(-2+59e^2)\sin(f+y_2)\\
&+3e(-52+105e^2)\sin(2f+y_2)\\
&-466e^2\sin(3f+y_2)\\
&-315e^3\sin(4f+y_2)\}\\
&+(1+3\theta^2)\{-15e^3\sin(3y_2)\\
&+70e^2\sin(f+3y_2)\\
&+e(-172+63e^2)\sin(2f+3y_2)\\
&-12(-18+35e^2)\sin(3f+3y_2)\\
&-e(-1156+189e^2)\sin(4f+3y_2)\\
&+1670e^2\sin(5f+3y_2)\\
&+693e^3\sin(6f+3y_2)\}]\cos(3y_3)\\
&+[3\theta(-1+\theta^2)\{105e^3\cos(2f-y_2)\\
&-18e^2\cos(f-y_2)\\
&-5e(-4+45e^2)\cos(y_2)\\
&+4(-2+59e^2)\cos(f+y_2)\\
&+3e(-52+105e^2)\cos(2f+y_2)\\
&-466e^2\cos(3f+y_2)\\
&-315e^3\cos(4f+y_2)\}\\
&+\theta(3+\theta^2)\{-15e^3\cos(3y_2)\\
&+70e^2\cos(f+3y_2)\\
&+e(-172+63e^2)\cos(2f+3y_2)\\
&-12(-18+35e^2)\cos(3f+3y_2)\\
&-e(-1156+189e^2)\cos(4f+3y_2)\\
&+1670e^2\cos(5f+3y_2)\\
&+693e^3\cos(6f+3y_2)\}]\sin(3y_3)\Big]\\
&-\frac{3}{256}\mu C_3\frac{(na)^3}{\eta^3 n_{In}^4}\frac{a_{In}^3}{r^7}\\
&\Big[[-(-1+5\theta^2)\{-105e^3\sin(2f-y_2)\\
&+18e^2\sin(f-y_2)\\
&-5e(-4+45e^2)\sin(y_2)\\
&+4(-2+59e^2)\sin(f+y_2)\\
&+3e(-52+105e^2)\sin(2f+y_2)\\
&-466e^2\sin(3f+y_2)\\
&-315e^3\sin(4f+y_2)\}\\
&-5(-1+\theta^2)\{-15e^3\sin(3y_2)
\end{aligned}
$$

$$
\begin{aligned}
&+70e^2\sin(f+3y_2)\\
&+e(-172+63e^2)\sin(2f+3y_2)\\
&-12(-18+35e^2)\sin(3f+3y_2)\\
&-e(-1156+189e^2)\sin(4f+3y_2)\\
&+1670e^2\sin(5f+3y_2)\\
&+693e^3\sin(6f+3y_2)\}]\cos(y_3)\\
&+[-\theta(-11+15\theta^2)\{105e^3\cos(2f-y_2)\\
&-18e^2\cos(f-y_2)\\
&-5e(-4+45e^2)\cos(y_2)\\
&+4(-2+59e^2)\cos(f+y_2)\\
&+3e(-52+105e^2)\cos(2f+y_2)\\
&-466e^2\cos(3f+y_2)\\
&-315e^3\cos(4f+y_2)\}\\
&-5\theta(-1+\theta^2)\{-15e^3\cos(3y_2)\\
&+70e^2\cos(f+3y_2)\\
&+e(-172+63e^2)\cos(2f+3y_2)\\
&-12(-18+35e^2)\cos(3f+3y_2)\\
&-e(-1156+189e^2)\cos(4f+3y_2)\\
&+1670e^2\cos(5f+3y_2)\\
&+693e^3\cos(6f+3y_2)\}]\sin(y_3)\Big]
\end{aligned}
$$

For intermediate periodic terms

$$S^* = 0$$

For long periodic terms

$$S^{**} = 0$$